Peptide Phosphorylation in the Design of a Vector for Intracellular Drug Delivery based on the Cell-Penetrating Peptide Penetratin

INAUGURALDISSERTATION

zur Erlangung der Würde eines Doktors der Philosophie

vorgelegt der Philosophischen-Naturwissenschaftlichen Fakultät

der Universität Basel

von Reto Sauder aus Lupsingen, Basel-Landschaft

Basel, 2013

Genehmigt von der Philosophisch-Naturwissenschaftlichen Fakultät auf Antrag von

Prof. Dr. Joachim Seelig
Prof. Dr. Sebastian Hiller

Basel, den 11.12.2012

Prof. Dr. Jörg Schibler
(Dekan)

Table of contents

i) Abbreviations

4NPP	4-nitrophenyl phosphate
ANTS	8-aminonaphthalene-1,3,6-trisulfonic acid
APPK	Alkaline phosphatase (from porcine kidney)
ATP	Adenosine triphosphate
CAM	Cell adhesion molecule
CHO	Chinese hamster ovaries
CPP	Cell-penetrating peptide
ddH_2O	Double distilled water
DIC	Differential interference contrast
DLS	Dynamic light scattering
DMEM	Dulbecco's modified Eagle's medium
DMSO	Dimethyl sulfoxide
DOPE-PEG	1,2-dioleoyl-*sn*-glycero-3-phosphoethanolamine-N-(methoxy(polyethylene glycol)-2000)
DPX	*p*-xylene-bis-pyridinium bromide (DPX)
EPR	Electron paramagnetic resonance
FCS	Fetal calf serum
GUV	Giant unilamellar vesicle
HIV	Human immunodeficiency virus
HPLC	High-performance liquid chromatography
ITC	Isothermal titration calorimetry
LUV	Large unilamellar vesicle
NMR	Nuclear magnetic resonance
OD	Optical density
PBS	Phosphate buffered saline
PDI	Polydispersity index
PEG	Poly(ethylene glycol)
PEI	Polyethyleneimine
pen-2AL	Penetratin mutant $A_9A_{10}L_{13}$

pen-Antp	Penetratin peptide (RQIKIWFQNRRMKWKK)
pen-AYL	Penetratin mutant $A_9Y_{10}L_{13}$
pen-A(pY)L	Penetratin mutant $A_9(pY)_{10}L_{13}$
PMT	Photomultiplier tube
POPC	1-palmitoyl-2-oleoyl-*sn*-glycero-3-phosphocholine
POPG	1-palmitoyl-2-oleoyl-*sn*-glycero-3-phospho-*rac*-glycerol
PTD	Protein transduction domain
RNA	Ribonucleic acid
SLS	Static light scattering
SUV	Small unilamellar vesicle
TAMRA	Tetramethylrhodamine
TAT	Trans-activator of transcription
TBS	Tris buffered saline
TEMPO	(2,2,6,6-tetramethylpiperidin-1-yl)oxyl
TFA	Trifluoroacetic acid
Tris	Tris(hydroxymethyl)aminoethane
Trp	L-Tryptophan
TX100	Triton X-100
Tyr	L-Tyrosine
UV-vis	Ultraviolet-visible (light)
WR_9	Nona-arginine (WRRRRRRRRR)

ii) Summary

The fruitful research in molecular biology over the course of the last 50 years has revolutionized our comprehension of the processes that happen inside a cell. Understanding of intracellular regulatory pathways and the protein synthesis by translation of gene transcripts allow the development of powerful methods to fight a broad spectrum of human health issues that are traditionally very hard to treat. An important requisite, however, is access of the agent to the cell interior. In this respect, the plasma membrane of eukaryotic cells poses an efficient barrier for many potential agents and methods that allow an agent's transit across it are therefore in high demand.

Promising vectors in this regard are cell-penetrating peptides (CPPs): short polycationic peptides that were shown to be capable of transporting compounds of interest inside eukaryotic cells. To date, the mechanism of their translocation is still under much debate. Also, their application as drug vector is potentially delicate because some CPPs showed a concentration dependent toxicity for cells.

Penetratin (pen-Antp) is among the best studied CPPs. Interestingly, it does not show translocation across model membranes such as unilamellar vesicles (LUVs). A more hydrophobic pen-Antp mutant called pen-2AL, however, does show permeation of model membranes. We were interested in the *potential modification of pen-2AL with a phosphorylated tyrosine (named pen-A(pY)L) in order to create a CPP which is only active after dephosphorylation* e.g. by a protein phosphatase. In doing so, we aimed for an inducible CPP that would only be activated by cellular phosphatases.

In the following chapters we discuss various aspects of the design of the pen-A(pY)L peptide and the investigation of its effect on both model and biological membranes. In **Chapter 1** we present the methodical basis for the investigation of the interaction of CPPs with model membrane systems. Both the creation of lipid model membranes and their thermodynamical characterization in presence of CPPs are described and supplemented with minute protocols for every method. Exemplary data show that pen-2AL destabilizes model membranes in a detergent-like manner whereas

pen-Antp does not. Furthermore, we show that the use of multivalent fluorescent dyes can introduce a critical measurement bias upon interaction with CPPs.

In **chapter 2** we discuss the design of the pen-A(pY)L peptide and show its effect on LUVs and CHO cells by means of a permeation (leakage) assay and confocal microscopy, respectively. Our leakage data suggest that the phosphorylated pen-A(pY)L does not permeate LUVs at low micromolar concentrations whereas the unphosphorylated pen-AYL shows strong permeation at these conditions. We could also successfully activate pen-A(pY)L by dephosphorylation as demonstrated by inducible dye leakage from LUVs after addition of a phosphatase. Lastly, CHO cells show uptake of TAMRA-labeled pen-A(pY)L after incubation with 20 µM of the CPP. The peptide seems also to successfully reach the cytosol without damaging the cells.

We then investigated the effect of the used medium during incubation of CHO cells with either peptide as discussed in **chapter 3**. Using plain phosphate buffered saline (PBS) as incubation medium led to strong detachment of the cells during incubation with low peptide concentration. In contrast, this could not be observed after incubation with either peptide dissolved in DMEM/F12. Furthermore, the images made with differential interference contrast suggest that incubation of CHO cells with 20 µM TAMRA-pen-AYL is toxic for the cells.

In **chapter 4** we describe the observed propensity of pen-A(pY)L for gel formation at low millimolar concentration. The peptide gets compared with its unphosphorylated counterpart in order to assess their tendency to aggregate under various conditions in order to identify the potential molecular interactions that promote gel formation. We thereby find that it is probably hydrophobic attraction between the peptide that leads to the clustering of pen-A(pY)L which may have been introduced by the tyrosine's phenol group. However, the bulk of peptide seems to remain dissolved at low micromolar concentrations i.e. at the relevant concentration for a potential application of the CPP.

Lastly, as a consequence of the earlier observed bias due to the interaction of multivalent fluorescent dyes with certain CPPs we propose in **chapter 5** an alternative molecular probe for the detection of membrane permeation by CPPs. Instead of the dequenching of fluorescent dye we exploit the concentration dependence of the electron paramagnetic resonance (EPR) signal of spin labels to detect their leakage out of LUVs.

We can show that the EPR signal is, in contrary to fluorescent dyes, independent of the presence of CPPs. However, we also experienced difficulties in enclosing sufficient spin label concentrations into LUVs. Nevertheless, we value electron-spin labels as promising option for such an assay.

Chapter 1:

Thermodynamics of Lipid Interactions with Cell-Penetrating Peptides[1]

1.1. General introduction to cell-penetrating peptides

The transition from classical screening in drug design to rational drug design including drug delivery

Drug design underwent a rational evolution during the last decades because of combined advances in the disciplines molecular genetics, combinatorial chemistry and high throughput screening. Originally, many drugs were designed to target enzymes and cell-surface receptors. Most of these drugs were water soluble compounds with a molecular mass low enough to still enable passage over biological membranes (Lipinski's "rule of 5") (2). However, proteomics has identified many more interesting signaling proteins involved in intracellular regulatory pathways. Further intracellular drug targets were identified because the structures responsible for protein biosynthesis i.e. the very target of gene therapy or RNA silencing are located in the cell interior as well. The challenge in exploiting these targets for modern medicine thus lies in the

[1] Sections 1.2. to 1.7. of this chapter consist of the publication "Thermodynamics of lipid interactions with cell-penetrating peptides" (1. Sauder R, Seelig J, Ziegler A. 2011. Methods in molecular biology 683: 129-55).

combined efforts to design the ligands and develop reagents that provide their effective delivery inside cells of specific tissues or organs.

Cell membranes as obstacle for intracellular drug delivery

The main barrier in this regard is the ~60 to 70 Å thick cell membrane (only accounting for the lipid part including hydrated headgroups; the thickness increases when glycosylated membrane proteins are included) which delineates not only distinct intracellular compartments ("organelles"), but also the whole biological cell from the outside. The cell membrane (described in more detail in (3, 4)) consists of two parts: a double layer of phospholipid[2] molecules (the so-called lipid bilayer) and the therein embedded proteins which maintain both signaling and transport of cellular nutrients, electrolytes, water or metabolic waste products across the membrane. The phospholipids of the membrane predominantly provide its barrier function by means of the hydrophobic nature of the fatty acid part of the various lipids. This hydrophobic core of the lipid bilayer drastically reduces its permeability of most common solutes of the cytosol, the extracellular fluid or the blood plasma (e.g. electrolytes, ATP, glucose or proteins) due to the high energy needed for such molecules to passively diffuse across (5). As a consequence, the drug design must not only respect specific binding to the target, but also shape, size, solubility and permeability to actually reach the target that might be located intracellularly (2). This is especially true for gene therapy methods using nucleic acids that are highly negatively charged because of their phosphate backbone. The delivery of such compounds into biological cells therefore poses a challenge. At best, the drug delivery is specific to a proper tissue (drug targeting) thus causing least side-effects to other tissue of the organism.

Vectors to transport compounds across cell membranes

There are established methods for intracellular drug delivery in simple biological systems: for example, cell culture of eukaryotic cells is an excellent model system to study the delivery of desired compounds across a biological membrane. Techniques

[2] Technically, the lipid bilayer does not exclusively consist of phospholipids (e.g. ceramides) but they form the bulk of it.

such as electroporation (6), viral vectors (7, 8), nanoparticles (9), or liposomes (10) have all been shown to successfully deliver a broad range of compounds into cells in culture and could, in some cases, even be applied to treat human diseases (e.g. viral vectors for severe combined immunodeficiency (11)). However, most of those methods have a limited efficacy or transport capacity for drugs; also toxic side effects might restrict their use in humans. The interest in alternative approaches for intracellular drug delivery is thus ongoing.

CPPs - Alternative vectors

Promising candidates for intracellular drug delivery are so-called cell-penetrating peptides (CPPs, also termed Trojan peptides or protein transduction domains (PTD); reviewed in (12, 13)). CPPs are a group of short cationic peptides that have the capacity to permeate biological membranes at low micromolar concentration; they can be conjugated to biologically relevant (macro)molecules such as peptides (14, 15), proteins (16, 17) or nucleic acids (18). Their discovery in the late 80's by the cellular uptake of both the HIV-1 TAT (19-21) and the penetratin peptide (derived from the Antennapedia transcription factor from *Drosophila melanogaster* (22)) was, to some degree, anticipated from earlier work on the cellular uptake of large polycationic homopolymers or proteins (23). Compounds such as polylysine (23) or polyethylenimine (24) were shown to help delivering conjugated drug molecules or nucleic acids into living cells. As these polycationic molecules bind to anionic, cell-surface bound polysaccharides (25), the proposed uptake mechanism was of endocytotic nature (26). Upon closer inspection, endocytotic uptake routes comprise several independent and highly regulated pathways (27, 28) involving signaling receptors and protein machinery driven by ATP hydrolysis. However, as cellular uptake of CPPs could be observed at low temperature (≤4 °C) (21, 22, 29-32) (where endocytosis does not take place), in the presence of endocytosis inhibitors (30, 31, 33), with CPPs as D-isomers (34, 35) or (retro-)inverso sequence (36, 37) it became clear that membrane permeation by CPPs was not exclusively based on a common endocytotic pathway. The need for a broader perspective on the topic became apparent when further investigations (38-40) corrected some of those observations as possible artifacts of the cell fixation.

Interaction of CPPs with model lipid bilayers

Alternative mechanisms of membrane permeation were suggested considering the hypothesis that CPPs not only interact with cell-surface proteins or carbohydrates, but also with the lipid portion of a biological membrane. In the latter case, the permeation should be observable when using a corresponding lipid bilayer model. One frequent lipid bilayer model are, for example, liposomes, that are spherules composed of desired mixtures of lipid molecules of synthetic or natural origin (41). Phospholipids serve as a well-established and easy-to-handle model for the lipid portion of biological membranes (reviewed in (42) and (43); already in the 1960s, Bangham et al. used this model to study the permeability of model membranes to ions and nonelectrolytes (44, 45)). Depending on their mode of preparation, both small (SUVs (46)) and large unilamellar vesicles (LUVs (47, 48)) with a homogeneous size distribution at an approximate diameter of 30 and 100 nm, respectively, were widely used in the past decades to study permeation of lipid bilayers by CPPs. The diameter of LUVs is in the same dimension as endosomes found in biological cells and is thus especially suited to study a potential intracellular escape from such structures.

The combination of spectroscopic methods with thermodynamic analysis yields important parameters of the interaction between CPPs and model lipid bilayers, such as the binding constant, conformational change or bilayer stability in presence of the CPP. For example, it was shown that the affinity of an individual CPP to the lipid bilayer might dependent on both the amphipathicity and the anionic lipid content of the bilayer (13), depending on the structure of the CPP. In the in vivo situation, binding to other potential cell-surface molecules, such as extracellular polysaccharides, might exceed binding to membranes of low anionic lipid content (49, 50) such as found in eukaryotic animal cell membranes (51).

Many studies consent that the highly charged CPPs do not permeate lipid bilayers by passive diffusion (13, 52, 53) unless they are of amphipathic nature (54-56) or in presence of a transmembrane potential (57, 58) (corresponding mechanisms were discussed in earlier reviews (59)). The observation that membrane permeation of model membranes is closely linked to the peptides' amphipathicity lead to classification of CPPs by their amphipathic nature (for details (13, 60)). This helped to resolve

controversial findings of a very heterogenous class of peptides with diverse structural properties that likely do not share a common uptake pathway. Depending on their structure, the various CPPs can be assigned with distinct uptake pathways.

The thermodynamic analysis of their interaction properties is therefore of great value when it comes to identify (un)favorable interactions between CPPs and potential binding partners as well as their ability to permeate model lipid membranes. Many experimental pitfalls may result when working with such highly charged molecules, so that the following publication covers the most important methods to investigate these peptides and their properties with detailed protocols. Specifically, the article addresses the i) preparation of lipid vesicles of desired lipid composition and size with particular focus to prevent aggregation with CPPs, ii) analytical determination of both lipid and peptide concentrations, iii) CPP-phospholipid interaction by isothermal titration calorimetry (ITC), iv) detection of membrane permeation by fluorescence spectroscopy and v) membrane stability in presence of CPPs by nuclear magnetic resonance (NMR)

1.2. Introduction to thermodynamics of lipid interactions with cell-penetrating peptides

Past (61, 62) and current research studies (63-65) have shown that eukaryotic cells take up polycationic compounds, such as cell-penetrating peptides (CPPs) or other cationic homopolymers (e.g. polyethylenimine (66) or DEAE-dextran (67)), at (sub)micromolar concentration by binding them to anionic cell-surface glycans and subsequent endocytosis. Entrapment of CPPs in endocytotic vesicles is of moderate biomedical interest, because a CPP-attached cargo (e.g. plasmid DNA, siRNA) would be rapidly degraded when passing from endocytotic vesicles to late endosomes or lysosomes. This way, no or only few cargo molecules would reach their intracellular target, e.g. the nucleus for gene expression.

In this respect, the work of Frankel (19) and Green (20) on the CPP HIV-1 Tat received much attention because the effect of extracellularly added Tat on cellular gene expression suggested that many more Tat molecules reached the nucleus than could be

provided by endocytosis. The delivery of CPPs into cytosol and nucleus thus became of high biomedical interest, and the work of Frankel and Green initiated a revival of research on cationic peptides, 20 years after the first studies on polylysine had been published (62).

Subsequent studies with fluorescently labeled CPPs confirmed that various CPPs could indeed enter the cytosol and reach the nucleus of biological cells (21, 32, 68-77). The translocation of CPPs into the cytosol was also observed in cells that were incompetent for endocytosis (e.g. bacteria) (78-80). Both observations were surprising, because this meant that some CPPs may overcome the cytoplasmic and/or endosome membrane in spite of their polycationic character that argues against a rapid passive diffusion across lipid bilayers (81). These experimental observations led to rather controversial views on the apparently "magic" (82) uptake into cytosol and cell nucleus.

Some of the observations could have been biased by experimental artifacts: Surface-bound CPP molecules, for example, may enter cells post-mortem, because the cell treatment with methanol, ethanol or paraformaldehyde typically used for cell fixation in microscopy can disrupt the membrane (40). This criticism does not apply to studies on living or unfixated cells (21, 32, 68-77). A detailed comparison of the conditions required for this cytosolic CPP entry suggests, however, that the cytosolic delivery of CPPs likely proceeds by more than one mechanism (13).

Some amphipathic CPPs have detergent-like properties. They have a high affinity for charged and uncharged lipids, they partition into the hydrophobic membrane core and disturb model membranes already at low micromolar concentrations - in analogy to many amphipathic antibiotic peptides (83, 84). These amphipathic CPPs translocate almost equally across pure lipid membranes (exempt of membrane proteins or glycans) or the plasma membrane of living cells (85). Molecular pathways of cell entry include, for example, pore and carpet formation – as can be demonstrated in model membranes (86, 87). In some cases, CPPs may also leak out of endosomes ("endosomolytic" or fusogenic peptides) as a result of their pH–dependant structural change and lipid interaction (75, 88, 89). As a drawback for their intrinsic membrane disturbing property, amphipathic CPPs typically have a higher cell toxicity than non-amphipathic CPPs (90,

91) which might render biomedical applications problematic which is also known from lipid-based transfection reagents.

In contrast, non-amphipathic CPPs, such as homopolymers of arginine, are less toxic (90), but they bind lipid membranes only with poor affinity, because the fraction of anionic lipids encountered in mammalian cells is usually quite low. Also, partitioning into the hydrophobic bilayer core is lacking (92-94). They do not induce membrane leakage at low micromolar concentrations even though they enter the cytosol of living cells at this concentration. This suggests that not the lipids, but other cellular compounds are required for their translocation into the cytosol (13). Their membrane permeation on *model* membranes (devoid of proteins or glycans) has been observed only for special conditions, e.g. high micromolar concentrations (electroporation-like), unphysiological counterions (95, 96), electro-chemical gradients (97), repeated lipid phase-cycling (98) or delicate vesicles (99, 100).

The present chapter describes protocols that allow for quantification and comparison of membrane interactions and perturbations of CPPs. Using selected CPPs it is shown that amphipathic CPPs destabilize model membranes already at low micromolar CPP concentration - in contrast to non-amphipathic CPPs. The distinction of both CPP classes resides on the strategy of making CPPs more amphipathic by either linking a membrane anchor to them ("acylation") (101) or by a previous report on an amphipahtic penetratin mutant ("p2AL") designed from helical wheel projections (55). Each protocol consists of an initial descriptive on required parameters and related literature, followed by the protocol itself. Conclusions from example data (see **Figures**) are described in **Subheading 1.5**.

1.3. Materials

1.3.1. Chemicals

1. Ammonium molybdate, $(NH_4)_6Mo_7O_{24}\cdot 4\ H_2O$ (Merck)
2. ANTS, 8-aminonaphthalene-1,3,6-trisulfonic acid, disodium salt (Molecular Probes)

3. Buffer for leakage experiments: 20 mM Tris, 134 mM NaCl, pH 8.5
4. Buffer for ITC experiments: 20 mM Tris, 100 mM NaCl, pH7.4
5. Calcein (Sigma-Aldrich)
6. Contrad 90 (Socochim)
7. DOPE, 1,2-dioleoyl-sn-glycero-3-phosphoethanolamine (Avanti Polar Lipids)
8. DOPE-PEG2000, 1,2-dioleoyl-sn-glycero-3-phosphoethanolamine-N-[methoxy(polyethylene glycol)-2000], ammonium salt (Avanti Polar Lipids)
9. Malachite green oxalate (Merck)
10. DPX, p-xylene-bis-pyridinium bromide (Molecular Probes)
11. Perchloric acid 70% (Merck)
12. Phosphoric acid 85% (Sigma-Aldrich)
13. POPC, 1-palmitoyl-2-oleoyl-sn-glycero-3-phosphocholine (Avanti Polar Lipids)
14. POPE, 1-palmitoyl-2-oleoyl-sn-glycero-3-phosphoethanolamine (Avanti Polar Lipids)
15. POPG, 1-palmitoyl-2-oleoyl-sn-glycero-3-phospho-(1'-sn-glycerol), sodium salt (Avanti Polar Lipids)
16. Potassium phosphate monobasic, KH_2PO_4 (Sigma-Aldrich)
17. Sepharose CL-6B (Sigma-Aldrich)
18. Tris, Tris(hydroxymethyl)aminomethane (Merck)
19. Triton X-100 (BioChemika)

1.3.2. Instruments

1. Fluorescence spectrophotometer F-4500 (Hitachi; Tokyo, Japan).
2. Isothermal titration calorimetry (ITC): itc200 (Microcal/GE Healthcare; Northampton, USA) having a reaction cell volume of 203.7 µL and a syringe volume of 38.45 µL.

3. NMR measurements: DRX-400 (Bruker; Karlsruhe, Germany) operating at a resonance frequency of 400 MHz for ^{1}H and 162 MHz for ^{31}P.
4. UV-visible spectrophotometer 8453 (HP; Waldbronn, Germany)

1.3.3. Vesicle preparation (MLVs)

A well-defined physical structure of model membranes facilitates many aspects in the thermodynamic analysis of peptide-lipid interactions, especially when the membrane passage of a peptide (i.e. access to inner leaflets or lamellae) is unknown. We therefore start reviewing important steps in the membrane preparation.

When dispersed in water, phospholipids, such as charge-neutral POPC, tend to self-associate: At the air-water interface, they slowly assemble to a monolayer and in the bulk phase rapidly to bilayer forming lipid vesicles ("liposomes") (102, 103). The dissociation constant of this self-assembly is in the order of 10^{-10} M^{-1} (104), the cross-sectional lipid area of POPC is 68$Å^2$ (105) and the thickness of the hydrophobic core and P-P distance in the fluid state is 27 and 38 Å, respectively (106). Length, number and position of double bonds of the acyl chains greatly influence the gel-to-fluid phase transition temperature (T_m) which characterizes the transition from the frozen (L_β; lamellar gel) to the fluid (L_α; liquid crystalline) phase. For POPC, this transition temperature is -2 °C (107).

Most biological membranes are in the liquid-crystalline phase (108), and cycling across the transition temperature renders bilayers leaky - even to larger compounds (109-111) which is important for observations on CPP leakage across model membranes (98). Lipid polymorphism is regulated, in part, by the ratio between cross-sectional area of lipid head groups compared to the cross section of the acyl chains. Lipids with a small headgroup, such as DOPE, do not form contiguous bilayers, but inverted hexagonal (H_{ii}) phases (112). As a result, DOPE is frequently used in transfection reagent mixtures for destabilizing membranes and improving their membrane translocation (113). In this regard, CPPs have been also proposed to form inverted lipid micellar structures as part of their membrane translocation (114).

Model membranes can be prepared by different methods, such as filter extrusion, sonication, reverse phase evaporation or detergent dilution (for a review see **ref.** (41)). Resulting vesicles differ not only in size, but also in stability, lipid packing density, outer/inner layer lipid stoichiometry, and binding enthalpies. Giant unilamellar vesicles (GUVs), for example, are particularly delicate (115). In contrast, large unilamellar vesicles (LUVs) with a defined diameter of ~100 nm produced by filter extrusion have a small polydispersity (116), excellent storage stability, a lateral packing density close to eukaryotes (28-35 mN/m) (117, 118) and a balanced inside/outside leaflet lipid stoichiometry. Finally, small unilamellar vesicles (SUVs) with a diameter of 30-50 nm, produced by sonication, have more lipid molecules on the outside than on the inside leaflet for sterical reasons (119). This is important when considering the lipid binding stoichiometry for peptides that have no access to the inner membrane leaflet. Peptide interactions with SUVs also might have different binding enthalpies in ITC experiments (as compared to LUVs) which can be favorable when working at low concentration (120). The number of water molecules (n_w) required for full hydration of a phospholipid molecule has been estimated to be 17-38 (121, 122), so that the lipid hydration must exceed ~0.4-0.9 g water/g lipid especially when working with concentrated NMR samples, and additional intravesicular water might be considered (123).

Lipid stock solutions in chloroform (Avanti Polar Lipids, Alabaster, USA) or in dichloromethane are more convenient to aliquot than greasy phospholipid "powders". On the other hand, the organic solvent requires non-plastic vials/pipets, pipetting at low room temperatures (the boiling point of dichloromethane and chloroform is 40 and 62 °C, respectively, at 760 mm Hg) and removal by rotary evaporation.

1. A lipid suspension (16 mM, 2 mL, molar ratio POPG/POPC = 1/1) is prepared as follows.

2. The weight of an empty 5-mL pear-shaped flask is noted. An aliquot of 12.16 mg of POPC (e.g. 0.608 mL of a 20 mg/mL stock) is pipetted into the flask. The solvent is removed by rotary evaporation and subsequent high-vacuum (0.1 mbar) for >4 hours. The weight of the flask is again noted.

3. The second lipid is added, e.g. 12.34 mg POPG (0.617 mL of a 20 mg/mL stock solution), and the solvent is also used to mix the second lipid with the first one. The solvent is removed by rotary evaporation and subsequent high-vacuum (0.1 mbar) for >4 hours. The weight of the flask is noted in order to determine the lipid weight ratio. The total lipid concentration is determined according to **Subheading 1.3.8**.

4. Additional lipids, such as pegylated lipids (DOPE-PEG2000), might be added in analogy to step 3 (see also **Subheading 1.3.7** Lipid choice).

5. The dry lipid film is hydrated with ~2.0 mL of buffer (the concrete volume is chosen according to measured lipid weight), topped with an Argon layer, vortexed and hydrated at room temperature during 1 h (44). Thereafter, the flask is again vigorously shaken using a table top shaker ("vortex") resulting in multilamellar vesicles (MLVs) of 16 mM total lipids and a wide size distribution range between 0.5-10 µm. Due to the large vesicle size, the light scattering is high and the appearance is milky. Occasional sediments may exist originating from slow hydration of inner lamellae, especially if hydration time was too short or lipid films after solvent evaporation to thick.

6. LUVs or SUVs are prepared by disrupting the MLVs using sonication (46) or freeze-thaw cycling followed by extrusion through a filter of defined pore size (47), as described under **Subheadings 1.3.4** and **1.3.5**, respectively.

1.3.4. LUVs

1. The MLV dispersion (prepared under **Subheading 1.3.3**) is subjected to 5 freeze-thaw cycles which reduces the lamellarity (124), vesicle size (<1 µm) and size distribution (125). This is done by placing the flask for 20 min into a -80 °C freezer followed by an ambient temperature water bath. Typically, no sediments are observed any longer after this step.

2. The suspension is aspired by a first 2.5-mL Hamilton syringe and extruded into a second Hamilton through a 19-mm syringe filter holder from Avanti Polar Lipids (Alabaster, USA), Avestin (Ottawa, Canada), or Eastern Scientific (Rockville, USA). The filter holder contains a stack of 2 polyethylene drain disks (art. 230300, Whatman;

Maidstone, UK), 2 polycarbonate nucleopore track-etch membranes with a 0.1 µm pore size (art. 800309, Whatman; Maidstone, UK), and again 2 drain disc. Importantly, extrusion is performed above the T_m of the lipids, because of the rapid vesicle fusion below T_m (126, 127). Depending on the lipid mixture, a heater block (Avanti Polar Lipids or Eastern Scientific) for the assembly is required. Without disconnecting the assembly, extrusion is repeated between the 2 syringes for at least 11 cycles (47, 128). The sample is recovered from the second syringe in order to ensure removal of any larger particles of the original suspension. Pore sizes available are 50, 100, or 200 nm; larger pores no longer produce narrow vesicle size distributions (128). For larger sample volumes, larger Hamilton syringes can be used or barrel extruders (Avestin; Ottawa, Canada; or Northern Lipids; Burnaby, Canada).

3. Because of the vesicle size reduction, the lipid dispersion becomes less opaque. Experimental verification of the vesicle size and distribution is recommended which is performed within a few minutes using dynamic light scattering (DLS).

4. The prepared vesicles are topped with Argon (to prevent oxidation) and stored at 4 °C (to prevent hydrolysis (129), so that the vesicles can be used during several days before fusion is observed (130). Freezing or cycling across the lipid phase transition temperature should be avoided (131, 132). The vesicle size is checked prior to experiments using DLS. Changes in vesicle size (fusion) and lamellarity occur after days or months, where the kinetics depends on lipid type and co-solutes. Generally, fusion is prevented by higher amounts of charged lipids, and promoted by high amounts of divalent ions or PEG. Studies on vesicle stability are summarized elsewhere (130, 131, 133).

1.3.5. SUVs

1. The MLV dispersion prepared under **Subheading 1.3.3** is sonicated during 40 min with a tip sonicator (e.g. model 250, Branson; Danbury, USA) and 35 Watt power setting. During sonication, the sample is protected under a nitrogen blanket and cooled with a 20-mL water bath (at a T just higher than T_m of the lipids). Duration, power-to-

volume ratio and ultrasound wavelength are critical to produce SUVs with low polydispersity (134). For instance, a sonication time of >35 min and 50W is required when using 10 mL volumes (135). Higher power-to-volume ratios might de-esterify phospholipids (136). In contrast, bath-type sonicators (e.g. model G112SP1T; Laboratory supplies; Hicksville, USA) are operated at higher power settings (80 W) and may produce vesicles of higher polydispersity (137) and lamellarity (138); using the latter method, fractions of larger vesicles can be separated by centrifugation or by chromatography with a Sephadex G-50 column (139). Considerations on optimum ultrasound frequency and vesicle formation by acoustic cavitations are published elsewhere (140). Finally, the tip sonicator can heat the liquid rapidly to temperatures > 60 °C which would lead to heat-induced lipid degradation so that cooling is required.

2. After sonication, the SUVs are transferred into 2 microcentrifugation test tubes (Eppendorf; Hamburg, Germany), and the titanium debris from the sonicator tip (which would disturb optical methods such as DLS) is removed by centrifugation at 16,000 g for 10 min. The prepared vesicles are filled into 4-mL storage vials (art. G075S-14, Infochroma; Zug, Switzerland), topped with Argon and stored at 4 °C. In contrast to LUVs, the outer surface of the vesicle bilayer contains twice as many lipid molecules than the inner leaflet (119) and their high energy curvature causes fusion to larger vesicles already after days (141).

1.3.6. NMR samples

MLVs for NMR are prepared in analogy to **steps 1-5** of **Subheading 1.3.3** with the following exceptions:

1. The membrane passage of CPPs to inner lamella of MLVs can't be assumed a priori. Therefore, the buffer (see **step 5** of **Subheading 1.3.3**) contains already the peptide, so that the CPP has access to all lamellae.

2. Prior to NMR measurements, the MLVs are subjected to 5 freeze-thaw cycles in order to reduce the polydispersity of the vesicles to a diameter of ~1 µm, to accelerate the hydration of inner lamellae and thus to improve spectral quality.

3. In case of rare and expensive lipids, smaller amounts of lipids (typically <5 mg) are dried directly inside the NMR vial (instead of a flask) to prevent losses. The organic solvent is removed by a gentle stream of nitrogen (because of the difficulty to connect it to a rotavapor). In this respect, chloroforom has not been classed as a greenhouse gas (142), but its inhalation might cause liver cancer (143) suggesting the work in a fume hood.

1.3.7. Lipid choice

1. A high POPC content is recommended for model membranes, because its transition temperature (T_m) is well below ambient temperature and since it is the major lipid in mammalian cell membranes (144). A detailed review on chain length and head-group composition of mammalian cells has been published (145).

2. In view of electrostatic interactions of CPPs, the addition of anionic lipids such as POPG (typical for plants and bacteria) or POPS (typical for eukaryotes) is recommended. The membrane content of anionic lipids can be up to 50-80% in Gram-positive bacteria (146, 147), but is only 2-12% in mammalian cells where they are primarily located in the inner leaflet of the plasma membrane of healthy cells (148). Only after cell death or apoptosis, they appear at the outer membrane leaflet which can be exploited for annexin V binding assays (apoptosis marker) (149). An anionic lipid content of 0-10% is thus reasonable for modeling eukaryotic membrane phospholipids.

3. Because of their polycationic character, CPPs may lead to intravesicular aggregation and sedimentation of anionic lipid vesicles (150). This leads to precipitates and light scattering which disturbs optical measurements (e.g. DLS, CD, fluorescence). The vesicle aggregation can be prevented by including 2-4 mol% PEGylated lipids in the lipid mixture (151). At higher ratios (>5-8 mol% depending on PEG chain length), a "mushroom-to-brush" transition of the PEG chains occurs (152-154) which may either increase (155) or diminish peptide binding (156).

1.3.8. Lipid quantification

Precise knowledge of the lipid concentration is essential in thermodynamic analysis of peptide-lipid interactions. Especially when preparing SUVs with a tip sonicator, solvent evaporation can occur. Phospholipid content is thus measured as phosphate content after oxidation of the phospholipids with perchloric acid. The liberated inorganic phosphate ion reacts with ammonium molybdate to phospho-molybdic acid which is measured spectrophotometrically. The sensitivity of the detection is increased in the presence of cationic malachite green (157). Dried KH_2PO_4 at 5-20 nmol is used for calibration. The assay is thus incompatible with phosphate based buffers. When using higher phosphate concentrations and readings later than 20 min after reagent addition, stabilization of the colored complex with surfactants such as Tween20 is required (158).

1. Wear protection glasses, gloves and lab coat.

2. Coloring reagent: 1.05 g of ammonium molybdate ($(NH_4)_6MoO_{24}\cdot 4H_2O$) is dissolved in 15 mL of 6 N HCl; this is added to 0.12 g of Malachite Green previously dissolved in 85 mL of H_2O. After 30 min of stirring, the reagent is filtered (filter paper #1,Whatman; Maidstone, UK). The reagent is stored at room temperature and is freshly filtered prior to use (0.2·µm PTFE syringe filter, Whatman; Maidstone, UK). The reagent is stable for 6 weeks. Thereafter, the assay leads to increased OD values and non-linearity in the standard curve.

3. An aliquot of ~150 nmol of phospholipids (e.g. 30 µL of a 5 mM POPC suspension) is placed into a 8x60 mm borosilicate glass tube (art. 26.013.201, Glas Keller; Basel; Switzerland)

4. 100 µL of perchloric acid (70%) are added.

5. Behind a protection shield and in a fumehood, the vial is hold with a forceps (tube opening opposed to the body) and is gently boiled with a bunsen burner for approximately 3-4 min, so that the solution first turns yellow and, after a short burst of

white smoke, gets clear again leaving ~1/2 of the original volume. After cooling, the solution is completed with water to 1.0 mL.

6.1. A tenth of it (100 µL; triplicate) is placed into a disposable plastic cuvette (1 cm path length), and 900 µL of the freshly filtered coloring reagent is added and immediately mixed.

6.2. For the blank, 100 µL of water are placed in a cuvette and 900 µL of the coloring reagent are added and mixed.

6.3. For the standard curve, 5, 10, 15 ad 20 µL of a 1 mM KH_2PO_4 solution are placed into a cuvette, followed by completion with water to 100 µL and addition of 900 µL of the coloring reagent.

7. A time-scan (light absorbance at 660 nm) of the most concentrated standard is recorded (i.e. 20 nmol of KH_2PO_4) , where the OD signal will increase after ~10 min to a ΔOD of ~ 0.9 (with regard to the blank) and will stay stable for ~30 min.

8. The interval between addition of the coloring reagent and achievement of stable signal (i.e. ~10 min) is kept equal for all samples.

1.3.9. Peptide quantification

Precise knowledge of the peptide content is essential - especially for CPPs. Current synthesis and purification procedures typically lead to a peptide purity of >98%, not meaning that the peptide content of the lyophilized powder is >98%: the presence of anionic counterions, such as trifluoro acetate or acetate, is considerably high after purification because of the high content of cationic arginines and lysines in CPPs. The CPP R_9, for example, may contain 9 TFA counter-ions after purification with HPLC using TFA as an ion pairing reagent. As a result, the mass content of TFA in the lyophilized peptide could be 40% or higher. Therefore, elemental analysis (comparing experimental versus theoretical nitrogen content) or amino acid analysis (quantifying amino acids by fluorescent tags after acid peptide lysis) (159) are required whenever working with CPPs.

Because spectrophotometers are in most laboratories, insertion of a light absorbing amino acid, such as tryptophane, at the N-terminus of the CPP sequence is also a good alternative for peptide quantification (e.g. WR_9). This allows for fast quantification during each peptide handling step using the molar extinction coefficient of 5'500 for tryptophane at 280 nm during denaturation in 6 M guanidine hydrochloride (160).

Peptides used in present protocols were made by solid-phase peptide synthesis using a Fmoc strategy (161) and a Rink amide resin. The carboxy terminus was amidated and thus uncharged. Acylation at the N-terminus with fatty acids of varying lengths (C_{14}, C_{16}, or C_{18}) was performed on-resin by activation with PyBOP/NMM. The single-letter code for the peptides used are WRRRRRRRRR (WR_9), myristoyl- (C_{14}-WR_9), palmitoyl- (C_{16}-WR_9), and stearoyl-WR_9 (C_{18}-WR_9), RQIKIWFQNRRMKWKK (penetratin; Antp) and RQIKIWFQAARMLWKK (penetratin p2AL, see **ref.** (55)). When observed in a helical wheel projection (162), WR_9 and Antp are considered to be non-amphipathic – in contrast to the acylated WR_9 derivatives ("primary amphipathic" according to **ref.** (13, 86)) and p2AL ("secondary amphipathic" according to **ref.** (13, 86)).

1.3.10. Fluorescent membrane leakage dyes

Calcein is a zwitterion having a maximum of 6 negative and 2 positive charges. Because of the uncertainty about its pKa_4 (163, 164), the net charge at pH7 is considered to be -3 (165, 166) or -4 (164). On the basis of published pK_a values, the net charge of further fluorescent leakage dyes, such as ANTS, carboxyfluorescein, and fluorescein, is -3, ~-2.7 (167), and ~-1.6 (163) at pH 7, respectively. Because of its multivalency, the encapsulation of calcein (typically 70 mM) into vesicles produces a high ionic strength. The ionic strength (I) of a solution containing n ionic species is defined by

$$I = \frac{1}{2}\sum_{i}^{n} c_i z_i^2 \qquad (1)$$

where c_i is the concentration of ion i, and z_i is its charge number.

Assuming z = -3 or -4 for calcein at neutral pH (disodium salt), a 70 mM calcein solution results in an ionic strength of 0.42 or 0.7 M, respectively, which is much higher than that of physiologic saline (0.154 M). This is important when considering ionic gradients as a potential mechanism for CPP membrane disturbance (168).

1.4. Methods

1.4.1. Membrane leakage (calcein dequenching)

The fluorescent dyes used in this assay are generally anionic in nature. As a result, they cannot cross the membrane because of the high Born charge energy barrier (81). Spontaneous dye leakage across the membrane proceeds only over days, but dyes of little charge (fluorescein, carboxfluorescein) leak faster than trivalent dyes (e.g. calcein, ANTS) (166). On the other hand, the multivalency of the latter dyes has the disadvantage of interacting with the cationic peptides (see **Fig. 1.1F** and **G**) and creating a strong ionic gradient across the membrane (see **Subheading 1.3.10**).

The membrane leakage assay (166) resides on the principle that the dye is entrapped in vesicles at self-quenching concentrations. Fluorescent dyes such as carboxyfluorescein are self- quenching at concentrations > 0.2 M because of non-fluorescent dimer formation and energy transfer to the dimer (169). In addition, the high light absorbance of the dyes causes an inner filter effect, so that the concentration for maximum fluorescence is observed already at low micromolar concentration depending on the cuvette dimension (see **Fig. 1.1A**). Adding a membrane-perturbing peptide then leads to the release of the dye out of the vesicles. Its dilution into the much larger extravesicular volume results in increased fluorescent signal intensity. In addition to self-quenching, collisional quenchers might be encapsulated (e.g. cationic DPX for anionic dye ANTS) so that their dilution upon membrane leakage causes also an increase of the fluorescence signal.

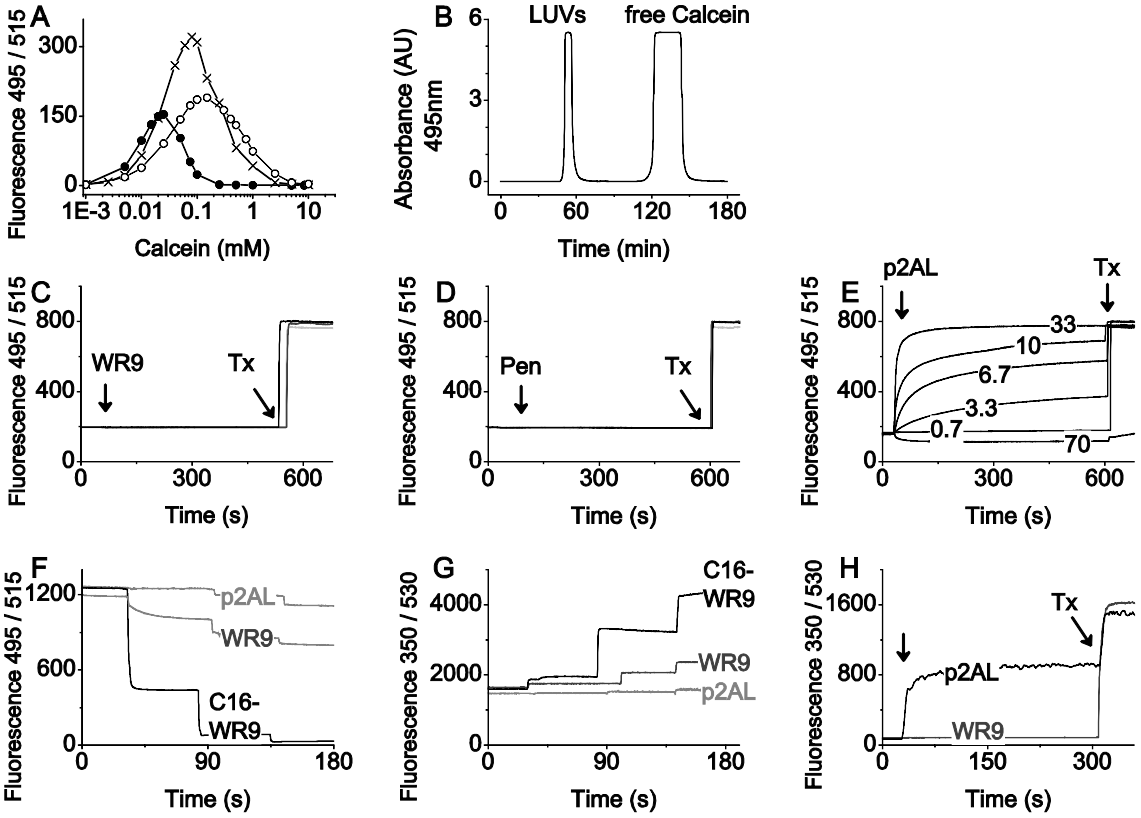

Fig. 1.1. Membrane leakage assay. (A) Because of the high optical absorbance of calcein, the observed maximum fluorescence at given concentration depends not only on quenching, but also on cuvette dimensions (i.e. inner-filter effect) as shown for a (●) 10 mm, (x) 5 mm and (○) 2 mm cuvette using same photomultiplier and bandwidth settings for the cuvettes. Small path lengths are thus preferred, especially when working with vesicles that stray light. **(B)** Separation of calcein-loaded LUVs from free calcein on a Sepharose CL-6B column (absorbance detection at 495 nm; 1.6 x 23 cm column, flow rate 0.3 mL/min). **(C)** Leakage assay for non-amphipathic WR_9: under permanent stirring, 100 µL of 10 µM (black), 100 µM (gray) and 1000 µM (light gray) WR_9 are added (at 60s) to 1.4 mL of LUVs (total lipid = 0.45 mM, molar ratio POPC/POPE/POPG/DOPE-PEG = 32/32/31/5; 13 mM calcein). Final peptide concentration is 0.7, 6.7 and 67 µM, respectively. At 600 s, 100uL of 5% Triton X-100 is added to release the entire vesicle content. **(D)** Same leakage assay, but using non-amphipathic penetratin. **(E)** Same leakage assay, but using amphipathic penetratin mutant p2AL. Indicated are final peptide concentrations (µM). The low fluorescence at highest p2AL concentration (70 µM) suggests interaction of anionic calcein with cationic CPPs. **(F)** Titration of 1.4 mL of 10 µM calcein with a 1 mM solution of 3 different CPPs. 10, 40 and 50 µL of the CPP are added at 40 s, 80 s, and 150 s, respectively, indicating the interaction of anionic dye with cationic CPPs. **(G)** Same titration, but using 100 µM ANTS. In contrast to (F), the dye-peptide interaction produces a signal *increase* which is favorable for improved sensitivity of the leakage assay. **(H)** Leakage assay using 12.5 mM of the dye ANTS (and 45 mM of its quencher DPX) inside the vesicles. Despite the improved sensitivity of this assay, no membrane leakage with non-amphipathic WR_9 is observed. Buffer allover: 20 mM Tris, 134 mM NaCl, pH 8.5.

1. LUVs are prepared as described in **Subheading 1.3.4** (total lipid concentration typically 15 mM) with the exception that the buffer (20 mM Tris) contains calcein (13 mM; ionic strength of 104 mM at pH 8.5), no NaCl, and the pH is 8.5, i.e. 3 pH units higher than pKa_3 of calcein. For this purpose, acidic calcein is first dispersed into the buffer, and the pH is adjusted to pH 8.5 using NaOH bringing calcein into solution.

2. Free calcein is removed by SEC using a glass column (i.d. 1.6 cm) filled to a height of 23 cm with Sepharose CL-6B (Sigma-Aldrich; fractionation range of 0.01-4 MDa for globular proteins) as stationary phase and a running buffer of 20 mM Tris, 134 mM NaCl pH 8.5. In order to protect the fluorescent dye against bleaching, the column is wrapped with an aluminum foil. When using carboxyfluorescein as dye, spontaneous dye leakage occurs faster than for calcein (166) so that chromatography at 4 °C is recommended.

3. Flow rate of the pump is 0.3 mL/min.

4. Absorbance of calcein is monitored at 495 nm.

5. Fractions of 1 mL are collected into Eppendorf tubes.

6. Fractions between 51 and 57 min (containing calcein-loaded vesicles) are collected (see **Fig. 1.1B**).

7. Fractions between 120 and 145 min (containing free calcein) are discarded.

8. The size of the vesicles is checked with DLS.

9. The lipid concentration is measured (see **Subheading 1.3.8**). The dilution factor as caused by present SEC column is typically ~6.

10. Lipids are diluted to a final concentration of 0.1-0.45 mM, i.e. a concentration close to total phospholipid content of cells in culture (e.g. 68 µM respecting 25 mL culture medium (170)).

11. Using a 1 cm fluorescence cuvette, 1.4 mL of the calcein loaded vesicles are placed into the cuvette containing a magnetic stir bar.

12. Under continuous stirring, a time scan of calcein fluorescence is recorded. After 60 s of baseline recording, a small volume (see **Fig. 1.1E**) of the CPP is added to produce a final peptide concentration in the micromolar range.

13. When at equilibrium (e.g. 10 min), 100 uL of 5% Triton X-100 are added in order to release the entire vesicle content.

14. The relative membrane leakage (F_{rel}) induced by the CPP can be calculated according to

$$F_{rel} = \frac{F_{CPP} - F_0}{F_{triton} - F_0} \tag{2}$$

where F_0, F_{CPP} and F_{triton} denote the initial (quenched) fluorescence, increased fluorescence after CPP addition, and maximum fluorescence after triton addition, respectively. Although calcein at self-quenching concentrations in 1-cm cuvettes (>0.2 mM) has almost no fluorescence (see **Fig. 1.1A**), F_0 in this assay is typically higher than zero, because of lower inner filter effects when calcein is encapsulated in diluted vesicles.

15. Reporting percentual dye release according to **Eq. 2** relies on a linear relation between dye concentration and fluorescence intensity. This is valid only when the fluorescence is not quenched, i.e. at a concentration below the concentration for maximum fluorescence (consider the logarithmic scale in **Fig. 1.1A**). The maximum fluorescence for calcein in a 1-cm cuvette, for example, is observed at a concentration of ~20 µM (see **Fig. 1.1A**). Based on a cross-sectional area of 68 $Å^2$ per POPC and a sample volume of 1.4 mL, a 0.45 mM POPC LUV preparation (vesicle radius of 50 nm) has a total intravesicular volume of 2.15 µL. Full membrane leakage thus produces a dye dilution factor of 1.4 mL/2.15 µL = 651. A linear correlation between fluorescence intensity and concentration is thus achieved for a vesicular calcein concentration of 651 x 20 µM = 13 mM and lower. When using a higher calcein concentration, the vesicle concentration must be decreased accordingly.

1.4.2. Membrane integrity (^{31}P NMR spectroscopy)

Phosphorous-31 NMR is a simple method to distinguish between lipid bilayers, hexagonal structures and isotropically moving phospholipids (171). Because of the slow rotation on a NMR time scale, MLVs produce a chemical shift anisotropy (see **Fig. 1.2A**). In contrast, rapidly tumbling structures (LUVs, SUVs, detergent-solubilized lipids "mixed micelles") show an isotropic NMR signal (see **Fig. 1.2B**).

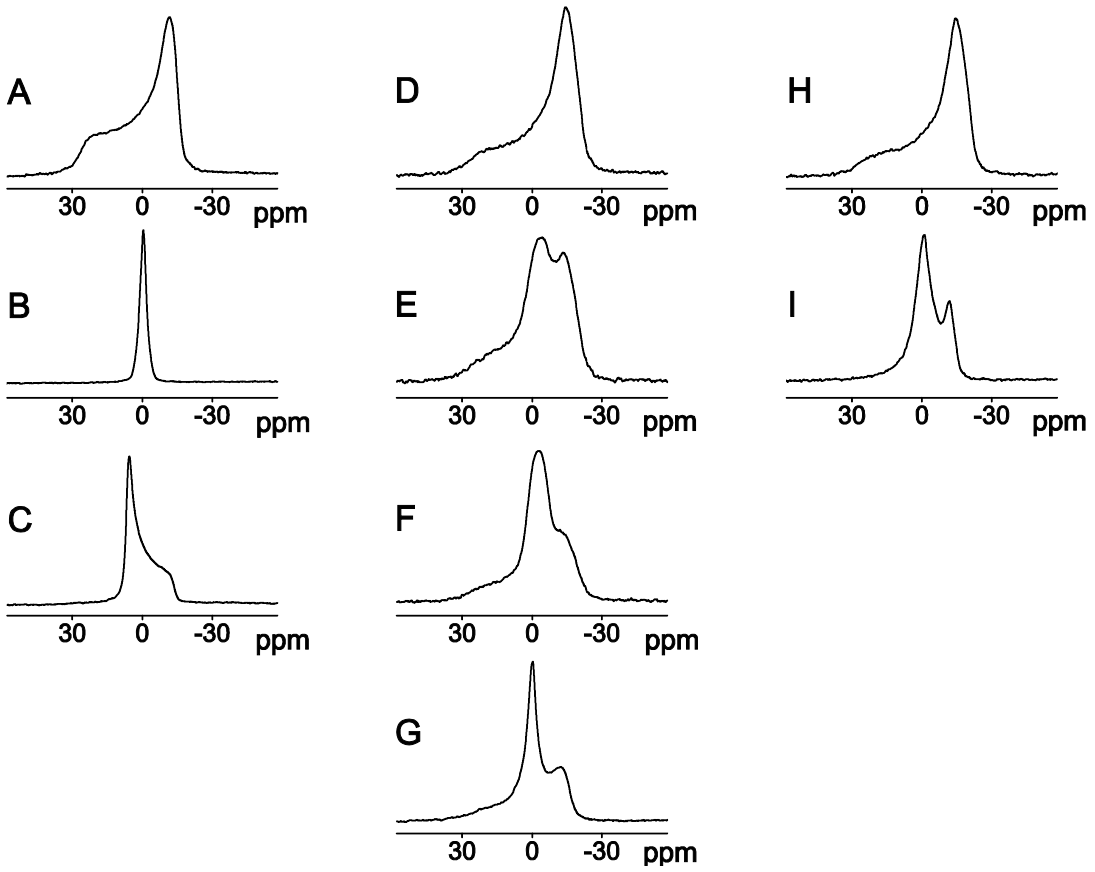

Fig. 1.2. Polymorphic phase behavior of phospholipids as studied by 31P NMR spectroscopy. Left column: **(A)** intact bilayer of POPC/POPG (= 3/1) prepared as MLVs; **(B)** same bilayer solubilized by Triton; **(C)** hexagonal phase (DOPE), occasionally termed "inverted micelles" in the CPP field (61). Middle column: same bilayer as (A) but prepared in the presence of different CPPs (at 4 mM): **(D)** non-amphipathic WR9, **(E)** amphiphilic analogue C14-WR9, **(F)** C16-WR9 and **(G)** C18-WR9. Right column: same bilayer as (A), but prepared in the presence of **(H)** non-amphipathic Antp or its **(I)** amphiphilic analogue p2AL. Spectra were recorded at 25 °C and are referenced to external H3PO4 85% at 0 ppm. Typically, 5 mg total lipid, 130 µL H2O and 1.4 mg peptide were used.

The assay therefore requires the work with MLVs. Because of potential vesicle aggregation and subsequent precipitation with CPPs (150), a horizontally aligned NMR radiofrequency coil (covering the entire sample tube) is preferred over a standard vertical high-resolution NMR probehead where aggregates sedimentate out of the sensitive volume of the probehead. Our laboratory typically uses a 4-turn solenoid of 14 x 8 mm inner diameter. Sample tubes are borosilicate tubes (Fiolax, Duran; Mainz, Germany) or house-made screw vials with internal volumes of 400 and 150 µL, respectively.

1. This assay is incompatible with phosphate-based buffers. MLVs are produced as described under **Subheading 1.3.6**. For rare lipids, only 5 mg total lipid and 150 µL of liquid are used, but lipid quantities can be increased up to 100 mg lipid / 100 mg of liquid (check hydration number for specific lipid) which leads to more signal and thus to faster experiments.

2. For external calibration, 200 µL of concentrated phosphoric acid (85%) are used (sealed in a borosilicate tube). After magnetic field homogenization with the ^{1}H frequency ("shimming") to the vial geometry, the ^{31}P signal of concentrated phosphoric acid is calibrated to 0 ppm (pH dependant). Because of the steady magnetic field drift, this procedure is repeated every day, where 1 scan typically yields sufficient signal.

3. The lipid samples are subsequently recorded using the same magnetic shim values and chemical shift calibration.

4. Because of the broad chemical shift dispersion, NMR spectra are recorded with a set-up for solid-state like compounds, i.e. fast digitizer, high power amplifier, and a probehead that can withstand that power .The inverse relation of excitation bandwidth and pulse length in FT NMR requires 90° pulses in the low µs range (typically 5 µs) for full spectral excitation.

5. ^{31}P NMR spectra are recorded using a Hahn echo sequence (90°-τ-180° with τ = 40 µs), broadband proton decoupling, a recycle delay of 5 s (i.e. ~5 times T_1), spectral width of 50 kHz, and 4K data size. Typically, 8000 transients are averaged, and the free induction decay is exponentially multiplied prior to Fourier transformation

corresponding to a 200 Hz line broadening. Compared to a simple pulse-and-acquire NMR sequence, the delayed acquisition of the Hahn echo sequence reduces contributions of preamplifier and resonance coil ringing after strong radio-frequency pulses (172).

1.4.3. Membrane binding (isothermal titration calorimetry)

The membrane binding of peptides can be driven by a variety of forces, such as hydrophobic partitioning, electrostatic attraction to charged lipid headgroups or stabilization through a conformational change (e.g. helix formation). As a consequence, membrane-peptide interactions are characterized by a variety of affinity constants, and these have not only different magnitudes, but also different molecular meanings (13, 173):

- The surface partition constant K_p, as defined here, describes the hydrophobic interaction. The molar amount of peptide bound (n_P) to accessible (i.e. outer leaflet) lipid (n_L), $X_b = n_P/n_L$, is used to calculate

$$K_p = \frac{X_b}{c_m} \tag{3}$$

where c_m is the peptide concentration close to the membrane surface. For uncharged lipids and uncharged peptides, the peptide concentration close to the membrane surface (c_m) equals the free peptide concentration in bulk at equilibrium (c_{eq}), so that a plot of c_{eq} versus X_b yields a straight line with the slope K_P (173). However, this correlation is not linear when electrostatic interactions are involved. In this case,

- the apparent membrane partitioning constant K_{app} is used including both hydrophobic and electrostatic interactions, and we define

$$K_{app} = \frac{X_b}{c_{eq}} \tag{4}$$

The electrostatic interactions between cationic peptides and anionic lipids cause the concentration of the peptide near the membrane (c_m) to be higher than in bulk (c_{eq}). Obviously, K_{app} is larger than K_p because of $c_{eq} << c_m$. Characteristically, K_{app} decreases with increasing peptide concentration because of electrostatic screening. Thus, a plot of c_{eq} versus X_b is not linear for charged compounds. Using the Gouy-Chapman theory, c_m and the membrane surface potential (Ψ_0) can be calculated (150, 173-175) which, in turn, allows the calculation of K_p. This way, hydrophobic and electrostatic contributions to the peptide-lipid interaction can be differentiated, and a plot of c_m versus X_b becomes linear (173).

Several studies agree that non-amphipathic CPPs such as R_9, Tat and PLL do not partition into to the hydrophobic core of model membranes but remain superficially bound (93, 94, 150, 176-178). Their interaction is thus best described by

- a complex (L_nP) formation of *n* lipids (L) with the peptide (P) according to

$$n\,L + P << L_nP \tag{5}$$

This way, peptide binding can be visualized in terms of a multi-site binding model. Here, a complex formation constant K of defined stoichiometry is used. In contrast, K_P and K_{app} make no assumptions on the reaction stoichiometry. Assuming *n* identical binding sites on the multivalent peptide P, the binding of lipid L to individual sites on P can be defined by a single-site ("microscopic") binding constant

$$k = \frac{[\text{filled sites}]}{[\text{empty sites}][L]} \tag{6}$$

where [ ] represents concentration. For statistical reasons (13), the first lipid (i.e. non-saturating conditions) binds with a higher affinity than the last one (i.e. saturating conditions). Determination, of the CPP-lipid affinity by ITC relies on the principle that the peptide in the reaction cell (200 µL) is progressively saturated by repeated additions (19 x 2 µL) of the lipid, while the heat of reaction is recorded during each injection. For a precise fit of experimental data, sufficient data points in the transition region (i.e. 3-10

data points) must be available in the thermogram and, ideally, an initial plateau for the first few titrations (see **Fig. 1.3C**). As a rule of thumb, both conditions are met, if the starting concentration of the peptide (A_0) in the reaction cell is close to

$$A_0 = 50 \cdot k_d / n \quad (7)$$

where k_d is the estimated dissociation constant ($k_d = 1/K$).

Because of the volume ratio of the cell/syringe of ~5, and a desired 2-fold excess of B at the end of the titration series, the concentration of the ligand B is chosen to be $500 \cdot k_d$ (which results from $B = 5 \cdot 2 \cdot n \cdot A_{0,}$ where A_0 is equivalent to **Eq. 7**).

If A_0 is 2 magnitudes higher than defined in **Eq. 7**, the transition region of the thermogram is almost rectangular (see **Fig. 1.3C**), so that the fitted k_d represents only a upper limit of k_d. If A_0 is 2 magnitudes lower than in **Eq. 7**, the isotherm is very flat and the endpoint is uncertain, so that the fit to the data no longer produces clear-cut results (see **Fig. 1.3C**). If the concentration cannot be increased in the latter case for experimental reasons (e.g. high polydispersity and lamellarity for lipids > 100 mM, or protein self-aggregation at high concentration), the syringe can be refilled a second time (see **Fig. 1.3B**), or the content of syringe and reaction cell can be inversed.

1. Prepare 4 mL of a peptide solution (sufficient for 6 experiments considering ~300 µL per pre-run cell rinsing and subsequent titration experiment) and 2 mL of SUVs (sufficient for 30 experiments considering ~60 µL per syringe filling) according to **Subheading 1.3.5**. The solutions are filled into a 4 mL glass vial and are degassed under stirring (ThermoVac, Microcal; Northampton, USA) at 0.7 atm during 7 min. Degassing is important especially for experiments above room temperature, because air bubbles lead to increased noise and baseline jumps in ITC due to the air compression and friction during stirring at high speeds (typically 1000 rpm). Prior to filling the instrument, the solutions are kept at experimental temperature in order to minimize the delay between cell filling and start of the first injection (which is typically 10-20 min for present instrument).

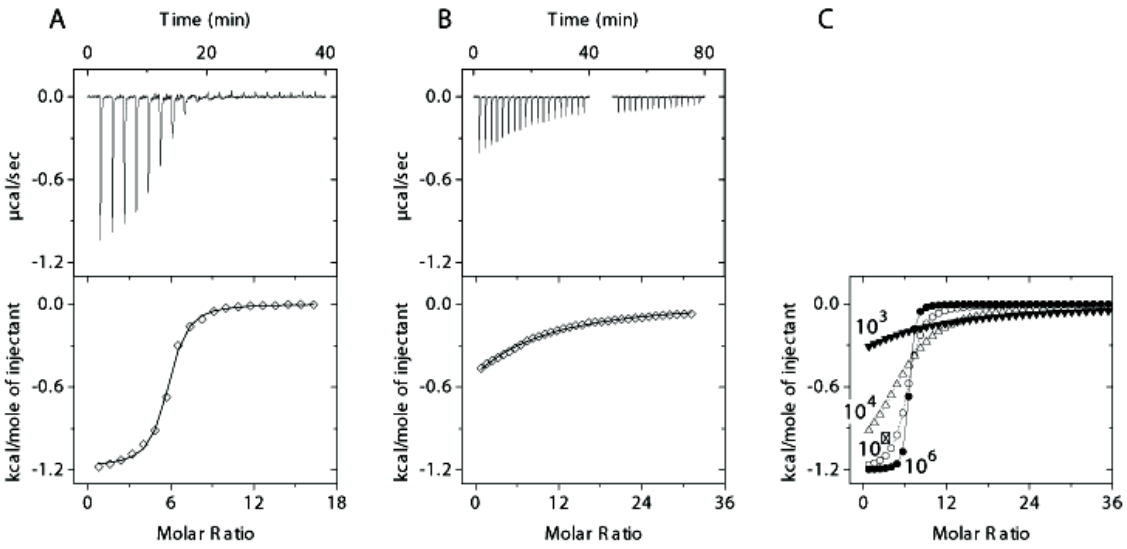

Fig. 1.3. Isothermal titration calorimetry (ITC). The reaction cell was filled with 204 µL of 60 µM WR_9. Every 2 min, 2 µL of lipid vesicles (SUVs) composed of neutral POPC and anionic POPG were added (25 °C). The concentration of POPG was held constant (8 mM), but POPC was varied in different experiments, so that the charge density of the membrane varied as follows: **(A)** POPG/POPC = 1/1 (typical for bacterial inner membrane), **(B)** POPG/POPC = 1/9 (typical for eukaryotic cell membrane). The heat release (raw data, upper panel) during each injection was integrated to yield the experimental heats of reaction (◊; lower panel). The line in the lower panel represents best fit to the experimental data using a multi-site binding model ***(28)***, where **(A)** $K = 1.91 \times 10^5$, n = 5.51 POPG/WR_9, ΔH = 1.18 kcal/mol $POPG_{out}$.; **(B)** $K = 1.08 \times 10^3$, n = 6.12 POPG/WR_9, ΔH = 1.69 kcal/mol $POPG_{out}$. Because of the low degree of binding in (B), the empty syringe was refilled after the 19th injection (i.e. at 40 min). After refilling, the injection series was continued which is feasible within 10 min using latest ITC technology. Precise determination of even lower binding constants would require much higher peptide and lipid concentrations; however, total lipid concentration is already at a high limit (80 mM in B) for obtaining unilamellar vesicles and low polydispersity. **(C)** Experimental simulations of the binding isotherm according to the multisite binding model using various K (10^6, 10^5, 10^4 and 10^3, as indicated) and similar conditions as in (A) and (B), i.e. 204 µL of 60 µM WR_9, 36 x 2- µL injections of 8 mM POPG (which is 4.8 mM POPG on outer leaflet of SUVs), fixed n = 6.0 $POPG_{out}/WR_9$, and ΔH = -1.2 kcal/mol $POPG_{out}$.

---

2. In a first experiment ("blank" experiment), SUVs are titrated into buffer in order to measure the heat of lipid dilution which is subtracted in subsequent experiments.

3. After the blank experiment, the reaction cell is cleaned, typically with 2% Contrad 90 (Socochim; Lausanne, Switzerland) during 15 min, followed by ample water rinsing.

4. The cell of the calorimeter thereafter contains smaller amounts of water from precedent cleaning procedures which could lead to dilution of the peptide. The cell is thus filled once with the peptide and the content is discarded. Thereafter the cell is filled again with the peptide for the proper experiment.

5. Selection of the injection volumes is a compromise between sufficient signal/noise per injection and sufficient data points to construct an isotherm: the syringe content (38.5 µL) is typically divided into 19 x 2 µL aliquots, but the injector could handle smaller volumes with high precision which can be exploited whenever the reaction enthalpy is high. The spacing between the injections depends on the reaction kinetics (and stirrer speed): fast reactions such as ethanol dilutions can be recorded with an interval of 60 s, but present multi-site binding reaction is slower and is best recorded with an interval of 90-120s (awaiting reaction equilibrium) so that the total experiment time from cell filling to end is typically 1 h.

6. The raw data (see **Fig. 1.3A** upper panel) are integrated to yield the heat per injection and thus a binding isotherm when plotting it against the molar ratio of the reactants (see **Fig. 1.3A** lower panel). A visual inspection yields a first approximation: in the case of an initial plateau, the ligand is almost completely bound, so that the heat (per mol of ligand) in the plateau region corresponds to the reaction enthalpy. The molar ratio at half of the plateau value allows one to estimate the stoichiometry of the reactants; finally the slope in the transition region serves as a rough approximation of the binding affinity; in the case of an initial plateau, the dissociation constant k_d is typically << A_0. Exact values of these parameters are determined by a fit to the data:

7. A fit to the experimental isotherm (see **Fig. 1.3A** lower panel) using the multi-site binding model (see **Eq. 6**; for further details see **ref.** (13)) yields K, n, the reaction enthalpy ΔH and entropy ΔS. Because non-amphipathic CPPs typically do not diffuse across the bilayer (93, 94, 150, 176-178), only the outer leaflet is accessible to the CPP, and this lipid concentration is approximately 60% of the total lipid concentration for SUVs (119).

8. Repeating the experiment at different temperatures is recommended for 2 reasons: on the one hand, a reaction might be driven entirely by entropy, so that the enthalpy would

be zero and the calorimeter would not detect any signal (despite the ongoing binding reaction). On the other hand, the slope of ΔH versus T yields the change in molar heat capacity (ΔC_P^0) which gives important information about hydrophobic (typically negative ΔC_P^0) and electrostatic (typically positive ΔC_P^0) contributions to the reaction. Electrostatic contributions to the binding can be also assessed by repeating the experiment at different salt concentrations.

9. Repeating the experiments with different buffers results in valuable information about protonation reactions (e.g. histidine rich CPPs) which can be detected by ITC because of the different ionization enthalpies of the buffers (179).

1.5. Notes

1.5.1. Membrane leakage (calcein dequenching)

1.) Using this protocol, it is observed that non-amphipathic WR_9 and penetratin do not produce membrane leakage (see **Fig. 1.1C** and **D**). In contrast, the amphipathic penetratin mutant p2AL leads to pronounced membrane leakage already at low micromolar concentrations (see **Fig. 1.1E**).

2.) The electrostatic interaction between the anionic dyes and cationic CPPs also affects the result. For example, the interaction of WR_9 with calcein results in a decrease of the fluorescence which could, in principle, mask the membrane leakage (Fig 1F). This effect is even stronger for the acylated WR_9 derivatives (see **Fig. 1.1F**) and p2AL at high concentration (see **Fig. 1.1E**). In contrast, the CPP interaction with the dye ANTS leads to an *increase* in fluorescence (see **Fig. 1.1G**), so that smaller membrane leaks should be detected with improved sensitivity.

3.) Even under these improved conditions using ANTS (see **Fig. 1.1H**), no membrane leakage is observed for WR_9. These data agree with previous studies where non-amphipathic CPPs could not produce membrane leakage at physiologically relevant conditions (52, 94, 150, 180-182). However, they have caused membrane leakage under particular conditions such as a higher molar CPP/lipid ratios (>0.2), more permeable

dyes (carboxyfluorescein), ionic gradients over the membrane, and pH >7.5 (183) which is considered to play a limited role in the *in vivo* CPP transduction (183).

1.5.2. Membrane integrity (^{31}P NMR spectroscopy)

Using this protocol, it is observed (see **Fig. 1.2**) that none of the investigated CPPs forms inverted micelles with lipids that are typical for physiological membranes - even at very high peptide concentration (4 mM). However, all amphipathic CPPs damaged the membrane in a detergent-like manner supporting the membrane leakage data (see **Fig. 1.1**). The critical micellar concentration of C_{18}-, C_{16}-, and C_{14}-WR_9 were found to be 26 µM, 49 µM, and ~5 mM, respectively, as determined by surface activity measurements (data not shown).

1.5.3. Membrane binding

1.) CPP uptake in biological cells is typically observed at low micromolar concentrations, (= similar concentrations as used in **Fig. 1.3**). Using the present ITC protocol, it is observed that the non-amphipathic CPP WR_9 has a poor affinity ($K \sim 10^3$) for model membranes that have an anionic lipid contents typical for mammalian cells (see **Fig. 1.3B**). This is in contrast to the high affinity of the CPP for other anionic compounds of the cell membrane such as heparan sulfate ($K \sim 10^5$) (161).

2.) The lipid affinity of non-amphipathic WR_9 becomes, however, important (even at micromolar concentrations) when the membrane has a high anionic lipid content (see **Fig. 1.3A**) such as encountered in bacterial membranes. This might be important for species selectivity of transfection reagents.

1.5.4. Applications

1.) Using a variety of different protocols on model membranes, it is concluded that non-amphipathic CPPs, such as WR_9 and penetratin, likely do not traverse cell membranes by direct interaction with lipids.

2.) This is in stark contrast to amphipathic CPPs, such as acylated WR_9 or amphipathic penetratin derivate p2AL that both considerably disturb the model membrane already at low micromolar concentration.

1.6. Acknowledgments

This work was supported by the Swiss National Science Foundation (SNF) Grant # 31.107793.

1.7. References

1. Sauder R, Seelig J, Ziegler A. 2011. *Methods in molecular biology* 683: 129-55
2. Lipinski CA, Lombardo F, Dominy BW, Feeney PJ. 2001. *Advanced drug delivery reviews* 46: 3-26
3. Singer SJ, Nicolson GL. 1972. *Science* 175: 720-31
4. Wiener MC, White SH. 1992. *Biophysical journal* 61: 428-33
5. Parsegian A. 1969. *Nature* 221: 844-6
6. Neumann E, Schaefer-Ridder M, Wang Y, Hofschneider PH. 1982. *The EMBO journal* 1: 841-5
7. Limberis MP. 2012. *Acta biochimica et biophysica Sinica* 44: 632-40
8. Douglas JT. 2007. *Molecular biotechnology* 36: 71-80
9. Singh R, Lillard JW, Jr. 2009. *Experimental and molecular pathology* 86: 215-23
10. Slingerland M, Guchelaar HJ, Gelderblom H. 2012. *Drug discovery today* 17: 160-6
11. Cavazzana-Calvo M, Hacein-Bey S, de Saint-Basile G, Le Deist F, Fischer A. 2000. *Transfusion clinique et biologique : journal de la Societe francaise de transfusion sanguine* 7: 259-60
12. Lundberg P, Langel U. 2003. *Journal of Molecular Recognition* 16: 227-33
13. Ziegler A. 2008. *Advanced Drug Delivery Reviews* 60: 580-97
14. Oehlke J, Scheller A, Wiesner B, Krause E, Beyermann M, et al. 1998. *Biochimica et biophysica acta* 1414: 127-39
15. Theodore L, Derossi D, Chassaing G, Llirbat B, Kubes M, et al. 1995. *The Journal of neuroscience : the official journal of the Society for Neuroscience* 15: 7158-67
16. Fawell S, Seery J, Daikh Y, Moore C, Chen LL, et al. 1994. *Proceedings of the National Academy of Sciences of the United States of America* 91: 664-8
17. Rojas M, Donahue JP, Tan Z, Lin YZ. 1998. *Nature biotechnology* 16: 370-5
18. Dokka S, Toledo-Velasquez D, Shi X, Wang L, Rojanasakul Y. 1997. *Pharmaceutical research* 14: 1759-64
19. Frankel AD, Pabo CO. 1988. *Cell* 55: 1189-93
20. Green M, Loewenstein PM. 1988. *Cell* 55: 1179-88
21. Vives E, Brodin P, Lebleu B. 1997. *The Journal of biological chemistry* 272: 16010-7

22. Derossi D, Joliot AH, Chassaing G, Prochiantz A. 1994. *The Journal of biological chemistry* 269: 10444-50
23. Ryser HJ, Hancock R. 1965. *Science* 150: 501-3
24. Boussif O, Lezoualc'h F, Zanta MA, Mergny MD, Scherman D, et al. 1995. *Proceedings of the National Academy of Sciences of the United States of America* 92: 7297-301
25. Persiani S, Shen WC. 1989. *Life sciences* 45: 2605-10
26. Ryser HJ, Drummond I, Shen WC. 1982. *Journal of cellular physiology* 113: 167-78
27. Conner SD, Schmid SL. 2003. *Nature* 422: 37-44
28. Doherty GJ, McMahon HT. 2009. *Annual review of biochemistry* 78: 857-902
29. Derossi D, Calvet S, Trembleau A, Brunissen A, Chassaing G, Prochiantz A. 1996. *The Journal of biological chemistry* 271: 18188-93
30. Pooga M, Hallbrink M, Zorko M, Langel U. 1998. *FASEB journal : official publication of the Federation of American Societies for Experimental Biology* 12: 67-77
31. Rhee M, Davis P. 2006. *The Journal of biological chemistry* 281: 1233-40
32. Thoren PE, Persson D, Isakson P, Goksor M, Onfelt A, Norden B. 2003. *Biochemical and biophysical research communications* 307: 100-7
33. Suzuki T, Futaki S, Niwa M, Tanaka S, Ueda K, Sugiura Y. 2002. *The Journal of biological chemistry* 277: 2437-43
34. Gammon ST, Villalobos VM, Prior JL, Sharma V, Piwnica-Worms D. 2003. *Bioconjugate chemistry* 14: 368-76
35. Wender PA, Mitchell DJ, Pattabiraman K, Pelkey ET, Steinman L, Rothbard JB. 2000. *Proceedings of the National Academy of Sciences of the United States of America* 97: 13003-8
36. Brugidou J, Legrand C, Mery J, Rabie A. 1995. *Biochemical and biophysical research communications* 214: 685-93
37. Futaki S, Suzuki T, Ohashi W, Yagami T, Tanaka S, et al. 2001. *The Journal of biological chemistry* 276: 5836-40
38. Drin G, Cottin S, Blanc E, Rees AR, Temsamani J. 2003. *The Journal of biological chemistry* 278: 31192-201
39. Lundberg M, Johansson M. 2001. *Nature biotechnology* 19: 713-4
40. Richard JP, Melikov K, Vives E, Ramos C, Verbeure B, et al. 2003. *The Journal of biological chemistry* 278: 585-90
41. Szoka F, Papahadjopoulos D. 1980. *Annual Review of Biophysics and Bioengineering* 9: 467-508
42. Sessa G, Weissman.G. 1968. *Journal of Lipid Research* 9: 310-&
43. Henn FA, Thompson TE. 1969. *Annual Review of Biochemistry* 38: 241-&
44. Bangham AD, Standish MM, Watkins JC. 1965. *Journal of Molecular Biology* 13: 238-&
45. Bangham AD, Standish MM, Weissman.G. 1965. *Journal of Molecular Biology* 13: 253-&
46. Huang CH. 1969. *Biochemistry* 8: 344-&
47. Hope MJ, Bally MB, Webb G, Cullis PR. 1985. *Biochimica et biophysica acta* 812: 55-65
48. Olson F, Hunt CA, Szoka FC, Vail WJ, Papahadjopoulos D. 1979. *Biochimica Et Biophysica Acta* 557: 9-23
49. Goncalves E, Kitas E, Seelig J. 2005. *Biochemistry* 44: 2692-702
50. Ziegler A, Seelig J. 2004. *Biophysical Journal* 86: 254-63
51. Zachowski A. 1993. *Biochemical Journal* 294: 1-14

52. Kramer SD, Wunderli-Allenspach H. 2003. *Biochimica Et Biophysica Acta-Biomembranes* 1609: 161-9
53. Ross MF, Filipovska A, Smith RAJ, Gait MJ, Murphy MP. 2004. *Biochemical Journal* 383: 457-68
54. Binder H, Lindblom G. 2003. *Biophysical Journal* 85: 982-95
55. Drin G, Demene H, Temsamani J, Brasseur R. 2001. *Biochemistry* 40: 1824-34
56. Magzoub M, Eriksson LEG, Graslund A. 2003. *Biophysical Chemistry* 103: 271-88
57. Magzoub M, Pramanik A, Graslund A. 2005. *Biochemistry* 44: 14890-7
58. Terrone D, Sang SLW, Roudaia L, Silvius JR. 2003. *Biochemistry* 42: 13787-99
59. Deshayes S, Morris MC, Divita G, Heitz F. 2006. *Biochimica Et Biophysica Acta-Biomembranes* 1758: 328-35
60. Fernandez-Carneado J, Kogan MJ, Pujals S, Giralt E. 2004. *Biopolymers* 76: 196-203
61. Morad N, Ryser HJP, Shen WC. 1984. *Biochimica Et Biophysica Acta* 801: 117-26
62. Ryser HJP. 1967. *Nature* 215: 934-&
63. Belting M, Mani K, Jonsson M, Cheng F, Sandgren S, et al. 2003. *Journal of Biological Chemistry* 278: 47181-9
64. Kaplan IM, Wadia JS, Dowdy SF. 2005. *Journal of Controlled Release* 102: 247-53
65. Lundberg M, Wikstrom S, Johansson M. 2003. *Molecular Therapy* 8: 143-50
66. Kopatz I, Remy JS, Behr JP. 2004. *Journal of Gene Medicine* 6: 769-76
67. Zenke M, Steinlein P, Wagner E, Cotten M, Beug H, Birnstiel ML. 1990. *Proceedings of the National Academy of Sciences of the United States of America* 87: 3655-9
68. Fischer R, Fotin-Mleczek M, Hufnagel H, Brock R. 2005. *Chembiochem : a European journal of chemical biology* 6: 2126-42
69. Fretz MM, Penning NA, Al-Taei S, Futaki S, Takeuchi T, et al. 2007. *Biochemical Journal* 403: 335-42
70. Mano M, Henriques A, Paiva A, Prieto M, Gavilanes F, et al. 2006. *Biochimica Et Biophysica Acta-Biomembranes* 1758: 336-46
71. Marinova Z, Vukojevic V, Surcheva S, Yakovleva T, Cebers G, et al. 2005. *Journal of Biological Chemistry* 280: 26360-70
72. Mitchell DJ, Kim DT, Steinman L, Fathman CG, Rothbard JB. 2000. *Journal of Peptide Research* 56: 318-25
73. Ter-Avetisyan G, Tunnemann G, Nowak D, Nitschke M, Herrmann A, et al. 2009. *The Journal of biological chemistry* 284: 3370-8
74. Tunnemann G, Ter-Avetisyan G, Martin RM, Stockl M, Herrmann A, Cardoso MC. 2008. *Journal of peptide science : an official publication of the European Peptide Society* 14: 469-76
75. Wadia JS, Stan RV, Dowdy SF. 2004. *Nature medicine* 10: 310-5
76. Zaro JL, Rajapaksa TE, Okamoto CT, Shen WC. 2006. *Molecular Pharmaceutics* 3: 181-6
77. Ziegler A, Nervi P, Durrenberger M, Seelig J. 2005. *Biochemistry* 44: 138-48
78. Geueke B, Namoto K, Agarkova I, Perriard JC, Kohler HPE, Seebach D. 2005. *Chembiochem : a European journal of chemical biology* 6: 982-5
79. Holm T, Netzereab S, Hansen M, Langel U, Hallbrink M. 2005. *Febs Letters* 579: 5217-22
80. Nekhotiaeva N, Elmquist A, Rajarao GK, Hallbrink M, Langel U, Good L. 2004. *FASEB journal : official publication of the Federation of American Societies for Experimental Biology* 18: 394-6
81. Glaeser RM, Jap BK. 1984. *Biophysical Journal* 45: 95-7
82. Nishihara M, Perret F, Takeuchi T, Futaki S, Lazar AN, et al. 2005. *Organic & biomolecular chemistry* 3: 1659-69

83. Bechinger B, Lohner K. 2006. *Biochimica Et Biophysica Acta* 1758: 1529-39
84. Scheller A, Oehlke J, Wiesner B, Dathe M, Krause E, et al. 1999. *Journal of peptide science : an official publication of the European Peptide Society* 5: 185-94
85. Takeshima K, Chikushi A, Lee KK, Yonehara S, Matsuzaki K. 2003. *The Journal of biological chemistry* 278: 1310-5
86. Deshayes S, Plenat T, Aldrian-Herrada G, Divita G, Le Grimellec C, Heitz F. 2004. *Biochemistry* 43: 7698-706
87. Shai Y. 1999. *Biochimica Et Biophysica Acta* 1462: 55-70
88. Cho YW, Kim JD, Park K. 2003. *The Journal of pharmacy and pharmacology* 55: 721-34
89. Subbarao NK, Parente RA, Szoka FC, Jr., Nadasdi L, Pongracz K. 1987. *Biochemistry* 26: 2964-72
90. Jones SW, Christison R, Bundell K, Voyce CJ, Brockbank SMV, et al. 2005. *British Journal of Pharmacology* 145: 1093-102
91. Saar K, Lindgren M, Hansen M, Eiriksdottir E, Jiang Y, et al. 2005. *Analytical biochemistry* 345: 55-65
92. Macdonald PM, Crowell KJ, Franzin CM, Mitrakos P, Semchyschyn DJ. 1998. *Biochemistry and cell biology = Biochimie et biologie cellulaire* 76: 452-64
93. Roux M, Neumann JM, Bloom M, Devaux PF. 1988. *European biophysics journal : EBJ* 16: 267-73
94. Tiriveedhi V, Butko P. 2007. *Biochemistry* 46: 3888-95
95. Esbjorner EK, Lincoln P, Norden B. 2007. *Biochimica Et Biophysica Acta* 1768: 1550-8
96. Sakai N, Takeuchi T, Futaki S, Matile S. 2005. *Chembiochem : a European journal of chemical biology* 6: 114-22
97. Henriques ST, Costa J, Castanho MA. 2005. *Biochemistry* 44: 10189-98
98. Afonin S, Frey A, Bayerl S, Fischer D, Wadhwani P, et al. 2006. *Chemphyschem : a European journal of chemical physics and physical chemistry* 7: 2134-42
99. Thoren PE, Persson D, Esbjorner EK, Goksor M, Lincoln P, Norden B. 2004. *Biochemistry* 43: 3471-89
100. Thoren PE, Persson D, Karlsson M, Norden B. 2000. *FEBS letters* 482: 265-8
101. Futaki S, Ohashi W, Suzuki T, Niwa M, Tanaka S, et al. 2001. *Bioconjugate chemistry* 12: 1005-11
102. Qiu R, MacDonald RC. 1994. *Biochimica Et Biophysica Acta* 1191: 343-53
103. Schindler H. 1979. *Biochimica Et Biophysica Acta* 555: 316-36
104. Smith R, Tanford C. 1972. *Journal of molecular biology* 67: 75-83
105. Altenbach C, Seelig J. 1984. *Biochemistry* 23: 3913-20
106. Lewis BA, Engelman DM. 1983. *Journal of molecular biology* 166: 211-7
107. Santaren JF, Rico M, Guilleme J, Ribera A. 1982. *Biochimica Et Biophysica Acta* 687: 231-7
108. Cullis PR, Hope MJ, Tilcock CP. 1986. *Chemistry and physics of lipids* 40: 127-44
109. Fabrie CH, de Kruijff B, de Gier J. 1990. *Biochimica Et Biophysica Acta* 1024: 380-4
110. Langner M, Hui SW. 1993. *Chemistry and physics of lipids* 65: 23-30
111. Volodkin D, Mohwald H, Voegel JC, Ball V. 2007. *Journal of controlled release : official journal of the Controlled Release Society* 117: 111-20
112. Marsh D. 1996. *Biophysical Journal* 70: 2248-55
113. Felgner JH, Kumar R, Sridhar CN, Wheeler CJ, Tsai YJ, et al. 1994. *The Journal of biological chemistry* 269: 2550-61
114. Prochiantz A. 1996. *Current opinion in neurobiology* 6: 629-34
115. Fischer A, Oberholzer T, Luisi PL. 2000. *Biochimica Et Biophysica Acta* 1467: 177-88

116. Elorza B, Elorza MA, Sainz MC, Chantres JR. 1993. *Journal of pharmaceutical sciences* 82: 1160-3
117. Herbig ME, Fromm U, Leuenberger J, Krauss U, Beck-Sickinger AG, Merkle HP. 2005. *Biochimica Et Biophysica Acta* 1712: 197-211
118. Seelig A. 1987. *Biochimica Et Biophysica Acta* 899: 196-204
119. Michaelson DM, Horwitz AF, Klein MP. 1973. *Biochemistry* 12: 2637-45
120. Wieprecht T, Apostolov O, Beyermann M, Seelig J. 2000. *Biochemistry* 39: 442-52
121. Ruocco MJ, Shipley GG. 1982. *Biochimica Et Biophysica Acta* 684: 59-66
122. Zhou Z, Sayer BG, Hughes DW, Stark RE, Epand RM. 1999. *Biophysical Journal* 76: 387-99
123. Newman GC, Huang C. 1975. *Biochemistry* 14: 3363-70
124. Kaasgaard T, Mouritsen OG, Jorgensen K. 2003. *Biochimica Et Biophysica Acta* 1615: 77-83
125. Traikia M, Warschawski DE, Recouvreur M, Cartaud J, Devaux PF. 2000. *European biophysics journal : EBJ* 29: 184-95
126. Larrabee AL. 1979. *Biochemistry* 18: 3321-6
127. Suurkuusk J, Lentz BR, Barenholz Y, Biltonen RL, Thompson TE. 1976. *Biochemistry* 15: 1393-401
128. Mayer LD, Hope MJ, Cullis PR. 1986. *Biochimica Et Biophysica Acta* 858: 161-8
129. Grit M, Crommelin DJA. 1992. *Chemistry and physics of lipids* 62: 113-22
130. Lasic DD. 1988. *The Biochemical journal* 256: 1-11
131. Lichtenberg D, Freire E, Schmidt CF, Barenholz Y, Felgner PL, Thompson TE. 1981. *Biochemistry* 20: 3462-7
132. Petersen NO, Chan SI. 1978. *Biochimica Et Biophysica Acta* 509: 111-28
133. Winterhalter M, Lasic DD. 1993. *Chemistry and physics of lipids* 64: 35-43
134. Maulucci G, De Spirito M, Arcovito G, Boffi F, Castellano AC, Briganti G. 2005. *Biophysical Journal* 88: 3545-50
135. Pereira-Lachataignerais J, Pons R, Panizza P, Courbin L, Rouch J, Lopez O. 2006. *Chemistry and physics of lipids* 140: 88-97
136. Hauser HO. 1971. *Biochemical and biophysical research communications* 45: 1049-55
137. Woodbury DJ, Richardson ES, Grigg AW, Welling RD, Knudson BH. 2006. *Journal of liposome research* 16: 57-80
138. Frimer AA, Strul G, Buch J, Gottlieb HE. 1996. *Free radical biology & medicine* 20: 843-52
139. Andrews SB, Hoffman RM, Borison A. 1975. *Biochemical and biophysical research communications* 65: 913-20
140. Yamaguchi T, Nomura M, Matsuoka T, Koda S. 2009. *Chemistry and physics of lipids* 160: 58-62
141. Martin FJ, MacDonald RC. 1976. *Biochemistry* 15: 321-7
142. McCulloch A. 2003. *Chemosphere* 50: 1291-308
143. Constan AA, Wong BA, Everitt JI, Butterworth BE. 2002. *Toxicological sciences : an official journal of the Society of Toxicology* 66: 201-8
144. Blixt Y, Valeur A, Everitt E. 1990. *In vitro cellular & developmental biology : journal of the Tissue Culture Association* 26: 691-700
145. White DA. 1973. In *Form and function of phospholipids*, ed. GB Ansell, Hawthorne, J.A. and Dawson, R.M.C., pp. pp. 441-82
146. Beining PR, Huff E, Prescott B, Theodore TS. 1975. *Journal of Bacteriology* 121: 137-43
147. Epand RM, Epand RF. 2009. *Biochimica Et Biophysica Acta* 1788: 289-94
148. Devaux PF. 1991. *Biochemistry* 30: 1163-73

149. Martin SJ, Reutelingsperger CP, McGahon AJ, Rader JA, van Schie RC, et al. 1995. *The Journal of experimental medicine* 182: 1545-56
150. Ziegler A, Blatter XL, Seelig A, Seelig J. 2003. *Biochemistry* 42: 9185-94
151. Persson D, Thoren PE, Lincoln P, Norden B. 2004. *Biochemistry* 43: 11045-55
152. Garbuzenko O, Barenholz Y, Priev A. 2005. *Chemistry and physics of lipids* 135: 117-29
153. Hristova K, Needham D. 1994. *Journal of Colloid and Interface Science* 168: 302-14
154. Tirosh O, Barenholz Y, Katzhendler J, Priev A. 1998. *Biophysical Journal* 74: 1371-9
155. Allende D, Simon SA, McIntosh TJ. 2005. *Biophysical Journal* 88: 1828-37
156. Kaasgaard T, Mouritsen OG, Jorgensen K. 2001. *International journal of pharmaceutics* 214: 63-5
157. Itaya K, Ui M. 1966. *Clinica chimica acta; international journal of clinical chemistry* 14: 361-6
158. Baykov AA, Evtushenko OA, Avaeva SM. 1988. *Analytical Biochemistry* 171: 266-70
159. Vemuri S. 2005. *The journal of peptide research : official journal of the American Peptide Society* 65: 433-9
160. Edelhoch H. 1967. *Biochemistry* 6: 1948-54
161. Ziegler A, Seelig J. 2008. *Biophysical Journal* 94: 2142-9
162. Schiffer M, Edmundson AB. 1967. *Biophysical Journal* 7: 121-35
163. Iritani N, Miyahara T. 1973. *Japan Analyst* 22: 174-8
164. Wallach DFH, Surgenor DM, Soderberg J, Delano E. 1959. *Analytical Chemistry* 31: 456-60
165. Garcia MA, Paje SE, Villegas MA, Llopis J. 2002. *Applied Physics a-Materials Science & Processing* 74: 83-8
166. Niesman MR, Khoobehi B, Peyman GA. 1992. *Investigative Ophthalmology & Visual Science* 33: 2113-9
167. Aschi M, D'Archivio AA, Fontana A, Formiglio A. 2008. *The Journal of organic chemistry* 73: 3411-7
168. Rothbard JB, Jessop TC, Lewis RS, Murray BA, Wender PA. 2004. *Journal of the American Chemical Society* 126: 9506-7
169. Chen RF, Knutson JR. 1988. *Analytical Biochemistry* 172: 61-77
170. Gavino VC, Miller JS, Dillman JM, Milo GE, Cornwell DG. 1981. *Journal of lipid research* 22: 57-62
171. Seelig J. 1978. *Biochimica Et Biophysica Acta* 515: 105-40
172. Soubias OaG, K. 2001. *Methods in molecular biology* 400: 77-88
173. Seelig J. 2004. *Biochimica Et Biophysica Acta* 1666: 40-50
174. Beschiaschvili G, Seelig J. 1990. *Biochemistry* 29: 10995-1000
175. Persson D, Thoren PE, Herner M, Lincoln P, Norden B. 2003. *Biochemistry* 42: 421-9
176. Dennison SR, Baker RD, Nicholl ID, Phoenix DA. 2007. *Biochemical and biophysical research communications* 363: 178-82
177. Franzin CM, Macdonald PM. 2001. *Biophysical Journal* 81: 3346-62
178. Macdonald PM, Crowell KJ, Franzin CM, Mitrakos P, Semchyschyn D. 2000. *Solid state nuclear magnetic resonance* 16: 21-36
179. Baker BM, Murphy KP. 1996. *Biophysical Journal* 71: 2049-55
180. Lamaziere A, Burlina F, Wolf C, Chassaing G, Trugnan G, Ayala-Sanmartin J. 2007. *PloS one* 2: e201
181. Thoren PE, Persson D, Lincoln P, Norden B. 2005. *Biophysical chemistry* 114: 169-79
182. Yi D, Guoming L, Gao L, Wei L. 2007. *Biochemical and biophysical research communications* 359: 1024-9
183. Fuchs SM, Raines RT. 2004. *Biochemistry* 43: 2438-44

Chapter 2:

Enzymatic tyrosine de-phosphorylation activates the cell-penetrating peptide pen-A(pY)L[3]

2.1 Introduction

A variety of diseases is characterized by altered regulatory pathways inside biological cells. The correction of these intracellular pathways by pharmaceutical means is believed to improve the outcome in diseases, where efficient treatment with small molecule drugs is not available. Drug candidates for that purpose are small-interference RNA (siRNA) and specific intracellular antibodies ("intrabodies"). Their action on intracellular regulatory pathways is transient as compared to stable gene therapies, so that eventual side effects are supposed to be easier manageable. The benefit of these drug candidates has been repeatedly confirmed on cells in culture. In contrast, their widespread use in intact organisms is delayed, mainly because of difficulties to get these rather large and charged drug entities across membranes of living cells. Diverse physical procedures, such as electroporation and gene guns, exist to destabilize cell membranes for that purpose, but these procedures are not approved for use in higher

[3] Sections 2.1 to 2.3.4 consist of a manuscript for a publication.

organisms. Also chemical procedures exist for that purpose, such as cell-penetrating peptides (CPPs) that act by both increasing the cell surface concentration of the drug and by membrane destabilization. Depending on the structure of the CPP, the membrane destabilization is provided by electrostatic actions (e.g., non-amphipathic CPPs) or by insertion into the lipid bilayer of the membrane due to hydrophobic attraction (e.g., amphipathic CPPs). Because of the property of small amphipathic CPPs to destabilize membranes, there is often only a small difference between concentrations required for efficient membrane destabilization and their toxicity which is typically designated as narrow therapeutic index (NTI) in clinical pharmacology. For example, CPPs such as transportan, MPG, and TP10 are membrane-lytic at low micromolar concentrations, but similar concentrations are required to assure their efficient delivery of drugs or fluorophores across biological membranes. Transient membrane damage and eventual cell losses might be tolerated on cells in culture, where surviving transfected cells will rapidly recover and proliferate. In contrast, the use of drug and gene delivery techniques in larger organisms requires more specific procedures to make the membrane destabilization confined to particular tissues of interest.

We here propose a new technique that might help to increase the tissue-specificity and therapeutic index of CPPs. The technique is based on the action of phosphatases – enzymes that are present in numerous tumour cells and also endocytotic vesicles. For this purpose, we introduced a tyrosine phosphate by substituting A_{10} in the hydrophobic face of the model peptide penetratin p2AL ((1) which destabilizes synthetic membranes at low micromolar concentrations. We hypothesized that the charged phosphate in the hydrophobic face prevents the deep membrane insertion of the model peptide Penetratin $A_9(pY)_{10}L_{13}$ (Pen-A(pY)L) thus reducing its membrane perturbation. Upon enzymatic de-phosphorylation of the peptide to Penetratin $A_9Y_{10}L_{13}$ (Pen-AYL), the hydrophobic face of the peptide should be restored likely restoring its membrane-lytic property. The influence of the (de-)phosphorylation of the tyrosine (Y_{10}) residue on the membrane perturbation of the peptide was tested on phospholipid model membranes and also on living CHO-K1 cells in culture.

2.2. Materials and Methods

2.2.1. Materials

The lipids POPC, POPG, and DOPE-PEG were purchased from Avanti Polar Lipids (Avanti Polar Lipids, Alabaster, USA). The fluorescent dye ANTS and its quencher DPX were from Molecular Probes/Invitrogen (Luzern, Switzerland). The cross-linked dextran gel Sephadex G-75 was from Pharmacia/GE Healthcare (Uppsala, Sweden). Tris was purchased from Merck (Darmstadt, Germany). Alkaline phosphatase from porcine kidney, NaCl, Triton X-100 and all other chemicals were from Sigma-Aldrich (Buchs, Switzerland). The Tris-buffered saline contained 20 mM, Tris 100 mM NaCl (pH 7.4), and the buffer for the enzyme stock solutions was made of 20 mM glycine, 100 mM NaCl (pH 10). The peptides (all with amidated carboxy-terminus), including their phosphorylated and TAMRA-labelled derivatives, were purchased from Peptide 2.0 (Chantilly, VA) as trifluoroacetate salt (purity ≥97% as judged by HPLC). Gibco cell culture medium (DMEM/F12 1:1 w/o L-Glutamin), PBS pH 7.2, 0.05% Trypsin-EDTA, L-Glutamin, fetal calf serum, penicillin and streptomycin were all provided by Life Technologies (Paisley, UK).

2.2.2. Determination of peptide concentration

Peptides were first weighed on a microbalance and dissolved in Tris buffered saline (TBS). The pH was adjusted with diluted NaOH to 7.4 and TBS was added to make the final volume. Thereafter, the concentration of the stock solution was determined spectrophotometrically in their denatured state (2) using a molar absorptivity of 5500 M^{-1} cm^{-1} at 281 nm for Trp and data averaging of triplicate measurements. Stock solutions of pen-A(pY)L >1 mM were avoided because of gel formation at higher concentration.

2.2.3. Calculation of the mean hydrophobic moment

The mean hydrophobic moment of the peptides was calculated according to the procedure of Eisenberg (3). In short, the direction of the hydrophobic moment was calculated assuming an angle of 100° separating the side chains of the amino acids along the helical backbone plotted as helical wheel projections (4). The amplitude of the hydrophobic moment was calculated using the hydrophobicity scale of Fauchere & Pliska (5) that is based on the l-octanol/pH 7.1 aqueous solution partition ratios (P) for N-acetylated and C-amidated amino acids; the hydrophobic parameter π of a side chain is then estimated as the difference of log P (N-acetyl-amino acid) from that of N-acetyl-glycine amide having the side chain "H". In this scale, the most and least hydrophobic amino acids have π values of +2.25 (Trp) and -1.01 (Arg), respectively. For the phosphorylated tyrosine (N-acetyl, C-amide), a π of -0.38 was used based on logP calculations of a fragementation method (ChemBioDraw Ultra 12) in agreement with experimental observations for phosphorylated tyrosine (6).

2.2.4. Preparation of dye-loaded LUVs

The fluorescent dye ANTS and its quencher DPX were dissolved in 20 mM Tris pH 7.4 for final concentrations of 12.5 and 45 mM for ANTS and DPX, respectively, and the pH was adjusted to 7.4 with diluted NaOH. Desired quantities of lipid mixtures were calculated to yield a final concentration of 40 mM. The PEGylated lipid DOPE-PEG was included in order to prevent the aggregation of the vesicles upon contact with the multivalent CPPs (7). In short, chloroform/lipid mixtures were dried to a film under a stream of nitrogen, followed by evaporation overnight under high vacuum (0.1 mbar) at room temperature and dark. The dry lipid films were suspended with the dye solution, followed by 10 freeze-/thaw-cycles (30 min) and subsequent extrusion for 10 times through polycarbonate filters (100 nm pore size, Whatman, Maidstone, UK) with a barrel extruder (LIPEX, Northern Lipids, Burnaby, Canada) at ~15 bar. The resulting dye-loaded large unilamellar vesicles (LUVs) had a homogenous size distribution with a diameter of ~100 nm as confirmed by dynamic light scattering on a Zetasizer Nano ZS (Malvern; Worcestershire, UK).

Dye-filled vesicles were separated from extravesicular free dye by size-exclusion chromatography on a Sephadex G-75 column (43 x 1.8 cm). Running buffer was TBS. The size distribution of the harvested LUVs was measured again by dynamic light spectroscopy and 5-6 fractions with the lowest laser attenuation were combined. Thereafter, the total lipid content of the LUVs was determined by a phosphorous assay (8).

2.2.5. Leakage assay

Fluorescence measurements were carried out on a Jasco FP-6500 fluorescence spectrophotometer (JASCO Corp., Japan) under constant stirring. A quartz microcuvette (d = 5 mm) with a filling volume of 250 µL was used for measurements at room temperature. Excitation and emission wavelengths were set to 360 and 518 nm for ANTS-loaded vesicles. Both, excitation and emission slit widths were set to 3 nm. An aliquot of 8 - 35 µL of peptide stock solutions with indicated concentrations between 10 µM and 1 mM were added to the vesicles (~1.75 mM LUVs). The change of fluorescence intensity upon peptide addition, corresponding to release and de-quenching of ANTS, was constantly measured during 10 min. Thereafter, the vesicles were solubilized in order to release all encapsulated ANTS using 25 µL 5% (v/v) Triton X-100 to determine the maximum fluorescence intensity corresponding to full leakage. The percentage of dye release was estimated by the following equation

$$Leakage\,(\%) = 100(F - F_0)/(F_{max} - F_0)$$

where F and F_{max} correspond to the fluorescence intensity of ANTS before and after the addition of detergent at ~10 min, respectively, and F_0 represents the original fluorescence intensity of intact vesicles at t = 0 min.

2.2.6. Enzymatic de-phosphorylation

Alkaline phosphatase from porcine kidney (APPK) was chosen because it showed pronounced de-phosphorylation activity (on *p*-nitrophenyl phosphate) at neutral pH (not shown). For that purpose, 0.86 mg of APPK was dissolved in 1 mL Gly buffer (pH 10), resulting in 5.55 µM stock solution using the molecular weight of 155 kD (9). Leakage assays involving enzymatic de-phosphorylation of pen-A(pY)L were done under the same conditions as without protein. Peptide induced dye-leakage percentages after addition of APPK were calculated as stated above, but changed F_0 to the fluorescence intensity prior protein addition.

2.2.7. Cell Culture

Wild-type Chinese hamster ovary cells, CHO-K1 (ATCC; Manassas, VA), were grown in DMEM/F12 (1:1) medium supplemented with 10% (v/v) fetal calf serum (FCS), 1% (v/v) 200 mM L-Glutamine, 100 U/mL penicillin, and 100 µg/mL streptomycin using 75 cm^2 large vented cell culture flasks (BD Biosciences; Allschwil, Switzerland). The cells were incubated at 37 °C in humidified air containing CO_2 (5%). Every second day (at ~80% confluency), the cells were detached (using trypsin and EDTA.Na_4 at 0.5 and 0.2 g/L, respectively) and split at a ratio of 1:10 up to a maximum of 25 passages.

2.2.8. Confocal Laser Scanning Microscopy

CHO cells were seeded in 12-well dishes onto sterile noncoated microscopic coverslips and incubated for 48 h in order to obtain a confluency of ~80%. Thereafter, cells were rinsed three times with ~2 mL PBS to remove residual FCS and to avoid peptide scavenging by albumin. Subsequently, 2 mL of the peptide solution (2 or 20 µM peptide) in DMEM/F12 (1:1) (containing antibiotics, but no FCS) was added. In case of additional phosphatase, the enzyme was added directly to the peptide solution immediately prior incubation. After 30 min of contact time in the cell incubator, cells were rinsed three times with PBS, mounted upside down on top of 25 µL Fluoromount

G (Southern Biotechnology Associates, Birmingham, AL) and imaged immediately for no longer than 15 min. Confocal images were acquired with an inverted confocal laser scanning microscope (Fluoview FV1000, Olympus, Japan) using a Plan-Apochromat 60 × 0.7 NA lens with excitation at 559 nm (yellow laser diode) for TAMRA-labeled peptides and using differential interference contrast (DIC).

2.3. Results and discussion

2.3.1. Peptide design

Different theories have been proposed to explain the interaction of peptides with biological and model membranes. Among them, the hydrophobic moment (μ) of helical peptides is one of the most prominent parameters to estimate the potential interaction of the peptide with phospholipid membranes and especially their membrane lytic properties (10). In general, it appears that not a maximum hydrophobicity of the peptide, but polar-nonpolar asymmetry ("amphiphilicity") is key to membrane lysis (11), although other processes for membrane destabilization exist, such as self-aggregation and pore formation of peptides.

A large hydrophobic moment ($\mu \approx 0.5 - 1$) (12), for example, indicates that the helix is amphipathic perpendicular to its backbone, i.e. the hydrophobic and hydrophilic side chains of the amino acids are opposite each other along the long axis view of the peptide (**Fig. 2.1**) (13). The resulting amphipathicity (or "amphiphilicity") facilitates the peptide's partitioning into the interface region of phospholipid membranes which often destabilizes membranes more than a transmembrane orientation, such as studied with many antimicrobial peptides.

In contrast, a low hydrophobic moment ($\mu \approx 0 - 0.4$) affects the membrane interface to a lesser extent, and the peptides can be either transmembranous or globular, depending on the overall prevalence of hydrophobic or hydrophilic amino acids, respectively (13). From literature and own experiments with penetratin, we knew

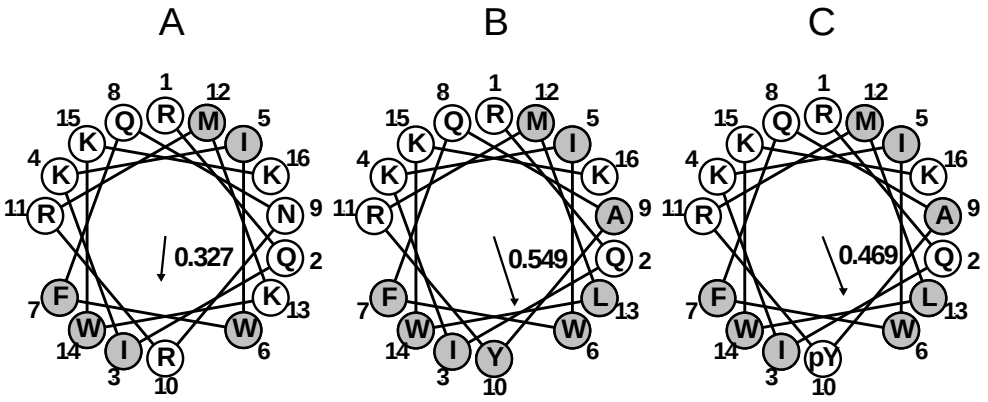

Fig. 2.1. Helical wheel projections of the peptides investigated. The 16 amino acids (single letter code) are plotted from the N-terminal end (1) to the C-terminus (16) using an angle of 100° between adjacent amino acids. The direction (arrrow) and amplitude of the mean hydrophobic moment are indicated in the middle of the wheel. Amino acids with hydrophobic side chains are displayed in grey. **(A)** wild-type penetratin (non-lytic at 20 µM). **(B)** more amphipathic pen-AYL mutant (lytic). **(C)** tyrosine phosphate (pY_{10}) in pen-AYL reduces the hydrophobic moment with consequences for lipid membrane binding.

---

that wild-type penetratin (µ = 0.327) is not lytic to model membranes at low micromolar concentrations. In contrast, when the amphiphilicity is increased by a 3-amino acid substitution to penetratin mutant pen-$A_9A_{10}L_{13}$ (pen-2AL; µ = 0.510), the peptide becomes highly lytic as a results of increased hydrophobic moment (1). The peptide's effect on the membrane integrity was almost detergent-like, as shown by ^{31}P NMR spectroscopy (14) and it showed full vesicle leakage at already low micromolar concentration. We assumed that a molecular switch between both molecules would offer a valuable biomedical tool for tissue-activated drug uptake or cell-specific lysis (e.g., for metastatic tissue), especially because biological phosphatases could be available to activate the peptide in-situ.

Based on this assumption, we modified pen-2AL in a way that the Ala_{10} in the hydrophibic face (**Fig. 2.1**) was replaced by a tyrosine, that could be either phosphorylated or not. It is known that even small changes in the hydrophobic moment (i.e., ($\Delta\mu \geq 0.06$) may considerably influence the membrane lysis of peptides (15). We therefore assumed that de-esterification of the phosphate group might provide a molecular switch between the presumably non-lytic phosphorylated pen-$A_9(pY)_{10}L_{13}$ (pen-A(pY)L; µ = 0.469) and presumably lytic de-phosphorylated pen-$A_9Y_{10}L_{13}$ (pen-

AYL; μ = 0.549). As next step after peptide design, we tested the effect of the $A_{10} \rightarrow Y$ substitution on model membranes, because the action of pen-2AL on model membrane was almost detergent-like, as shown by ^{31}P NMR spectroscopy (14).

2.3.2. Peptide action on model membranes (LUVs)

Aliquots between 8 and 35 µL peptide stock solutions were titrated under continuous stirring into 250 µL of 1.75 mM phospholipid model membranes (LUV suspensions filled with the self-quenching dye ANTS and an additional quencher DPX) to monitor the peptide's membrane permeation capacity. **Tab. 1** summarizes the final peptide concentrations and corresponding peptide/lipid (P/L) ratios using model membranes of both charged and uncharged phospholipids.

At low micromolar concentration, the unphosphorylated pen-AYL (μ = 0.549) lysed both uncharged model membranes (POPC/DOPE-PEG, 96:4 n/n) and charged model membranes (POPC/POPG/DOPE-PEG, 76:20:4 n/n) (**Fig. 2.2**, right panel) with

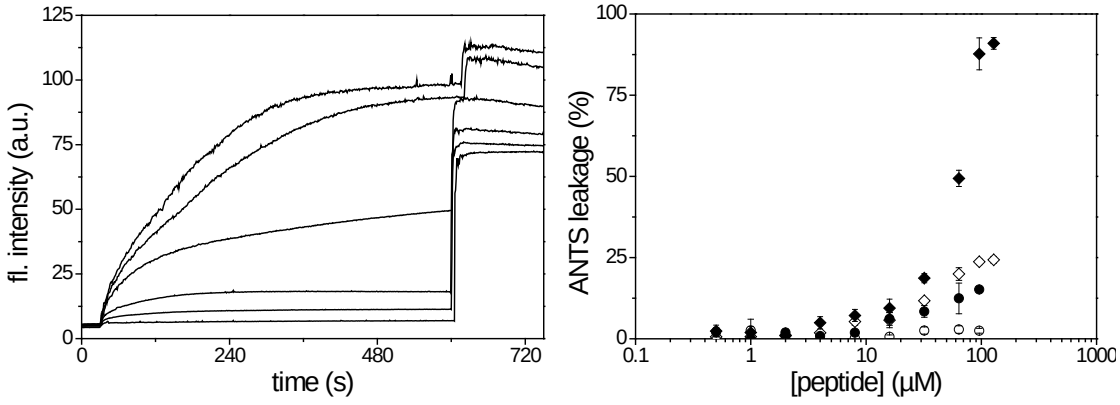

Figure 2.2. Peptide induced ANTS leakage from LUVs. (Left panel) Concentration dependent ANTS leakage from POPC/POPG/DOPE-PEG (76:20:4 mol%) LUVs as induced at s by the injection of unphosphorylated peptide Pen-$A_9Y_{10}L_{13}$. Peptide concentrations correspond to 4, 16, 32, 64, 96 and 128 µM (from bottom to top). At 600 s, Triton X100 was injected to determine the maximum fluorescence intensity corresponding to full leakage of vesicles; the maximum fluorescence intensity after triton addition was increased by the peptide, with the effect being less pronounced as compared to other fluorescent dyes,. **(Right panel)** Averaged ANTS leakage (n = 3 per concentration) from both charged (diamonds) and uncharged LUVs (circles) as induced by both pen-AYL (filled) and pen-A(pY)L (empty) as function of peptide concentration.

Tab. 1. Calculated dye-leakage from both charged and uncharged vesicles in presence of pAYL and pA(pY)L for 600 s.

		pen-AYL	***pen-A(pY)L***	***pen-AYL***	***pen-A(pY)L***
		Dye leakage (%)			
[peptide] (µM)	***P/L***	***uncharged LUVs***		***LUVs with 20% surface charge***	
0.5	***0.0003***	0.6	-0.3	2.4	2.1
1	***0.0006***	0.6	2.5	2.0	0.0
2	***0.0012***	1.1	-0.2	0.9	1.9
4	***0.0025***	1.8	-0.4	4.9	0.9
8	***0.005***	5.3	0.2	7.2	1.9
16	***0.01***	5.7	0.6	9.5	6.1
32	***0.02***	11.7	2.5	18.7	8.4
64	***0.04***	19.9	2.9	49.4	12.4
96	***0.06***	23.7	2.5	87.7	15.2
128	***0.08***	24.3	-	90.9	-

high efficiency (**Tab. 1**). Interestingly, the lipid composition affected both the kinetics and extent of dye-leakage of the cationic peptide.

In case of negatively charged vesicles, peptide-induced leakage was both larger and faster (**Fig. 2.2**, left panel) which could be explained by a higher membrane interface concentration of the peptide as a result of electrostatic attraction. For example, using same final peptide concentrations of 16 µM and 128 µM, the dye-leakage on charged membranes was 1.7 and 3.7 times more pronounced, respectively, as compared to uncharged membranes (**Tab. 1**). The difference of the peptide's potency to induce dye-leakage depending on the vesicle surface charge is readily visible at higher peptide concentrations e.g. at 96 µM, pen-AYL induces 87.7% and 23.7% dye-leakage for charged and uncharged, respectively.

2.3.3. Additon of pen-A(pY)L to LUVs

Titrations were done as described in the previous section. As evident in both **Fig. 2.2** and **Tab. 1**, the peptide's ability to permeate LUVs is strongly decreased upon phosphorylation of the Tyrosine residue. Comparison between induced dye-leakages of the two peptides (**Tab. 1**) shows that Tyr-phosphorylation of pen-AYL causes loss of its ability to induce significant dye-leakage from uncharged LUVs. However, permeation is still observable at peptide concentration ≥16 µM in charged LUVs with up to 15.2% dye-leakage at 96 µM i.e. membrane permeation of pen-A(pY)L is 6 times less than that of pen-AYL with charged vesicles.

Again, the concomitant increase of fluorescence emission intensity after TX100 addition with increasing peptide concentration is due to an enhancing effect of the peptide on fluorescence emission of ANTS, which is even more pronounced for pen-A(pY)L (data not shown). The "negative" leakage of uncharged vesicles in presence of pen-A(pY)L are probably due to the slight dilution (10:11) of the suspension upon peptide addition.

2.3.4. Enzymatic dephosphorylation of pen-A(pY)L in presence of LUVs

The design behind the pen-A(pY)L peptide aimed at using enzymatic phosphate cleavage as a molecular switch in order to turn the peptide from its phosphorylated, membrane-inactive form into a membrane-active form, which then should lead to adjustable dye-leakage from LUVs in a concentration dependent manner. However, the activity of protein phosphatases can be very specific regarding both their substrate and solvent condition. For that reason, several phosphatases were tested upon their activity in TBS. Enzyme activity was monitored by means of UV absorption spectroscopy, using the unspecific substrate 4-nitrophenyl phosphate (4NPP). Alkaline phosphatase from porcine kidney (APPK) showed reasonable activity in TBS i.e. 1 mM 4NPP was completely dephosphorylated by 0.55 μM APPK in approximately 90 min, which corresponds to an averaged reaction rate of 19.5 μmole/min/μM protein. As apparent in **Fig. 2.3**, 0.25 μM APPK is able to dephosphorylate the pen-A(pY)L peptide, turning it into the membrane permeating pen-AYL. One hour after addition of APPK, peptide-induced dye-leakage was 8.1 and 67.6% with 32 and 64 μM peptide, respectively. For comparison, pen-AYL (obtained from synthesis rather than phosphate cleavage) was able to induce 18.7 and 49.4%, respectively, at those two concentrations. Discrepancy between those values can partially be explained by kinetics. For instance, dye-leakage induced by 64 μM pen-AYL is still increasing after 600 s (**Fig. 2.2**) when the fluorescence intensity for calculation of leakage is taken. However, dye-leakage does not increase anymore after 300 s in the case of 32 μM pen-AYL (**Fig. 2.2**). It is thus reasonable to assume that most of the 64 μM peptide was dephosphorylated during the first 30 min after APPK addition. Hence, the reaction rate of pen-A(pY)L dephosphorylation by APPK would be 8.5 μmole/min, which is ~half of the 19.5 μmole/min/μM observed for 4NPP dephosphorylation. The slight decrease in fluorescence intensity right after addition of APPK is likely due to dilution.

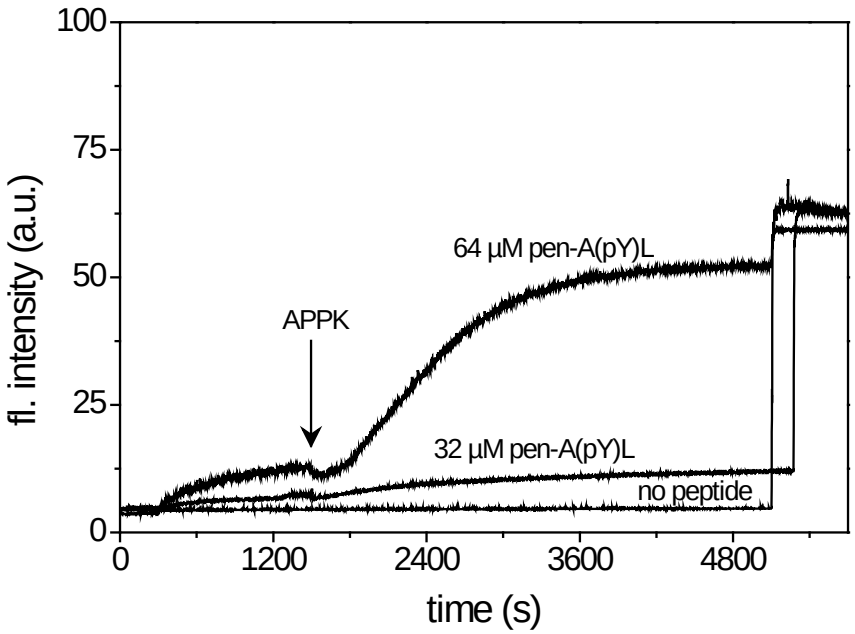

Figure 2.3. Alkaline phosphatase from porcine kidney (APPK) activates the phosphorylated peptide Pen-$A_9(pY)_{10}L_{13}$. 1.75 mM POPC/POPG/DOPE-PEG (76:20:4 n/n) LUVs show only weak leakage in presence of pen-A(pY)L. At 600 s, 32 µM of the phosphorylated peptide pen-A(pY)L causes only 8.4% leakage and thus much less vesicle leakage as compared to the unphosphorylated peptide (compare to **Fig. 2.2**; different time scale). APPK was added at 1500 s and activated the peptide as evident by e.g. 67.7% leakage with 64 µM pen-A(pY)L after 1 h (top trace). Full leakage was achieved with TX100 at ~5100 s.

2.3.5. Addition of TAMRA-pen-AYL to CHO cells

After having assessed the permeabilization of model membranes as induced by each peptide we investigated their uptake by living cells. For this purpose, we incubated CHO cells with TAMRA-labelled derivatives of each peptide for 30 min. The incubated cells were then investigated by means of confocal microscopy. Note that the fluorescence signal intensity is arbitrary and dependent on the voltage of the photomultiplier tube (PMT). We therefore indicated the applied voltage for each image to be able to compare the actual peptide concentrations in the cells. Differential interference contrast (DIC) images complement the fluorescence images by providing visual evidence of the cells' condition and possible toxic effects (e.g. by membrane destabilization as with pen-2AL; compare **Fig. 1.2 i** in **chapter 1**) – they are provided and discussed in **chapter 3**.

We incubated the CHO cells with peptide concentrations of 2 and 20 µM. The lower concentration corresponds to commonly used concentrations in the low micromolar range from 1-10 µM where CPPs show cellular uptake (16-18). The higher concentration was chosen for comparison with the obtained leakage data (**Fig. 2.2**) and corresponds to the onset of dye leakage (>5% at 16 µM beside pen-A(pY)L in uncharged LUVs) from LUVs in presence of either peptide.

The TAMRA signal of pen-AYL in CHO cells after incubation is shown in **Fig. 2.4**. At 2 µM, most cells show endocytotic uptake of the peptide as indicated by the punctate fluorescence pattern. Roughly 5-10% of the cells show additionally a fluorescence signal in the cytoplasm. At 20 µM the peptide manages to enter into the cytoplasm of all cells. However, the corresponding DIC images show that many of these cells are dead or heavily damaged (see **Fig. 3.5A** in **chapter 3**). Note that this is not the case for the lower peptide concentration (**Fig. 3.4A** in **chapter 3**).

2.3.6. Addition of TAMRA-pen-A(pY)L to CHO cells

Fig. 2.5 shows a typical image of CHO cells after incubation with either 2 or 20 µM TAMRA-pen-pA(pY)L. The cells show, in contrast to TAMRA-pen-AYL, almost no uptake at the lower peptide concentration (note the highest used PMT voltage). On the other hand, at 20 µM the peptide apparently manages to reach the cytosol in at least 25% of the cells (our numbers are chosen rather cautious because the arbitrariness of the fluorescence signal). The cells remained healthy at both peptide concentrations (see **Fig. 3.4B** and **3.5B** in **chapter 3**). Interestingly, TAMRA-pen-A(pY)L showed better relation between cellular uptake and toxicity than TAMRA-pen-AYL which, at the given conditions, either had low access to the cytosol or was toxic for the cells.

2.3.7. Addition of TAMRA-pen-A(pY)L with phosphatase to CHO cells

Finally, we incubated CHO cells with TAMRA-pen-A(pY)L in presence of 0.1 µM APPK. Note that the enzyme needs time to dephosphorylate the peptide. If we assume

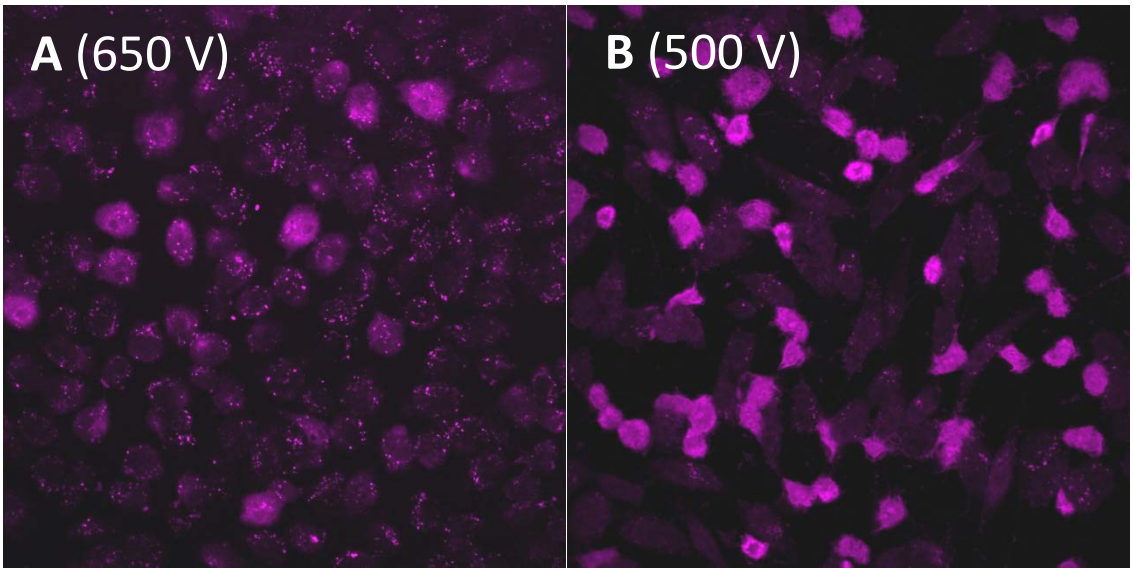

Fig. 2.4. Confocal microscopy images (fluorescence channel) of CHO cells after incubation with 2 (A) or 20 µM TAMRA-pen-AYL (B) for 30 min. (A) With 2 µM most cells show a punctate fluorescence pattern with single cells having an even distribution throughout the cytoplasm. This is indicative that most of the peptide is trapped in endosomes but some manages to enter the cytosol. **(B)** All cells show heavy uptake of TAMRA-pen-AYL (also indicated by the lower PMT voltage compared to (A)). However, the cells are mostly dead (as indicated by DIC images, see **chapter 3** for details), probably due to membrane permeation (compare with dye leakage in **Fig. 2.2**). (**in brackets**) PMT voltage.

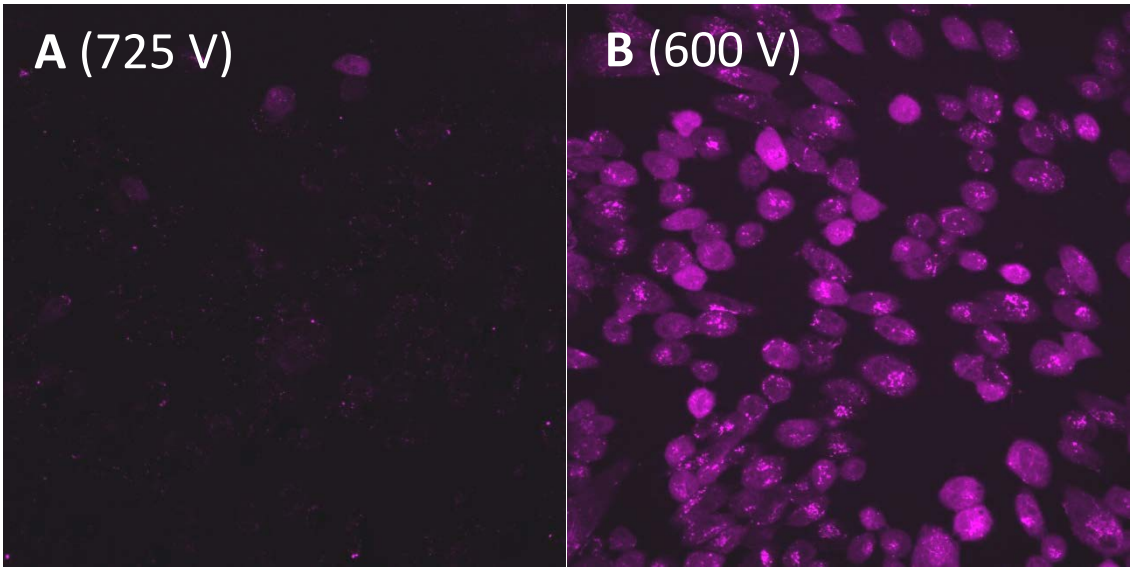

Fig. 2.5. Confocal images of CHO cells after incubation with 2 (A) or 20 µM TAMRA-pen-A(pY)L (B) for 30 min. (A) No visible uptake of 2 µM TAMRA-pen-pA(pY)L. **(B)** Most cells show both endocytotic uptake and presence of the peptide in the cytoplasm after incubation with 20 µM. The fluorescence pattern is comparable to the result obtained with 2 µM TAMRA-pen-AYL but here more cells show fluorescence in the cytoplasm. The cells were also still healthy (as judged by DIC, see **chapter 3**). (**in brackets**) PMT voltage

the rate of 8.5 µmole/min/µM as observed in the leakage assay 20 µM pen-A(pY)L would need 25 min to be completely dephosphorylated. The cells are therefore probably not exposed to activated peptide during the whole incubation period.

As shown in **Fig. 2.6** CHO cells show a very similar peptide uptake as without the addition of APPK. Intracellular TAMRA-pen-A(pY)L is almost not present after incubation at 2 µM. However, the peptide seems to be well distributed throughout the cells when incubated at 20 µM. Notable are the absence of punctate patterns and the needed PMT voltage of 500 V which was only as low as with 20 µM of the unphosphorylated TAMRA-pen-AYL.

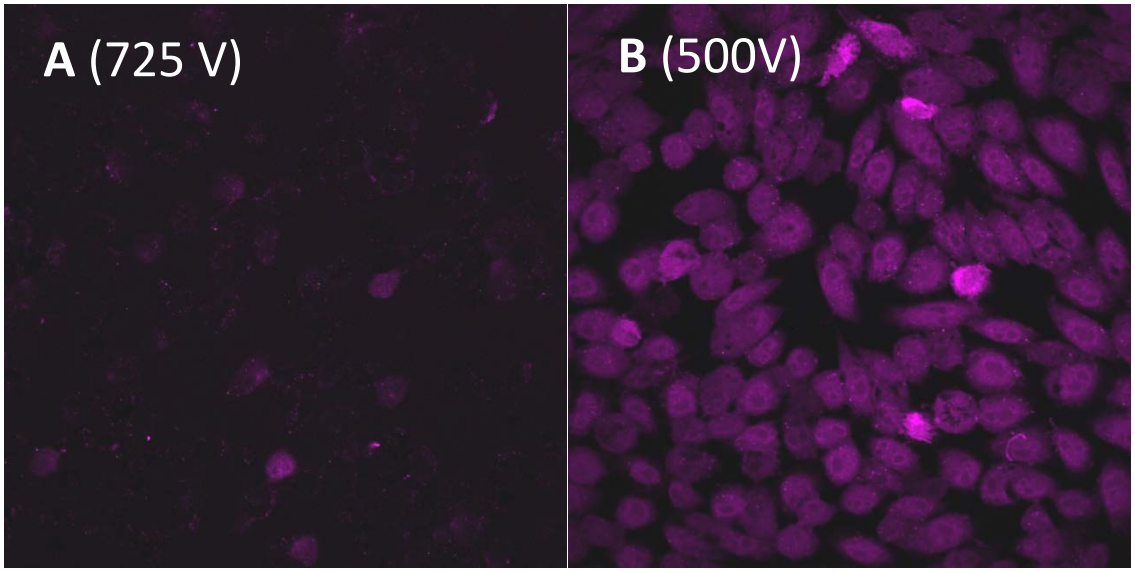

Fig. 2.6. CHO cells after incubation with 2 (A) or 20 µM TAMRA-pen-A(pY)L (B) in presence of 0.1 µM APPK. (A) The cells show only very little signal after incubation with low peptide concentration. **(B)** In contrast, at higher concentration the peptide seems to be evenly distributed in the cells. The difference to incubation in absence of the enzyme is, however, not that pronounced.

2.3.8. Conclusion

In this chapter, we designed an inducible membrane permeation system based on the pen-2AL mutant (1) of the CPP penetratin. The substitution of A_{10} in pen-2AL by pY_{10} decreased the peptides' hydrophobic moment that membrane permeation was

strongly reduced as evident by the low dye leakage of LUVs in presence of pen-A(pY)L (**Fig. 2.2,** right panel). In contrast, unphosphorylated pen-AYL showed strong dye leakage from LUVs similar to pen-2AL (**Fig. 2.2,** right panel) indicating increased membrane permeation. The membrane inactive pen-A(pY)L then could be activated by enzymatic dephosphorylation by APPK at submicromolar concentration (**Fig. 2.3**). Finally, we could demonstrate by fluorescence confocal microscopy the cellular uptake of pen-A(pY)L by living CHO cells (**Fig. 2.5B**). Additionally provided APPK caused the peptide to further locate to the cytoplasm (**Fig. 2.6B**) illustrating its potential benefit for drug delivery.

2.4. References

1. Drin G, Demene H, Temsamani J, Brasseur R. 2001. *Biochemistry* 40: 1824-34
2. Edelhoch H. 1967. *Biochemistry* 6: 1948-54
3. Eisenberg D, Weiss RM, Terwilliger TC. 1982. *Nature* 299: 371-4
4. Schiffer M, Edmundson AB. 1967. *Biophysical Journal* 7: 121-35
5. Fauchere JL, Pliska V. 1983. *European Journal of Medicinal Chemistry* 18: 369-75
6. Allentoff AJ, Mandiyan S, Liang HB, Yuryev A, Vlattas I, et al. 1999. *Cell Biochemistry and Biophysics* 31: 129-40
7. Persson D, Thoren PEG, Norden B. 2001. *Febs Letters* 505: 307-12
8. Itaya K, Ui M. 1966. *Clinica chimica acta; international journal of clinical chemistry* 14: 361-6
9. Wachsmut.Ed, Hiwada K. 1974. *Biochemical Journal* 141: 273-82
10. Wieprecht T, Apostolov O, Beyermann M, Seelig J. 2000. *Biochemistry* 39: 442-52
11. Fernandez-Vidal M, Jayasinghe S, Ladokhin AS, White SH. 2007. *Journal of molecular biology* 370: 459-70
12. Eisenberg D. 1984. *Annual review of biochemistry* 53: 595-623
13. Eisenberg D, Schwarz E, Komaromy M, Wall R. 1984. *Journal of molecular biology* 179: 125-42
14. Sauder R, Seelig J, Ziegler A. 2011. *Methods in molecular biology* 683: 129-55
15. Wieprecht T, Dathe M, Krause E, Beyermann M, Maloy WL, et al. 1997. *Febs Letters* 417: 135-40
16. Drin G, Cottin S, Blanc E, Rees AR, Temsamani J. 2003. *The Journal of biological chemistry* 278: 31192-201
17. Richard JP, Melikov K, Vives E, Ramos C, Verbeure B, et al. 2003. *The Journal of biological chemistry* 278: 585-90
18. Ziegler A, Seelig J. 2011. *Biochemistry* 50: 4650-64

Chapter 3:

Effect of medium during incubation of CHO cells with pen-AYL and pen-A(pY)L

3.1. Introduction

The uptake of cell-penetrating peptides (CPPs) into a number of different living cells has been repeatedly reported in the past 20 years. The various cell types included bacterial, insect, mammalian, plant and yeast cells that typically differ in their membrane composition and their capacity for endocytosis. A common uptake mechanism, if at all existing, has therefore puzzled many investigators ever since.

It appears that CPPs are promising vectors for intracellular delivery of a broad variety of biologically relevant (macro)molecules such as nucleic acids (e.g. oligonucleotides, pDNA, siRNA), peptides and proteins (references (1,2) and also introduction of chapter 1). In in vitro experiments both the CPP alone and the corresponding conjugate with the aforementioned compounds have been shown to be taken up by a variety of cell lines.

Two major caveats, however, prevented their distribution in medical applications to date. Firstly, and probably most importantly, the actual mechanism of CPP uptake is not resolved yet. Both passive translocation and active uptake have been suggested according to the results of recent studies that imply variable uptake routes (3,4), usually

dependent on the applied concentration. Whenever referring to a potential common uptake mechanism, it is thus important to exclude artifacts of the observational methods and to review whether quantitative data of the uptake are available for comparison. The latter is rarely the case.

For example, it has been found that the highly cationic CPPs bind electrostatically to the cell membrane of many cell types. The adsorbed CPP can lead to artifacts, whenever cells are prepared for microscopy. Fixation with methanol, for example, can create leaky cell membranes where the adsorbed CPP appears in the (dead) cells to a much higher extent than in vivo uptake would produce.

Also, the high analytical sensitivity of the observation methods might create confusion as to what the CPP "uptake" is referring to. Fluorescent methods, such as confocal scanning laser microscopy and fluorescent cell sorting, have a measuring range of several orders of magnitude. Reports of absolute intracellular CPP content thus are challenging and rarely available for comparison. Likewise, gene expression can be technically amplified from a few molecules (e.g. copies of mRNA). As a result, it must be emphasized that the term "CPP uptake" was often used without specific quantitation and/or possibility for comparison.

Tab. 2. Used peptides and their corresponding primary structure. Positively or negatively charged residues and groups are in red and blue, respectively.

Peptide	sequence (single letter code)
TAMRA-pen-AYL	TAMRA-RQIK IWFQ AYRM LWKK
TAMRA-pen-A(pY)L	TAMRA-RQIK IWFQ A(pY)RM LWKK

Secondly, especially *amphipathic* CPPs (5) can be toxic to cells at low micromolar concentrations either by destabilizing the integrity of the lipid part of a membrane by membrane insertion (6) or by pore formation (7), similar to the action of some

antimicrobial peptides like melittin (8,9). Toxicity of CPPs on living cells is usually concentration dependent and does not necessarily concur with the concentration range where they succeed to enter cells.

As discussed in the previous chapter, we studied the effect of the penetratin mutants pen-AYL and its phosphorylated variant pen-A(pY)L (sequence **Tab. 2**) on both synthetic and biological membranes to assess their property to permeate these. In the present chapter it is described that the observed difference of both peptides depends on the culture medium which gives further information on the biological uptake processes. Most importantly, CPP uptake was higher a cell culture medium that promoted cell adherence to the cell culture support (i.e. plastic dish or glass cover slips) which eventually substantiates earlier findings that cells in suspension are difficult to transfect as they are not infiltrated by CPPs. Specifically, it was found that CPPs at low micromolar (2 µM) concentration tend to detach the cells – especially when CPP was administered in PBS (phosphate buffered saline) instead of cell culture medium. At higher concentration (20 µM), however, the CPP helped to attach the cells to the glass support, in analogy to earlier findings with polylysine.

3.2. Materials and methods

3.2.1. Materials

The TAMRA-labelled peptides (labelled at the amino-terminus; amidated carboxy-terminus) were purchased from Peptide 2.0 (Chantilly, VA) as trifluoroacetate salt (purity ≥97% as judged by HPLC). All materials for cell culture (see previous chapter) were provided by Life Technologies (Paisley, UK).

3.2.2. Cell Culture

See previous chapter for details.

3.2.3. Confocal Laser Scanning Microscopy

Microscopy was performed as already described in the previous chapter. Incubation of the cells was done at ~80% confluency for every sample. Only difference here was the choice of the incubation medium: immediately prior incubation, the TAMRA-labeled peptides were diluted from a 100 µM stock solution (buffer 20 mM Tris 100 mM NaCl pH 7.0) into either PBS pH 7.2 or pure DMEM/F12 (i.e. without serum, antibiotics or glutamine) to a final concentration of either 2 or 20 µM with a total volume of 2 mL. The cells grown on coverslips then were incubated with the corresponding peptide solution prior to microscopy.

3.3. Results

3.3.1. Cell adhesion when incubated with peptide dissolved in PBS

As described in the previous chapter, wild-type Chinese hamster ovary (CHO) cells were incubated with the TAMRA-labelled pAntp mutants TAMRA-pen-AYL and TAMRA-pen-A(pY)L in order to track the cellular uptake of these peptides by means of fluorescence microscopy. In order to avoid the introduction of methodical artifacts by cell fixation (10,11), we only monitored live which were not fixated. Furthermore it is important to note that the concentration of the CPPs did influence the effect of secondary amphipathic CPPs (5) on both model membranes (see previous chapters) and biological membranes (see Drin et al. (12) for uptake of pAntp by K562 cells). For that reason, two concentrations of the CPPs were chosen (2 and 20 µM) to monitor the effect of these peptides on living cells. At comparable peptide concentration (16 µM), pen-AYL showed 9% dye leakage out of large unilamellar vesicles (LUVs) composed of 1.75 mM POPC/POPG/DOPE-PEG 76:20:4 n/n. i.e. a membrane charge that reflects eukaryotic cells (see previous chapters for other peptide concentrations and lipid contents).

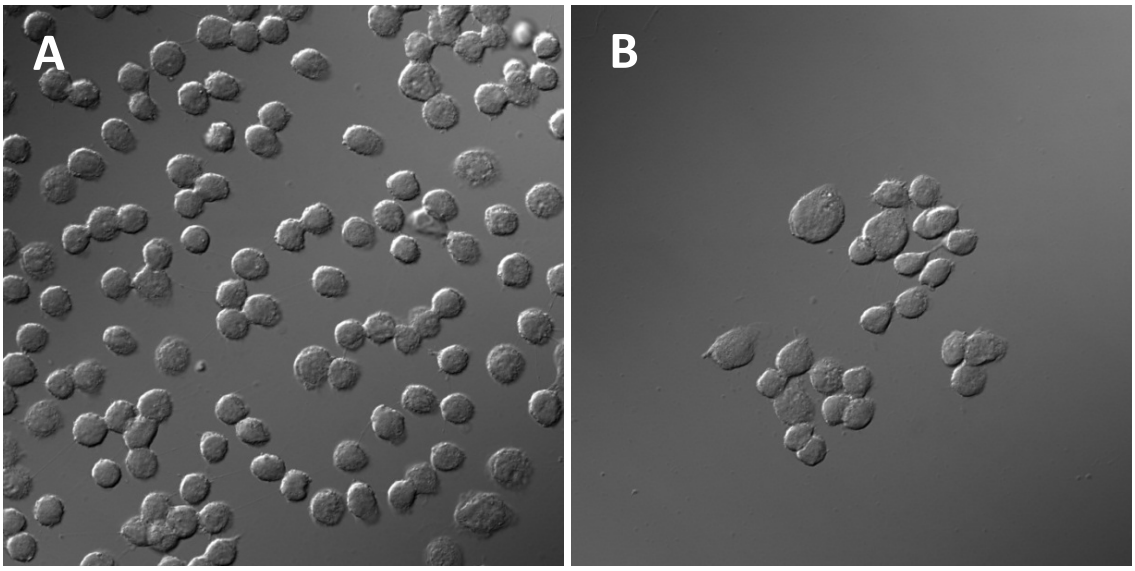

Fig. 3.1. DIC of cover slips originally covered with CHO cells (~80% confluency) after incubation in PBS for 30 min with 2 µM TAMRA-pen-AYL (A) or TAMRA-pen-A(pY)L (B). Note that the cover slips mostly showed sparse single cells (similar to **Fig. 3.3**) and the shown examples are rather exceptional. Generally, most cells were detached after incubation with 2 µM of either peptide

Prior to the 30 min incubation of the cells with the peptides, the cells were rinsed with phosphate buffered saline (PBS). After the incubation with either peptide (2 µM in PBS) the cells detached from the surface (see differential interference contrast (DIC) in **Fig. 3.1**) leading to sparse single cells or groups of cells. Despite of very gentle pipetting the PBS solution along the recipient wall, most parts of the cover slip were simply devoid of cells under these conditions. Cells were therefore assumed to be detached, which was also supported by the round shape of the cells with very little presence of adhesion structures.

In contrast, cells that are attached to the glass support were flat and showed many adhesion structures (compare to **Fig. 3.4**) when incubated with higher CPP concentrations which, in analogy to polylysine glass coatings, might act as a “glue” between cells and the glass support. Upon closer inspection of the individual steps of the experimental procedure it became apparent that the cell monolayer was detaching from the cover slips during the careful washing steps with PBS after incubation of cells with 2 µM of either peptide.

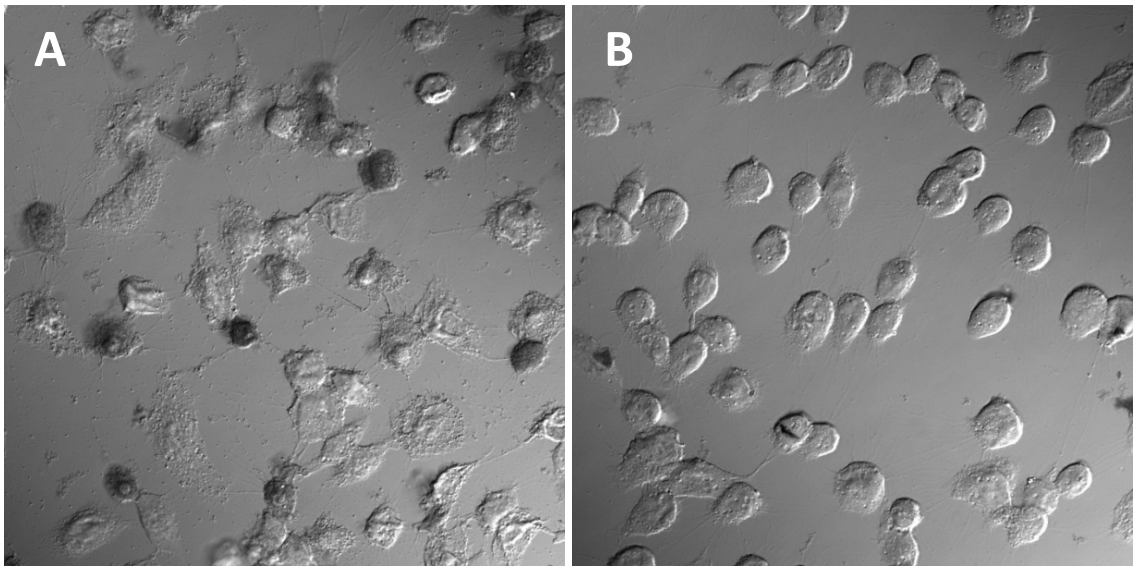

Fig. 3.2. DIC of CHO cells after incubation in PBS for 30 min with 20 µM pAntp mutants. Approximately half of the cells, and thus much more as in **Fig. 3.1**, remained at the cover slip during incubation and related washing steps. Cells incubated with 20 µM TAMRA-pen-AYL frequently died during the procedure **(A)**, whereas they remain healthy in presence of 20 µM TAMRA-pen-A(pY)L **(B)**.

At 20 µM peptide concentration a part of the cells clearly stayed attached to the cover slide. Nevertheless, as the incubation with peptide was done with cells at a confluency of approximately 80%, about 50% must have been detached even at the 20 µM peptide concentration (see **Fig. 3.2**). Despite the high fraction of adsorbed cells, it appears by visual examination of the cells incubated with 20 µM TAMRA-pen-AYL that some cells were destroyed by the peptide (indicated by both dark or empty cell ruins and cell debris across the cover slide; **Fig. 3.2A**). The inherent nature of the DIC imaging contrast suggests that the dark appearance of some cells is due to dense aggregates that might be caused by peptide binding to various cellular polyanions, such as DNA, RNA and heparin sulfate.

On the other hand, cells incubated with 20 µM of phosphorylated TAMRA-pen-A(pY)L appear to be undamaged (**Fig. 3.2B**). They show, however, a similar loss of approximately half of the cells originally attached to the cover slide as when incubated with 20 µM TAMRA-pen-AYL.

In conclusion, the incubation of CHO cells with TAMRA labeled pAntp mutants in PBS impairs cell adhesion and promotes detachment of the cells from the support glass at 2 µM, independent of the peptide (**Fig. 3.1**). In contrast, toxicity, as apparent from dense cell aggregates, is observed for the amphipathic TAMRA-pen-AYL, but not for the phosphorylated mutant. The cell detachment is reduced at higher peptide concentration (20 µM) for either peptide (**Fig. 3.2**).

3.3.2. Cell adhesion when incubated with pure PBS

As described above, higher peptide concentration markedly reduced the detachment of cells during the incubation period, so that CPPs might be considered as an adhesion factor for the cells. We therefore incubated CHO cells with pure PBS for 30 min in order to verify whether PBS alone (and the involved mechanical forces from pipetting) induces the cell detachment from the cover slides. Indeed, as evident in **Fig. 3.3**, incubation with PBS produces the same cell detachment as incubation with 2 µM of either peptide: Apparently, PBS alone (or in combination with the rinsing forces) causes detachment of the cells from the glass surface. 20 µM concentration of either peptide seems to counteract this effect, probably in a similar manner as coating glass surfaces with polylysine (see (13)) for improved cell adhesion.

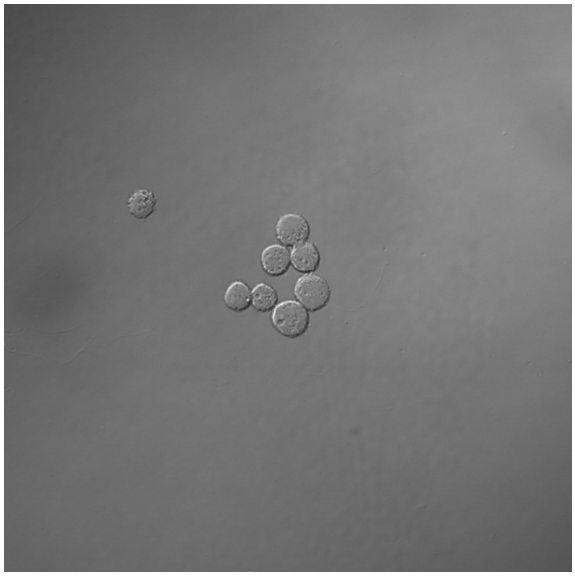

Fig. 3.3. Only spare single cells of the originally attached CHO cells remained on the glass cover slide after a 30 min incubation with pure PBS (originally confluency was ~80%). The incubation with PBS caused most cells to detach from the surface and being flushed away during the subsequent washing steps.

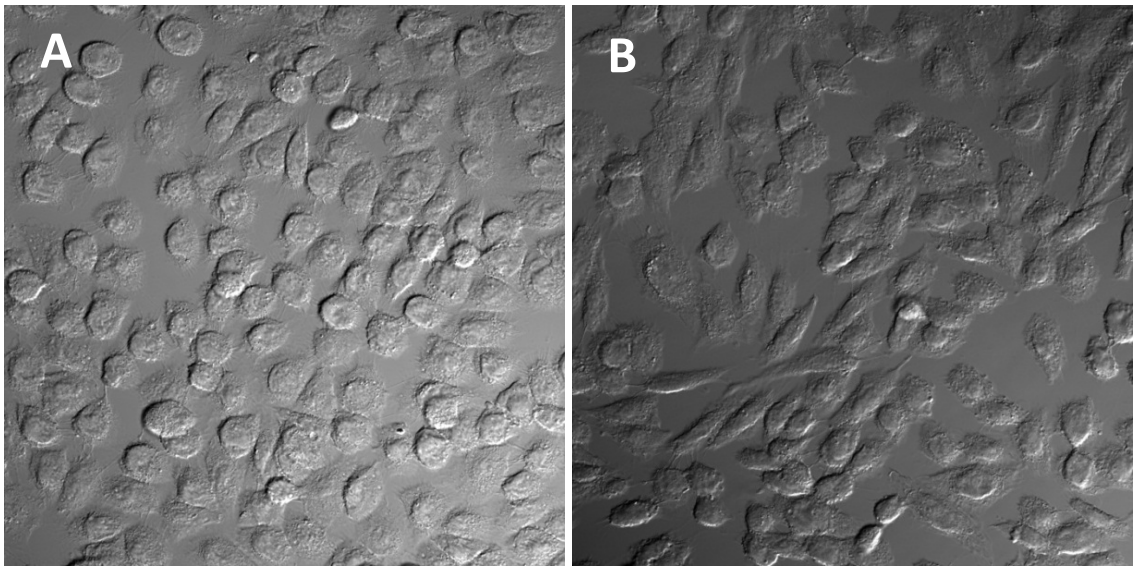

Fig. 3.4. DIC of CHO cells after incubation in DMEM/F12 for 30 min with 2 µM TAMRA-pen-AYL (A) or TAMRA-pen-A(pY)L (B). The cells stayed attached to the cover slip and appeared healthy after incubation with either peptide.

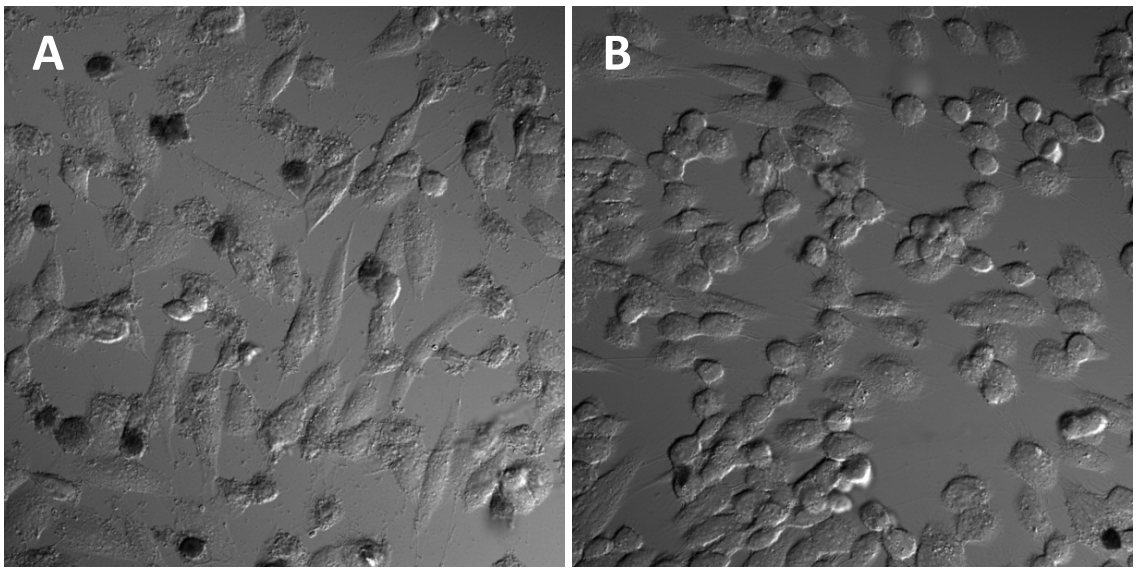

Fig. 3.5. DIC of CHO cells after incubation in DMEM/F12 for 30 min with 20 µM TAMRA-pen-AYL (A) or TAMRA-pen-A(pY)L (B). Although the cells did not detach during the incubation period, 20 µM TAMRA-pen-AYL seems to be much more toxic (as evident by cell ruins and debris) for the cells in contrast to the phosphorylated variant.

3.3.3. Cell adhesion when incubated with peptide dissolved in DMEM/F12

After observing the unfavorable loss in cell adherence upon incubation with PBS, we changed the solvent for incubation with the pAntp mutants to pure DMEM/F12 (1:1 v/v) without adding fetal calf serum (FCS) or other additives. In particular, addition of serum was omitted to prevent interaction or even precipitation between its protein components (especially albumin) and the CPP. When dissolved in DMEM/F12, incubation with either peptide did not cause the loss of cell adhesion that was observed after incubation in PBS. At 2 µM, both peptides did not cause cell detachment from the cover slips, and cells had a healthy aspect (**Fig. 3.5**), as apparent by the cell shape and multiple adhesion structures.

When increasing the concentration of the unphosphorylated TAMRA-pen-AYL to 20 µM, the cell adhesion still remained but, similar as with PBS, half of the cells appeared to be in critical condition, as again indicated by both dark or empty cell ruins and lots of cell debris (**Fig. 3.5A**). In contrast, the phosphorylated TAMRA-pen-A(pY)L peptide did not harm the cells at 20 µM as they still have a healthy appearance after incubation (**Fig. 3.5B**). For both peptides several dark spots are visible in the extracellular space which is probably caused by dense peptide aggregates that produce no fluorescence – most likely because of fluorescence quenching within the aggregates as reported previously (4).

In conclusion, the present observations suggest that the selection of the incubation medium has a profound effect on the ability of CHO cells to adhere on glass cover slips and thus the conclusion derived from the remaining cells on the CPP uptake. Cells being detached may represent more than 50% of the total cells and would not appear in the microscopic observations, so that CPPs effects on the detached cells would remain undocumented. Incubation of cells with peptides dissolved in DMEM/F12 prevents cell detachment during an incubation period of 30 min.

3.4. Discussion

We have investigated the effect of cell culture medium on CHO cells during the incubation with two CPPs, TAMRA-pen-AYL and TAMRA-pen-A(pY)L, at 2 and 20 µM. Both the effect on cell adhesion to the noncoated glass cover slips and CPP's toxicity were assessed by means of confocal microscopy using DIC which provided excellent visual assessment of cell morphology. The cells were incubated with peptide dissolved in either PBS or DMEM/F12.

3.4.1. Cell adhesion in dependence of incubation medium

The adhesion of CHO cells to the glass support after the incubation period was strongly dependent on the choice of incubation medium. In the absence of peptide or at low peptide concentration, incubation with PBS could not preserve the cell-glass contact leading to an almost complete loss of cell adherence to the glass support within 30 min. This effect could be attenuated by a tenfold increase of peptide concentration, where only half of the cells detached after incubation with 20 µM of either peptide. In contrast, cells incubated with peptide dissolved in DMEM/F12 stayed attached to the cover slips independent of peptide concentration.

In cell culture, attachment of cells to plastic or glass surfaces is dependent on various (extra)cellular adhesion molecules (CAMs; e.g. laminin or fibronectin) and membrane-spanning receptor proteins (integrins) that mediate the interaction between the supporting surface and the cell (14). Importantly, there is evidence that the binding of CAMs to the integrin receptor is regulated by divalent cations such as Mg^{2+} or Ca^{2+} (15,16). As PBS buffer is devoid of divalent cations we assume that their absence during incubation induced the overall cell detachment. In contrast, the DMEM/F12 mixture contains millimolar amounts of both Mg and Ca and therefore ensures proper function of the CAMs. Note that we hereby exclude insufficient supply with nutrition during the incubation period as a reason for cell detachment, mainly because the cells stay attached to the surface as well when incubated in presence of electrolytes.

On the other hand, we could observe a decreased detachment of cells after incubation in PBS with either peptide at 20 µM. A higher peptide concentration

therefore seems to diminish the effect of PBS on cell adhesion. A potential mechanism might be that the peptide acts as adhesive between cell and cover slip. A widespread fixation technique is surface coating with poly-L-lysine (13). Immobilization of cultured cells is achieved by electrostatic mediation between the negatively charged silicate groups and carboxylic acids of the glass (17) and cell surface (e.g. proteoglycans; see Kjellén for an extensive review (18)), respectively, by the highly cationic poly-L-lysine homopolymers. As both peptides are highly positively charged under the given conditions, we assume a similar principle to attach the cells to the glass surface with CPPs.

3.4.2. Cell toxicity of TAMRA-pen-AYL

In toxicity studies using peptide concentrations up to 100 µM, the wild-type penetratin did not show noticeable toxicity (19,20). At the same time, wild-type penetratin could not permeate model bilayers such as LUVs – unless under particular conditions such as with giant unilamellar vesicles (21) or in presence of a transmembrane potential (22). Substitution of the amino acids $N_9 \rightarrow A$, $R_{10} \rightarrow Y$ and $K_{13} \rightarrow L$ did change both toxicity and cell-uptake, and this has been described in the previous chapter. It thus might speculated whether cell uptake and cell permeation are coupled.

In particular, the toxicity of the peptide increased upon the 3 amino acid substitution and was concentration dependent as observed by means of DIC microscopy of CHO cells after incubation with TAMRA-pen-AYL. At 2 µM concentration, pen-AYL did not lead to apparent damage of the CHO cells, whereas incubation with 20 µM peptide showed clear cell toxicity, independent of the used incubation medium. At 20 µM most of the cells were obviously damaged as evident by cell ruins and scattered cell debris evident in DIC images.

The CPP uptake into living cells apparently correlates with the membrane perturbation observed on membrane models using LUVs (see previous chapter). Detectable membrane permeation of LUVs by pen-AYL started at a peptide concentration of ≥4 µM. At 16 and 96 µM pen-AYL, 10 and 88% dye leakage from

POPC/POPG/DOPE-PEG (76:20:4 n/n) LUVs was monitored, respectively. In contrast, the phosphorylated pen-A(pY)L induced only 6 and 15% dye leakage at 8 and 96 µM, respectively. In analogy to the CPP uptake, also the cell toxicity was dependent the CPP used and its concentration. During the 30-min incubation with the CPP at 20 µM, only pen-AYL, but not the phosphorylated pen-A(pY)L , damaged the cells leading to the question whether CPP uptake is not an early sign of cell damage.

In this respect, we have previously investigated the effect of pen-2AL (12), the precursor peptide of pen-AYL, on the membrane integrity with ^{31}P NMR spectroscopy. Pen-2AL showed pronounced disturbance of the membrane similar to the detergent Triton X-100 (**first chapter**; (23)). Taken these observations together, we assume that the mechanism responsible for membrane permeation in LUVs might be similar to cell toxicity under the described conditions. Furthermore, the effect is concentration dependent where approximately 10 µM concentrations separated toxic and non-toxic effects of TAMRA-pen-AYL on living CHO cells. Similar concentrations were required to initiate the cell permeation so that this concentration threshold seems to be the current tradeoff between transduction efficacy and toxicity for the particular system. The close concentrations for effective membrane permeation on the one hand and systemic toxicity on the other hand would not be tolerated for clinical applications. The here described CPP phosphorylation might thus prevent systemic CPP toxicity prior to reaching the organ of interest.

3.5. References

1. Lundberg, P., and Langel, U. (2003) J Mol Recognit 16, 227-233
2. Stewart, K. M., Horton, K. L., and Kelley, S. O. (2008) Org Biomol Chem 6, 2242-2255
3. Fischer, R., Kohler, K., Fotin-Mleczek, M., and Brock, R. (2004) J Biol Chem 279, 12625-12635
4. Ziegler, A., and Seelig, J. (2011) Biochemistry 50, 4650-4664
5. Fernandez-Carneado, J., Kogan, M. J., Pujals, S., and Giralt, E. (2004) Biopolymers 76, 196-203
6. Saar, K., Lindgren, M., Hansen, M., Eiriksdottir, E., Jiang, Y., Rosenthal-Aizman, K., Sassian, M., and Langel, U. (2005) Anal Biochem 345, 55-65
7. Deshayes, S., Plenat, T., Charnet, P., Divita, G., Molle, G., and Heitz, F. (2006) Biochim Biophys Acta 1758, 1846-1851
8. Dempsey, C. E. (1990) Biochim Biophys Acta 1031, 143-161
9. Raghuraman, H., and Chattopadhyay, A. (2007) Biosci Rep 27, 189-223
10. Lundberg, M., and Johansson, M. (2001) Nat Biotechnol 19, 713-714
11. Richard, J. P., Melikov, K., Vives, E., Ramos, C., Verbeure, B., Gait, M. J., Chernomordik, L. V., and Lebleu, B. (2003) J Biol Chem 278, 585-590
12. Drin, G., Cottin, S., Blanc, E., Rees, A. R., and Temsamani, J. (2003) J Biol Chem 278, 31192-31201
13. Mazia, D., Schatten, G., and Sale, W. (1975) J Cell Biol 66, 198-200
14. Yamada, K. M. (1983) Annu Rev Biochem 52, 761-799
15. Gailit, J., and Ruoslahti, E. (1988) J Biol Chem 263, 12927-12932
16. Plow, E. F., Haas, T. A., Zhang, L., Loftus, J., and Smith, J. W. (2000) J Biol Chem 275, 21785-21788
17. Behrens, S. H., and Grier, D. G. (2001) J Chem Phys 115, 6716-6721
18. Kjellen, L., and Lindahl, U. (1991) Annu Rev Biochem 60, 443-475
19. Jones, S. W., Christison, R., Bundell, K., Voyce, C. J., Brockbank, S. M. V., Newham, P., and Lindsay, M. A. (2005) Br J Pharmacol 145, 1093-1102
20. Mueller, J., Kretzschmar, I., Volkmer, R., and Boisguerin, P. (2008) Bioconjug Chem 19, 2363-2374
21. Thoren, P. E., Persson, D., Isakson, P., Goksor, M., Onfelt, A., and Norden, B. (2003) Biochem Biophys Res Commun 307, 100-107
22. Terrone, D., Sang, S. L. W., Roudaia, L., and Silvius, J. R. (2003) Biochemistry 42, 13787-13799
23. Sauder, R., Seelig, J., and Ziegler, A. (2011) Methods Mol Biol 683, 129-155

Chapter 4:

Gel formation of pen-Antp variants

4.1. Introduction

The Penetratin peptide (1) (see **Tab. 4.1** for peptide sequences) is among the best studied cell-penetrating peptides (CPP) (2), both in terms of its physicochemical properties and its effect on biological cells. Based on the more amphipathic Penetratin mutant called pen-2AL (designed and described by Drin et al. (3)) we designed a peptide pair to trigger membrane transduction in presence of a phosphatase. In the previous chapters, we could show that dephosphorylation by a phosphatase turns the membrane inactive peptide pen-A(pY)L into the membrane destabilizing pen-AYL (see **chapter 2** for details). We consider this system as an innovative concept for the intracellular delivery of large and/or anionic (macro)molecules that are unable to reach the cytosol, largely because the chemical properties of the cargo molecules naturally preclude passage of the cell membrane. We made, however, a unforeseen property of the peptides when prepared at >~500 µM concentrations, i.e. a self-clustering especially for the zwitterion pen-A(pY)L.

As described in **chapters 1** and **2** (see *determination of peptide concentration*), we prepared 1 mM stock solutions of each peptide by weighing desired amounts (e.g. 2.7 mg pen-AYL/mL solvent) as trifluoroacetate salt into a 2 mL glass vial followed by adding the approximate volume of corresponding buffer. Then the final peptide concentration has been determined spectrophotometrically using the 2 tryptophan

Tab. 4.1. Amino acid sequences of pen-Antp and its investigated variants. Positively or negatively charged residues and groups are in red and blue, respectively. Residues that were substituted from the original Penetratin peptide are underlined.

peptide	Sequence (single letter code)
pen-Antp (penetratin)	RQIK IWFQ NRRM KWKK
pen-2AL	RQIK IWFQ AARM LWKK
pen-AYL	RQIK IWFQ AYRM LWKK
pen-A(pY)L	RQIK IWFQ A(pY)RM LWKK

residues. The peptides dissolved quickly and the solutions were clear and did not show any aggregates visible by eye. If the pen-A(pY)L solution, however, was allowed to stand for ≥36 h at 4 °C, the dissolved peptide either settled to the bottom of the vial forming a gel-like structure (see **Fig. 4.1**) or turned the originally fluid solution into a viscous liquid that would not flow down when turned upside down indicating that the zwitterionic molecule might have a tendency for self-aggregation. The gel-like structure could be dissolved again by shaking with a vortex mixer and subsequent ultrasound bath[4]. Note that this visual observation could only be made for the 1 mM stock solutions but not with solutions of lower peptide concentration, be it diluted from stock or dissolved as powder directly into the desired liquid.

We were then interested in the reason of this behavior and therefore wanted to investigate the possible driving intermolecular force. With this respect, it is important to note that the only difference between this peptide and the also studied pen-AYL peptide, which did not show any aggregation at all, is a phosphor-ester at the tyrosine. Apparently, the negatively charged phosphate group alone is able to promote the interaction between individual peptides in a way that leads to some sort of gelation-

[4] All peptides solutions were treated accordingly immediately prior any dilution or addition in the leakage assay (see chapter 2). Specifically, the solutions were mixed for 1-2 s, followed by a 5 min bath in ultrasound.

hereby referred as peptide clusters - although the peptides' net charge is still largely positive.

Aggregation i.e. formation of clusters out of single dissolved peptides, brings mainly two technical issues when working with such solutions: i) it precludes a proper determination of the peptide concentration because of inhomogeneity and ii) concentrated stock solution thus must be avoided in order to prevent inaccurate dilutions during both preparations and the actual experiment itself.

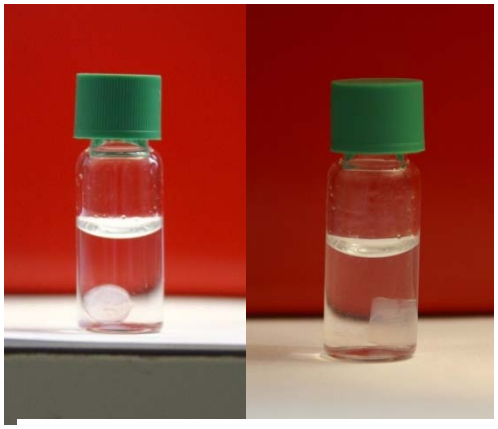

Fig. 4.1. 1 mM pen-A(pY)L in TBS. Note the gel-like structure at the bottom of the glass vial observed only at that high concentrations.

As an opportunity for investigating this effect, all investigated peptides include 2 tryptophan (Trp) residues, which allow i) examination of the concentration by means of optical absorbance and ii) changes in the polarity of the Trp proximity by means of fluorescence spectroscopy methods. In particular, the fluorescence emission of the Trp indole group is highly dependent on the polarity of its proximate environment i.e. around 350 nm in water with a blue shift when brought into a more hydrophobic environment (4). In addition to Trp residues, the peptide also contains a tyrosine (Tyr) moiety that is also a weak fluorophore, but its emission wavelength, in contrast to Trp, is not dependent on the environmental polarity.

The dependency of the Trp fluorescence emission on its environment polarity thus builds the basis for the following investigation to possibly identify the intermolecular force leading to the observed gelation of the pen-A(pY)L peptide. We therefore measured the Trp fluorescence emission of each peptide both at distinct concentrations and either presence or absence of salt in order to screen for electrostatic charge effect being responsible for the interaction. In the case of the charge of the phosphate group contributing to the aggregation we expect this effect to be more prominent in the absence of salt due to the diminished conductivity ("electrostatic screening").

To supplement the data gained by Trp fluorescence spectroscopy, all peptide solutions were further investigated by both dynamic and static light scattering and analytical ultracentrifugation.

4.2. Materials and methods

4.2.1. Materials

1. Buffer (unless indicated otherwise): 20 mM Tris 100 mM NaCl pH 7.4 (TBS).
2. DMSO (Dimethyl sulfoxide) (Sigma-Aldrich, Buchs, Switzerland)
3. L-Tryptophan (Sigma-Aldrich, Buchs, Switzerland).
4. L-Tyrosine (Sigma-Aldrich, Buchs, Switzerland).
5. PEI (Poly(ethyleneimine, 50% (w/v) in H_2O) (Sigma-Aldrich, Buchs, Switzerland).
6. Tris (Merck, Darmstadt, Germany).

4.2.2. Peptide solutions

All peptides were synthesized by Peptide 2.0 (Chantilly, VA) with amidated carboxy-terminus and supplied as trifluoroacetate salt. Purity was ≥97% as judged by HPLC. The 1, 10 and 100 µM stock solutions were prepared by dissolving 1 mg amounts in 90% of the final volume which would result in approximately the desired peptide concentration. Then the pH was adjusted to 7.4 and solvent added to make the final volume. 1 mM stock solutions were prepared the same way but weighing peptide amounts corresponding to a final volume of 1.5 mL. All peptide solutions were allowed to equilibrate for ≥24 h prior to investigation. Solvent volumes or amounts of peptide powder were calculated using the nominal weight of the corresponding trifluoroacetate salt.

4.2.3. Peptide concentration determination

The concentrations of the peptide solutions were determined by Trp absorbance (5) by means of UV-Vis spectroscopy using a single beam Hewlett-Packard 8354 spectrophotometer. Absorbance of 200 µL volumes was measured in quartz micro cuvettes with a path length of 1 cm at 280 nm after blanking with the corresponding buffer. The peptide concentration was then calculated with an extinction coefficient ϵ = 5'500 $M^{-1}cm^{-1}$ per Trp. In case of non-linear response (>1.5 OD), the solution was diluted in order to lower the OD below 1.5. Denoted standard deviations were calculated as

$$\sigma = \sqrt{\frac{\Sigma\,(x - \bar{x})^2}{n}} \qquad (1)$$

with x = sample value, $\bar{x}$ = sample mean average and n = sample number.

4.2.4. Fluorescence Spectroscopy

All experiments were done with a Jasco FP-6500 fluorescence spectrophotometer (JASCO Corp., Japan). Measurements were performed at room temperature using a 0.5 cm (inner diameter) rectangular quartz cuvette with a sample volume of 0.25 mL. Spectrophotometer settings were partially varied for different solute concentrations and are shown in **Tab. 4.2**. All peptide solutions, unless stated otherwise, were excited at 295 nm to minimize Tyr emission.

Specific settings such as excitation and emission wavelengths, slit width or photomultiplier voltage varied depending on the investigated fluorophore and its concentration and are indicated in the corresponding results section. Prior to measurements, the peptide solutions were dipped in an ultrasound bath for 5 min and quickly vortexed to break down eventual existing clusters. During the measurement, the

	[**fluorescent solute**] (μM)			
	1000	100	10	1
Slits (nm)	3	3	3	5
Response time (s)	0.1	0.1	0.1	0.2
PMT $(V)_a$	300	300	400	450
Data Pitch $(nm)_b$	0.5	0.5	0.5	0.5
Scan Speed $(nm/min)_b$	500	500	500	500

Tab. 4.2. Settings for fluorescence emission measurements.
Fluorescent solute refers to either the free L-amino acids or peptide. Response for 1 μM was increased to decrease signal noise.
[a] Photomultiplier tube (PMT) voltage was adjusted that maximum fluorescence intensities were approximately equal for all measurements.
[b] only for spectrum measurements.

samples were stirred with a tiny fluoropolymer coated stir bar magnet unless indicated otherwise. 3 fluorescence emission spectra were successively recorded, and the wavelength corresponding to maximal signal intensity was noted. All denoted values are arithmetic averages of a triplicate experiment with standard deviations calculated using equation (1).

4.2.5. Peptide adsorption to glass

For every measurement, pen-Antp was always freshly diluted from a 100 μM stock solution. In experiments involving PEI, the quartz cell was incubated for 30 minutes with 1% (w/v) PEI dissolved in distilled water and thoroughly flushed with water prior every measurement to prevent adsorption of the peptides to the glass. The settings of the spectrometer were as follows: ex/em bandwidths 3 nm, photomultiplier tube (PMT) voltage 550 V, response time 0.1 s and 0.5 s for single and constant excitations respectively, data pitch 1 s for constant excitations. Wavelengths for excitation and emission were set to 280 and 351 nm, respectively.

4.2.6. Dynamic light scattering

TBS and DMSO were filtered with Filtropure S 0.2 (PES, 0.2 µM; Sarstedt AG, Sevelen, Switzerland) and Fluoropore (PTFE, 0.45 µM; Millipore; Billerica, MA) membranes, respectively, prior both dissolution of peptide or mixing. Measurements were done on a Zetasizer Nano ZS ZEN3600 (Malvern, Worcestershire, UK) equipped with a HeNe laser (633 nm) and backscattering detection. 0.5 mL solutions were measured using rectangular PS semi-microcuvettes with an optical pathway of 10 mm (Sarstedt AG, Sevelen, Switzerland) at 25 °C. For peptide solutions ≤100 µM the measurement position (z) and light attenuation was set to 4.65 mm and 11 (100% transmission), respectively. All samples were measured in triplicates of 10 runs each. Intensity- and volume weighed size distributions, PDI and averaged diameters were all calculated by the Zetasizer software provided by Malvern.

4.2.7. Static light scattering

All measurements were done with the Jasco FP-6500 fluorescence spectrophotometer. Specifically, the following settings were used: 1 nm bandwidth, 2 s response time, 400 V PMT and both excitation and emission wavelengths at 400 nm. 250 µL peptide solutions were measured in a micro quartz cuvette (5 mm inner width) and constantly stirred with a tiny fluoropolymer coated stir bar magnet. The detector was at a 90° angle to the excitation beam. 5 measurements were acquired in 30 s intervals and averaged.

4.2.8. Analytical ultracentrifuge (AUC)

Sedimentation velocity data were measured on a Beckman XL-I (Beckman Coulter, Indianapolis, IN) analytical ultracentrifuge equipped with interference (RI) detection. Experiments either with or without salt were performed with an An50Ti (8 holes) or An60Ti (4 holes) rotor, respectively. Sample and buffer cells were loaded with 400 and 420 µL volumes, respectively, and had a light path length of 12 mm. 999 RI scans were recorded for each individual peptide solution at 3’000 rpm during ~150 minutes and 20

°C. Fitting of AUC data was done with the Sedfit program (6) (7) using the continuous c(s) distribution model. Meniscus and bottom for data of the liquid column, and the fit limits were adjusted graphically. The data were then fitted using the following parameters: resolution 100, s_min 0.0001, s_max 50-100, frictional ratio 1.4, partial spec. volume 0.73, buffer density 1.0054, buffer viscosity 0.01002, fitted baseline, RI Noise and Time Independent Noise.

4.3. Results

4.3.1. Preparation of experimental setup

In order to determine appropriate instrumental adjustments and experimental conditions, the dependence of Trp fluorescence emission on excitation wavelength, potential peptide adsorption and the component of Tyr fluorescence emission were investigated.

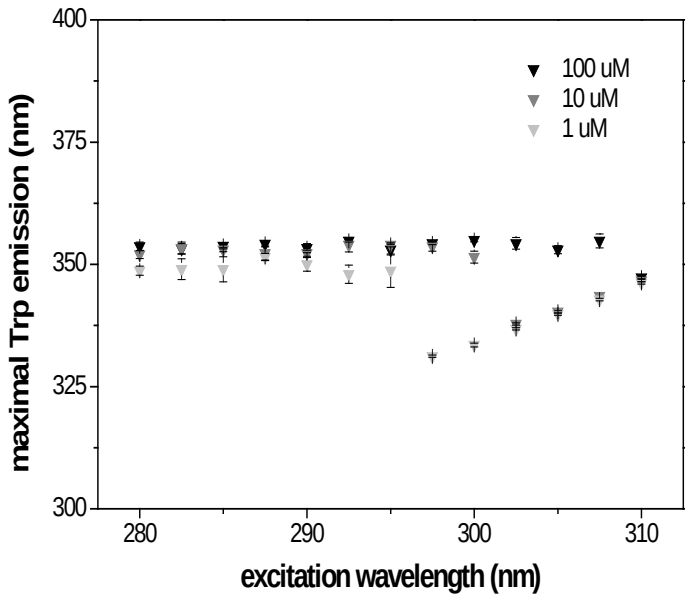

Fig. 4.2. Maximum Trp emission wavelength in dependence of excitation wavelength. 1, 10 and 100 µM L-Trp dissolved in TBS were excited at indicated wavelengths. Error bars are the standard deviation of every triplicate experiment. See text and **Fig. 3** for deviance of 1 and 10 µM Trp at wavelengths of >295 and >300 nm, respectively. At low concentration (1 µM), the curve fitting no longer allowed accurate determination of optimum λ_{em}, because of the presence of a shoulder peak that gave maximum signal when excited at 296-310 nm.

Dependence of maximal tryptophan emission on excitation wavelength.

First, the optimum excitation wavelength for maximum Trp emission was set. For this purpose, the maximum fluorescence emission and wavelength upon different excitation wavelengths for monomeric L-Trp dissolved in Tris buffered saline (TBS) was determined. This was done by measuring fluorescence emission spectra of 1, 10 and 100 µM L-Trp when excited at wavelengths in the near UV range. Because the maximum Trp absorbance is expected at 280 nm and potential Tyr absorption (up to 295 nm) ((5) and (8) page 446 ff.) in future measurements should be avoided, individual spectra were recorded with increasing excitation wavelengths. Specifically, spectra were recorded at excitation wavelengths every 2.5 nm in the range from 280 to 310 nm.

Emission wavelengths with maximal intensity were independent of the excitation wavelength for 100 µM Trp (**Fig. 4.2**). The same was observed for 10 µM and 1 µM at wavelengths of >300 nm and >295 nm, respectively (also **Fig. 4.2**). At low concentration (1 µM), the curve fitting no longer allowed accurate determination of optimum λ_{em}, because of the presence of a shoulder peak that gave maximum signal when excited at 297.5-310 nm (visible in **Fig. 4.3**). This peak was also observed for buffer (TBS) or distilled water (ddH_2O) (**Fig. 4.4**), so that it might originate either from the Raman band of water or from scattering in the instrument. Optimum emission wavelength of Trp was at ~350 nm and is shown in **Tab. 4.3**. It decreases by a couple of nm with lower concentration of Trp which might be the result of unclear maximum values in the curve fitting.

Fluorescence contribution from tyrosine.

In order to modify the pen-2AL peptide with a phosphate group, a Tyr (or pTyr) was introduced at the position of Ala_{10}. Tyr absorbs approximately at the same wavelength range as Trp, but its molar extinction coefficient is lower. Specifically, the absorption maximum of Tyr (at 275.5 nm) has ϵ = 1500 $M^{-1}cm^{-1}$ whereas Trp (at 280 nm) has ϵ = 5800 $M^{-1}cm^{-1}$ (5). In order to test whether the fluorescence of Tyr might interfere, the fluorescence emission of both fluorophores at the previously determined wavelength of maximal Trp emission (~350 nm) was measured. For this

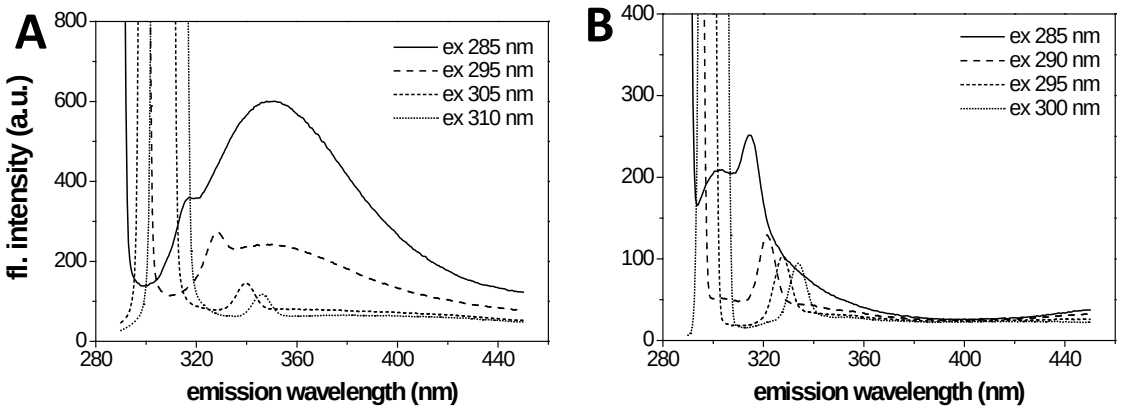

Fig. 4.3. Fluorescence emission spectra of 1 µM L-Trp (A) and 1 µM L-Tyr (B) as excited at indica ted wavelengths. (A) The fluorescence intensity of the shoulder peak left-hand of the Trp emission maximum exceeds at wavelengths >295 nm and shifts the value for maximum intensity to lower wavelengths. **(B)** A similar picture emerges for the Tyr emission spectra. The shoulder peak shifts together with the excitation wavelength and has its maximum approximately 25 nm above it in both measurements. At low concentration (1 µM), the curve fitting no longer allowed accurate determination of optimum λ_{em}, because of the presence of a shoulder peak that gave maximum signal when excited at 296-310 nm.

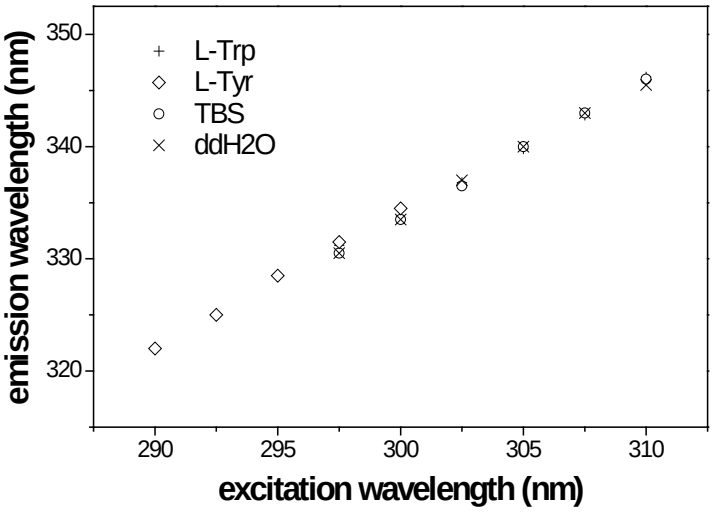

Fig. 4.4. Maximal emission intensity of the shoulder peak in various solutions. The correlation over distinct conditions and solutes implies a measuring artifact produced by the spectrophotometer.

[**L-Trp**] (µM)	Ø wavelength (nm)$_a$	Standard deviation$_b$
1	349.3	1.1
10	352.9	0.9
100	354.0	0.7

Tab. 4.3. Average (of triplicates) wavelength of maximal Trp fluorescence emission intensity.

[a] averages were calculated with values between 280-295, 280-300 and 280-307.5 nm for 1, 10 and 100 µM, respectively.

[b] calculated with (1) (see methods).

purpose, the emission spectra of free L-Tyr were measured with emission between 290 and 450 nm when excited between 280 and 300 nm (2.5 nm steps). The Tyr signal portion corresponding to the averaged emission intensities at wavelengths of maximal Trp fluorescence emission (as gathered in **Tab. 4.3**) relative to the Trp signal (=100%) where then calculated and are shown in **Tab. 4.4**.

[**L-Tyr**] (µM)	excitation wavelength (nm)				
	280	285	290	295	300
	Tyr signal relative to Trp signal (%)[a]				
100	**3.0**	**2.1**	**0.7**	**0.8**	**2.0**
10	**3.8**	**3.1**	**2.1**	**3.7**	**9.4**
1	**8.2**	**7.3**	**7.2**	**10.4**	**17.1**

Tab. 4.4. Average (of triplicates) of Tyr fluorescence emission intensity relative to Trp when excited at given wavelengths. Emission wavelengths correspond to rounded values as determined in **Fig. 4.4**. [a] Trp emission intensity corresponds to 100%.

Overall, the relative signal portion of L-Tyr is less than 5% at both 10 and 100 µM and, as expected, decreases with increasing excitation wavelength. However, at 1 µM the portion of L-Tyr signal exceeds 5% at all wavelengths and reaches its maximum with 17.1% at 300 nm. The increase of the Tyr signal portion at wavelengths ≥295 nm can partially be explained by the slight blue shift of the Trp maximum emission wavelength (**Tab. 4.3**). Some of the spectra of 1 µM L-Tyr are shown in **Fig. 4.3B** for closer inspection. Similar to the Trp emission spectra a peak appears approximately 25 nm above the excitation wavelength that raises the emission signal to relatively higher intensities when compared to 10 or 100 µM. As depicted in **Fig. 4.4** the wavelength of maximal intensity of this peak aligns again linearly with the excitation wavelength, further indicating a measurement artifact.

Regarding both the negligible portion of Tyr when excited at <295 nm and the fact that the peptides of interest contain 2 Trp but only 1 Tyr, we could safely chose to neglect the Tyr component of the fluorescence signal for further investigations on Trp fluorescence emission shifts.

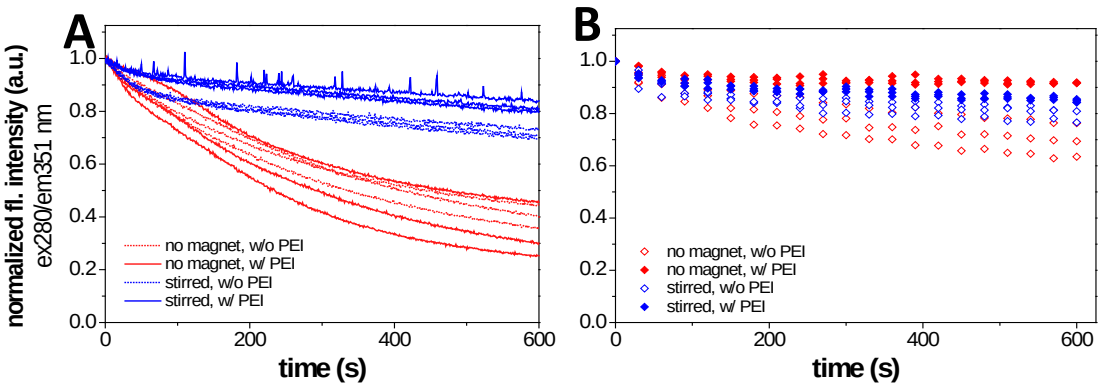

Fig. 4.5. Absorbance of 0.5 µM pen-Antp to the surface of the quartz cuvette over the time course of 10 min when excited constantly (A) or once every 30 s (B). (A) The fluorescence emission intensity decreases by ~60% when unstirred whereas the decrease is less than 20% when stirred. **(B)** The decrease of fluorescence is approximately halved when not constantly excited. Incubation of the cuvette with 1% (w/v) PEI before the measurement slightly diminishes this decrease in fluorescence emission for all conditions.

Peptide adsorption.

As reported by several authors (9-11), peptides with multiple positive charges such as pen-Antp (7 nominal positive charges) are prone to adsorption to glass- and fluorocarbon-based polymer surfaces. In the case of negatively charged quartz glass surfaces (e.g. in a glass cuvette used in spectroscopic measurements) (12) electrostatics dominate the adsorption whereas for plastic it is ascribed to hydrophobic interactions. Because pen-Antp can adopt a helical conformation possessing amphipathic properties, either interaction may take place depending on the present surface.

Pen-Antp was shown to be taken up by live cells at already low micromolar concentration (13-15). Potential peptide adsorption at such concentrations to glass or plastic surfaces may bias experiments. For instance, part of a study done by Persson et al. reports an approximate 70% loss of Trp fluorescence of a stirred 0.5 µM pen-Antp solution in a 10 x 10 mm quartz cell within one hour (11). However, a foregone 30 min incubation of the cell with 1% (w/v) polyethyleneimine (PEI) could diminish the fluorescence loss below 25% (11). As the pen-Antp variants in our study are still highly positively charged (5 nominal charges), we repeated the experiment done by Persson describing adsorption of pen-Antp to quartz glass and fluoropolymer surfaces by means of Trp fluorescence.

Fig 4.5A shows triplicates of the normalized time traces of a constantly excited 0.5 µM pen-Antp solution, both with and without magnetic stirrer in a 5 x 5 mm quartz cell either incubated with 1% (w/v) PEI for 30 min or not. Under these conditions, stirring of the solution during the measurement had a much more pronounced effect compared to incubation with PEI. The unstirred solution has a signal loss of approximately 60% whereas the stirred solution only loses 15 or 25% depending if incubated with PEI or not, respectively. Interestingly, the difference diminished when the solution was not excited constantly but only for single times every 30 s (**Fig 4.5B**). According to these results, photo-bleaching of the fluorophore seems to affect the fluorescence signal more than surface absorption of the peptide. Ultimately, incubation with PEI could prevent a relative signal decrease of 10% of a stirred 0.5 µM pen-Antp solution that is constantly excited with the mentioned parameters. In contrast to the results from Persson, stirring of the solution prevented the loss of fluorescence signal over time much more than incubation of the quartz cuvette with PEI. Since the solutions were continuously stirred and desorption of PEI might cause other (electrostatic) interferences, it was decided to not pre-saturate the glass with PEI.

peptide	***buffer***	***name***
pen-AYL	20 mM Tris pH 7.4	pen-AYL no salt
	20 mM Tris 100 mM NaCl pH 7.4	pen-AYL TBS
pen-A(pY)L	20 mM Tris pH 7.4	pen-A(pY)L no salt
	20 mM Tris 100 mM NaCl pH 7.4	pen-A(pY)L TBS

Tab. 4.5. Peptide solutions and their buffers. All solutions were prepared at peptide concentrations of 1, 10, 100 and 1000 µM.

4.3.2. Peptide solutions

The different peptide concentration were obtained in individual preparations in order to study the observed gel formation in 1 mM pen-A(pY)L stock solutions. We

chose peptide concentrations of 1, 10, 100 and 1000 µM of both pen-AYL and pen-A(pY)L to both investigate a potential concentration dependence of this event and avoid improper dilution from concentrated stock solutions. For every concentration two peptide solutions were prepared using either TBS or a buffer solution of 20 mM Tris omitting electrolytes. An overview of the composition of all investigated peptide solutions is given in **Tab. 4.5**.

Peptide concentration determination.

The concentration of every peptide solution was determined by means of Trp absorption (5) using UV-Vis spectroscopy. The observed imprecision (spectrophotometer and fitting routine) of this method is less than 10 mOD and all of the pen-Antp variants include two Trp resulting in a total extinction coefficient of 11'000 $M^{-1}cm^{-1}$. We therefore have a good signal-to-noise ratio with 1 mM peptide stock solutions (resulting absorbance of ~1.1 upon 1:10 dilution) and usually assessed a deviation of less than 5% from the calculated concentration e.g. a pen-2AL stock solution calculated as 1 mM was determined to have an apparent concentration of 0.96 mM (data not shown). Precision was sufficient (<10% coefficient of variation) for concentrations down to 10 µM e.g. the calculated OD of a 10 µM pen-Antp solution in a cell of 1 cm length is 0.11.

As apparent in **Tab. 4.6**, the measured peptide concentration is lower than calculated by weight (using the molecular weight of the corresponding trifluoroacetate salt). The small amounts weighed in for concentrations <100 µM added more error from the balance as compared to the imprecision of the spectrophotometric method. For example, the results from the 1 µM solutions were inconsistent because either i) some of them show negative absorbance or ii) a relatively high signal-to-noise ratio (e.g. 0.81 for 1 µM pen-A(pY)L without salt). The 10 µM peptide solutions have concentration deviations between 31.9 and 95.5%. The 100 µM peptide solutions are closest to the calculated concentrations with deviations ranging from 12.4 to 16.4%, so that this mode of preparation was preferred in the following. At 1 mM, we measured again larger deviations between 13.3 and 68.2% which might be due to the tendency of gel formation of the penA(pY)L peptide.

			20 mM Tris 100 mM NaCl pH 7.4				20 mM Tris pH 7.4			
			calculated pept. conc. (mM)				calculated pept. conc. (mM)			
			0.001	**0.01**	**0.1**	**1**[a]	**0.001**	**0.01**	**0.1**	**1**[a]
pen-AYL	sample (OD@280 nm)	1	-3.78E-03	7.06E-02	1.24E+00	1.08E+00	-9.88E-03	5.58E-02	9.30E-01	1.24E+00
		2	-3.22E-03	7.60E-02	1.23E+00	1.09E+00	-2.36E-02	5.36E-02	9.20E-01	1.27E+00
		3	-8.24E-03	7.38E-02	1.24E+00	1.09E+00	-2.62E-02	5.52E-02	9.20E-01	1.23E+00
	average		-5.08E-03	7.49E-02	1.24E+00	1.09E+00	-1.99E-02	5.44E-02	9.23E-01	1.25E+00
	standard deviation[b]		2.25E-03	2.22E-03	4.71E-03	4.71E-03	7.16E-03	9.29E-04	4.71E-03	1.70E-02
	conc. (mM)		**-4.62E-04**	**6.81E-03**	**1.12E-01**	**9.88E-01**	**-1.81E-03**	**4.95E-03**	**8.39E-02**	**1.13E+00**
	Δ absolute		-1.46E-03	-3.19E-03	1.24E-02	-1.21E-02	-2.81E-03	-5.05E-03	-1.61E-02	1.33E-01
	Δ %[c]		**-146.2**	**-31.9**	**12.4**	**-1.2**	**-280.8**	**-50.5**	**-16.1**	**13.3**
pen-A(pY)L	sample (OD@280 nm)	1	3.49E-02	2.40E-01	1.27E+00	1.88E+00	-5.88E-03	6.38E-02	9.30E-01	1.19E+00
		2	3.47E-02	2.20E-01	1.27E+00	1.82E+00	-5.58E-03	7.44E-02	9.10E-01	1.29E+00
		3	4.06E-02	2.10E-01	1.26E+00	1.85E+00	1.32E-02	6.56E-02	9.20E-01	1.29E+00
	average		3.67E-02	2.15E-01	1.27E+00	1.85E+00	5.80E-04	7.00E-02	9.20E-01	1.26E+00
	standard deviation[b]		2.74E-03	1.25E-02	4.71E-03	2.45E-02	8.92E-03	4.63E-03	8.16E-03	4.71E-02
	conc. (mM)		**3.34E-03**	**1.95E-02**	**1.15E-01**	**1.68E+00**	**5.27E-05**	**6.36E-03**	**8.36E-02**	**1.14E+00**
	Δ absolute		2.34E-03	9.55E-03	1.52E-02	6.82E-01	-9.47E-04	-3.64E-03	-1.64E-02	1.42E-01
	Δ %[c]		**233.9**	**95.5**	**15.2**	**68.2**	**-94.7**	**-36.4**	**-16.4**	**14.2**

Tab. 4.6. Concentration determination of the various peptide solutions by absorption at 280 nm. All concentrations were calculated as $c_{pep} = \frac{OD_{280nm}}{\varepsilon_{Trp}\, l}$ with ε_{Trp} = 5'500 $M^{-1}cm^{-1}$ and l = 1 cm. **(Red cells)** negative absorbance signal.

[a] diluted 1:10 prior measurement.

[b] calculated with (1)

[c] Δ % is the relative deviation of the apparent concentration from the calculated concentration (calculated concentration = 100%).

4.3.3. Trypthophan fluorescence emission shifts of pen-Antp variants

Because the Trp fluorescence is sensitive to changes in solvation, the potential clustering of peptides was investigated by means of the peptides Trp fluorescence shifts. Observations were done while varying both peptide concentration and presence of electrolytes (NaCl). Clustering of peptides was expected to shift the Trp fluorescence emission to shorter wavelengths (blue shift) if the Trp's indole moiety is brought into a more nonpolar environment.

Trp fluorescence of pen-2AL with salt.

We first investigated the Trp fluorescence of pen-2AL, which has been reported to have a random coil conformation in aqueous solution without reports of aggregation (3). This peptide sequence differs in only 1 amino acid from both pen-AYL and pen-A(pY)L. **Tab. 4.7** shows the averaged wavelengths corresponding to maximal Trp emission in TBS which all are between 351-352 nm. This value closely matches the emission maximum of Trp in aqueous solution which is around 350 nm (also shown in **Tab. 4.3**) and goes along with the aforementioned observation of a monomeric state of pen-2AL at the given conditions.

Trp fluorescence of pen-AYL.

1 mM stock solutions of the peptide did not show gel-like aggregation as observed with DLS. The measured Trp emission maxima of pen-AYL both with and without 100 mM NaCl are shown in **Tab. 4.8**. Similar to p2AL in TBS, the Trp emission maxima are ~ 352 nm for all but 2 conditions: at 100 µM with salt and at 1 mM without salt the emission shifts to shorter wavelengths of 345 and 348 nm, respectively, which might result from insufficient precision for the rather flat curve maximum observed. As the Trp emission maxima mostly resembled both that of pen-2AL and L-Trp in aqueous solution we assume that the two Trp of pen-AYL are in a polar, aqueous environment and therefore the peptide is primarily monomeric at the given conditions as well.

		average max wl (nm)	
		TBS pH 7.4	St. dev. (±)
[**pen-2AL**] (μM)	1	**351.2**	1.2
	10	**351.7**	1.0
	100	**351.9**	0.6
	1000	**350.9**	0.6

Tab. 4.7. Averaged (of triplicates) wavelengths corresponding to maximal Trp fluorescence emission intensity of pen-2AL dissolved in TBS at concentrations of 1, 10, 100 and 1000 μM.

		average maximum wavelength (nm)			
		TBS pH 7.4	St. dev. (±)	20 mM Tris pH 7.4	St. dev. (±)
[**pen-AYL**] (μM)	1	**351.9**	0.9	**352.6**	0.9
	10	**351.7**	0. 9	**352.4**	0.5
	100	**345.4**	1.0	**352.6**	0.6
	1000	**352.8**	0.3	**348.2**	0.7

Tab. 4.8. Averages (of triplicates) of maximal emission wavelengths of pen-AYL. Overall, emissin maxima are around 352 nm, matching that of Trp in aqueous solution. Exceptions are 100 μM with salt and 1 mM without salt showing blue shifts of 7 and 4 nm, respectively.

		average maximum wavelength (nm)			
		TBS pH 7.4	St. dev. (±)	20 mM Tris pH 7.4	St. dev. (±)
[**pen-A(pY)L**] (μM)	1	**351.6**	1.3	**352.6**	1.7
	10	**351.8**	0.6	**351.7**	1.1
	100	**350.6**	0.6	**352.3**	0.7
	1000	**342.6**	0.6	**344.4**	0.9

Tab. 4.9. Averages (of triplicates) of maximal emission wavelengths of pen-A(pY)L. The emission maximum of 1 mM both in presence and absence of salt is shifted to shorter wavelengths indicating a change of the polarity in the Trp proximity. Emission maxima of the other peptide solutions correspond to that free monomeric pen-2AL.

Trp fluorescence of pen-A(pY)L.

As shown in **Tab. 4.9**, the Trp emission maxima of 1, 10 and 100 µM pen-A(pY)L are again mainly around 351-352 nm, independent of the presence or absence of salt. The peptide is therefore assumed to be primarily monomeric at these concentrations as well. However, at 1 mM, the emission maxima of both solutions show a shift down to 342.6 and 344.4 nm with and without salt, respectively. This shift implies a change of polarity in the proximate environment of the Trps which correlates with the changes observed with DLS at these high concentrations.

4.3.4. Dynamic light scattering of peptide solutions

In a first attempt to assess the size of the peptide clusters we used dynamic light scattering (DLS) to investigate both peptides dissolved in TBS. The obtained size distributions (weighted with both signal intensity or volume) at both 100 µM and 1 mM are shown in **Fig. 4.6** (pen-AYL) and **Fig. 4.7** (pen-A(pY)L; the particle diameters of individual peaks in the volume-weighted graphs correspond to the average size distribution of three measurements). Solutions of 1 and 10 µM had not enough scattered signal for such small and monomeric peptides, so that measurements failed to deliver reliable data.

It is important to note that the signal in the intensity distribution profile is dependent on the 6^{th} power of the radius of the scattering particle. The signal intensity of registered particles accordingly increases by a factor of 10^6 for an order of magnitude in its size. This means the difference in signal intensity between two particles with a diameter of 10 and 1000 nm is 10^{12}! Accordingly, size determination of small particles cannot be reliably measured with this technique in the presence of even small amounts of larger particles. As an important consequence, the following observations only serve as a suggestion that *some* of the peptide molecules in a preparation might be aggregated, whereas the technique does not allow to determine how much of all peptide molecules are aggregated. This is especially important to note, because the method is not sensitive to resolve the peptide diameter at concentrations <1 mM even in the absence of aggregates.

Pen-AYL solutions in TBS.

The 1 mM pen-AYL peptide solution shows a distinct shift to larger particle sizes when compared to 100 µM (**Fig. 4.6B** and **D**). At 100 µM, the signal intensity distribution shows 3 peaks with comparable intensity (**Fig. 4.6A**), indicating that the main fraction of observable (!) particles has a size between 20 and 120 nm. There are, however, larger particles with a diameter around 700 nm present as well (**Fig. 4.6B**).

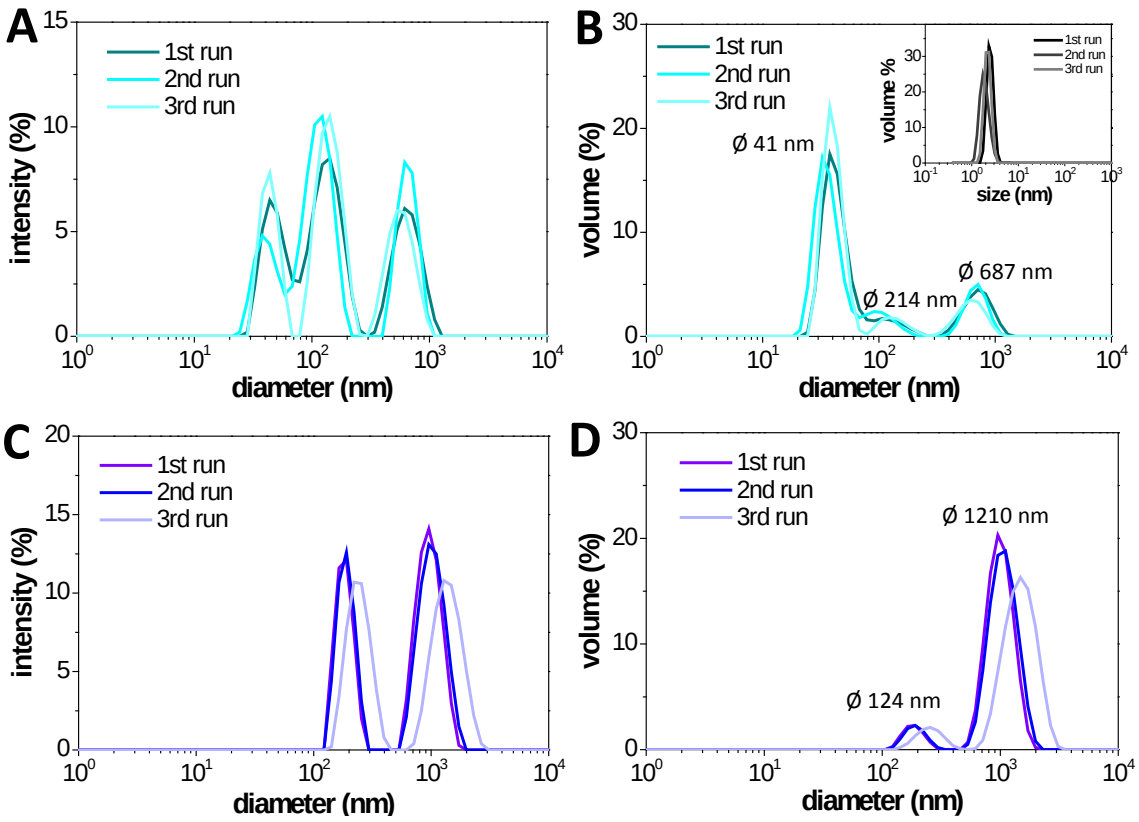

Fig. 4.6. DLS of 0.5 mL pen-AYL TBS solutions. Shown are the signal intensities **(A, C)** and corresponding volume-weighted **(B, D)** size distributions of 100 µM **(A, B)** and 1 mM **(C, D)** peptide, respectively. The peptide seems to mainly form two distinctly sized clusters; one at a dimension around 10 to 100 nm and another at 600 to 1200 nm. At 1 mM, equilibrium seems to shift to formation of the larger particles when compared to 100 µM. The indicated particle diameters were calculated from the averaged size distribution of the triplicate run. **(B; inset)** Volume-weighted size distribution of a 0.5 mL 340 µM pen-Antp TBS solution.

The polydispersity index[5] (PDI) was 0.653 with a light transmission of 30% which confirm a really broad size distribution. At peptide concentration of 1 mM the signal of larger particle sizes (diameter of 1200 nm) dominates (**Fig. 4.6D**). Smaller particles were still detected and probably correspond to the smaller species observed at 100 µM but a specific size description is not appropriate because the large difference in signal intensity (**Fig. 4.6C**). Accordingly, we detected a high PDI of 0.538 and a diminished light transmission to 0.1% which further attests to an increased population of larger sized particles.

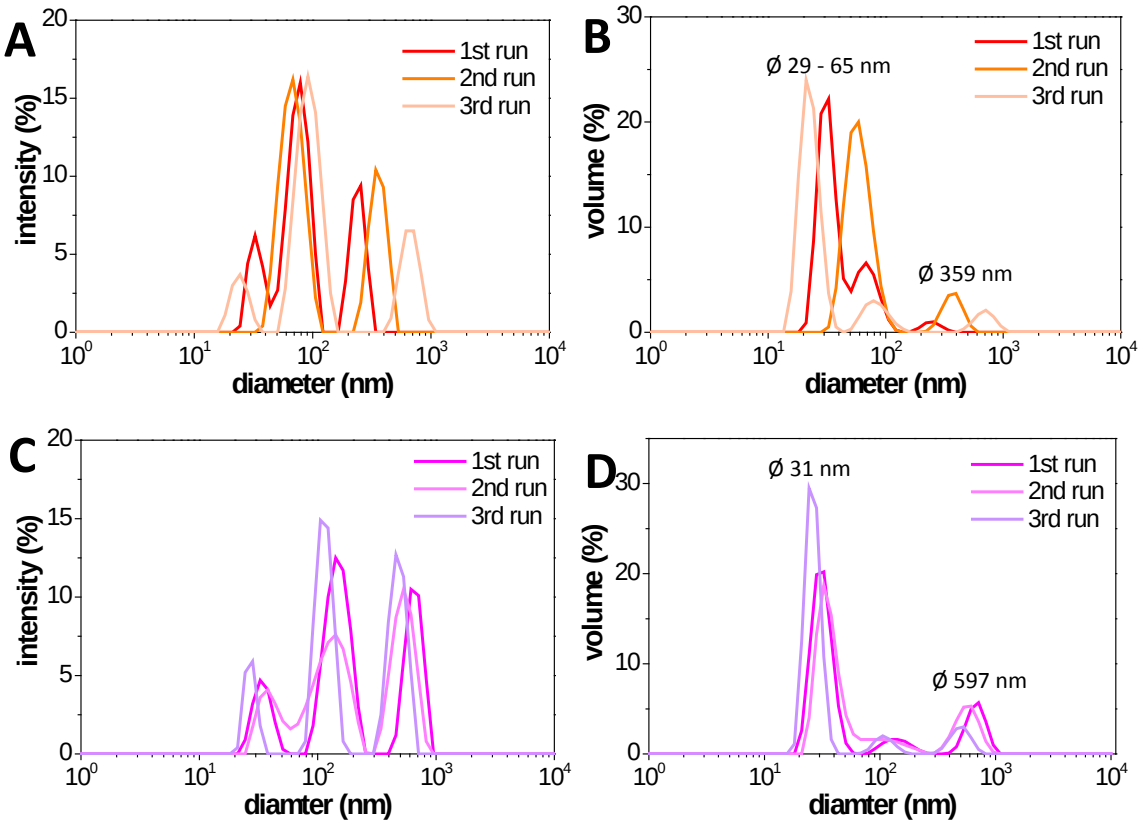

Fig. 4.7. DLS of 0.5 mL pen-A(pY)L TBS solutions. Shown are the signal intensities **(A, C)** and corresponding volume-weighted **(B, D)** size distributions of 100 µM **(A, B)** and 1 mM **(C, D)**, respectively. The peptide is distributed in two fractions of different size at both concentrations. The main fraction shows a smaller diameter of 20 to 120 nm whereas the less large particles exist at couple of hundreds nm. Indicated particle diameters were calculated from the averaged size distribution of the triplicate run.

[5] The PDI is a dimensionless parameter provided by a fit of the correlation data and describes the size distribution of the sample. A PDI of ≤0.05 corresponds to a monodisperse sample whereas a PDI of ≥0.7 indicates a very broad size distribution of registered particles.

Pen-A(pY)L solutions in TBS.

Solutions of 100 µM pen-A(pY)L show a similar signal distribution than 100 µM pen-AYL (**Fig. 4.7A**) suggesting the absence of larger aggregates (>1000 nm). Nevertheless, there are two size species, one between 10 to 100 nm and a second between 100 and 1000 nm. The corresponding diameters in **Fig. 4.7B** should be treated as rough estimates because of the apparent polydispersity of the sample. Specifically, the PDI amounts to 0.446 at 30% light transmission.

Interestingly, the signal distribution at 1 mM pen-A(pY)L (**Fig. 4.7C**) matches the one of 100 µM pen-AYL very closely. In fact, the solution seems to comprise the same two populations of 20 to 120 nm and approximately 600 nm (**Fig. 4.7D**). PDI and light transmission were 0.557 and 1%, again like the corresponding pen-AYL sample. This result suggests that pen-A(pY)L does not produce distinct aggregates at concentration >1mM, but rather a gel-like structure that produces correlation times too long to be assessed by DLS.

Pen-AYL and pen-A(pY)L in DMSO/TBS mixtures.

Optical investigation (**Fig. 4.1**) of both peptides pen-AYL and pen-A(pY)L dissolved in TBS showed unknown fractions of larger peptide assemblies (eventually resulting from the amphipathic structure)). Formation of such clusters apparently occurs without requirement for ionic interactions, as indicated by the Trp fluorescence experiments. An alternative interaction could be hydrophobic attraction. If this was the case, the interaction between individual peptide molecules should be weakened in a less polar solvent such as dimethyl sulfoxide (DMSO), which is widely used as solvent for many nonpolar compounds. We therefore investigated 100 µM solutions of peptide dissolved in mixtures of DMSO/TBS with varying composition of the two solvents, ranging from 10 to 90% (v/v) of one or the other by means of DLS. In contrast to the peptide dissolved in pure TBS, however, we were not able to detect any peptide assemblies in mixtures with a DMSO content ≥70% (v/v). Thus, DMSO seems to manage to properly dissolve the peptide, thereby dropping its signal intensity below the detection threshold of the used device (reflecting also the observation that the monomeric peptide diameter could not be assessed with this technique at that low

peptide concentration). The measured volume distribution of 340 µM pen-Antp in TBS is shown in the inset of **Fig. 4.6B** as comparison with the signal of a monomeric peptide of virtually the same size. We therefore chose to simply plot both the count rate and PDI of the measured peptide solutions against the DMSO content to display the dependence of peptide cluster formation on the solvent composition.

Fig. 4.8A shows the count rate of 100 µM peptide in dependence of its DMSO content (at constant measurement depth (4.65 mm) and light attenuation (100% transmission). Both peptides show a similar tendency to assemblies at a DMSO content of ≤40% (v/v). The small difference in count rate, however, suggests that the fraction of

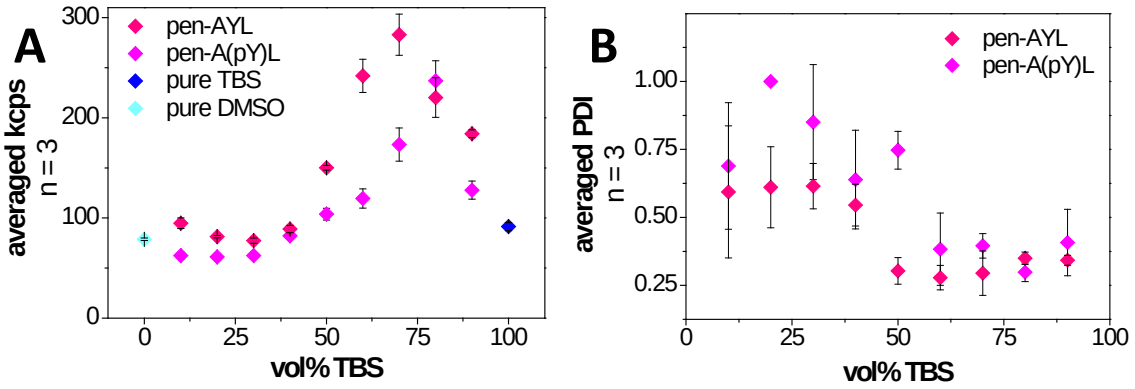

Fig. 4.8. DLS of 100 µM pen-AYL and pen-A(pY)L in mixtures of TBS and DMSO. (A) Averaged count rate (in kcps using same attenuator and z-position settings of 11 and 4.65 mm) in dependence of the volume content of TBS. The signal below 50% (v/v) TBS corresponds to that of pure DMSO what we interpret as dissolved peptide. Count rates for both pure TBS and DMSO are indicated for reference**. (B)** PDI of the same measurements. At a TBS content below 50% (v/v) the polydispersity escalates accordantly to the decrease in count rate in A.

assemblies is likely representing a minor part of all peptide molecules. Above 40% (v/v) DMSO, the signal basically corresponds to that of pure DMSO what we interpreted with monomeric peptides. The observed molecule size slightly increased at 20 and 30% (v/v) DMSO and ultimately dropped again above. A very similar dependence on the DMSO content of the solvent is apparent for the PDI of the investigated peptide solutions (**Fig. 4.8B**). The samples show a very high polydispersity and, more importantly, a large

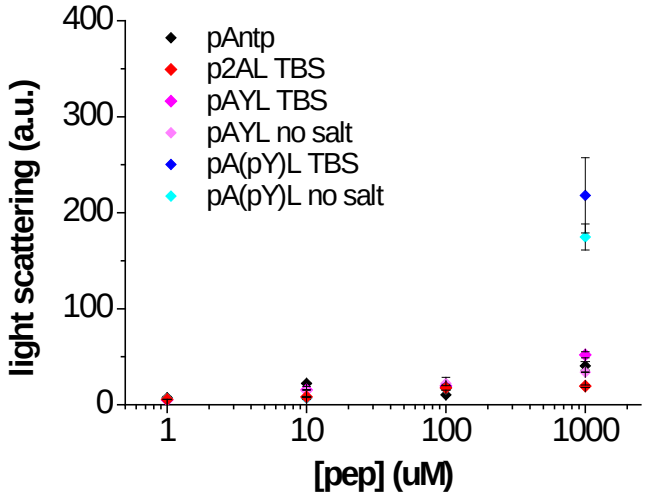

Fig. 4.9. Static light scattering of pen-Antp and its variants.
Pen-Antp and pen-AYL both with and without salt show an approximately linear correlation between concentration and light scattering, implying a monomeric state at the given conditions.
In contrast, pen-A(pY)L in both conditions and pen-2AL show a clearly increased signal at 1 mM, but not at lower concentrations.

fluctuation in solvent with a DMSO content of ≥50% (v/v). The large fluctuation might be explained by the absence of a scattering signal and thus an insufficient precision of the method for peptide monomers. Formation of peptide clusters is then further indicated by the decrease of the PDI to approximately 0.3 at a DMSO content of ≤50% (v/v).

4.3.5. Static light scattering of peptide solutions

In order to compare the signs for assemblies of the amphipathic peptide at concentrations >100 µM, the data obtained from the Tryptophan fluorescence with a distinct technique, we harnessed static light scattering (SLS) of the same peptide solutions. The solutions were irradiated with monochromatic light with a wavelength of 400 nm, thereby avoiding specific absorption by atomic groups of the peptides (specifically, Tyr and Trp around 280 nm and the peptide bond around 230 nm). As the scattering of light is dependent on the 6^{th} power of the diameter of the scattering particle, the signal intensity is expected to linearly increase with the peptide concentration for monomeric peptides. The signal by peptide clusters, however, is expected to increase non-linearly because of increasing size of the particles. With only 4 concentrations for every peptide and the low signal with diluted solutions, however, we lack in sufficient data for a quantitative analysis such as Zimm plots.

Fig. 4.9 shows the results of SLS. For reference of a monomeric peptide solution, we included solutions of pen-Antp as well. The light scattered by pen-p2AL and pen-AYL either with or without salt had similar intensities as the corresponding pen-Antp solutions indicating a monomeric state for those peptides at the given conditions as well. In contrast, both pen-A(pY)L solutions scattered approximately 4 times more at concentrations >100 µM, which in turn correlates with the blue shift of the Trp emission of these solutions (see **Tab. 4.9**). Overall, the pen-2AL peptide showed the least scattering of all peptides.

4.3.6. Sedimentation velocity by analytical ultracentrifugation of peptide solutions

Theoretical background.

The Brownian motion of a dissolved macromolecule, such as a peptide, depends on a number of factors including its physical properties such as mass, shape and density (mathematically described by the Einstein–Smoluchowski relation). On the other hand, its diffusion in a solvent is described by Fick's Laws. When an external force, such as centrifugal force, is applied, the peptide then moves with a certain velocity against diffusion and flotation described by the sedimentation flux. Thus, we can obtain a peptide's mass by investigation of its migration during centrifugation. This fact forms the basis for determination of several parameters such molecular mass, shape or size distribution by analytical ultracentrifugation (AUC).

In an actual AUC experiment, sample cells get loaded with the sample solution assuming a homogeneous distribution of the dissolved molecule of interest across the cell. Optical detection of the peptide distribution is done by either absorbance measurements if it exhibits a chromophore or by interference created by differences of the refractive index in the solution caused by the molecule. In both cases, the signal from the sample cell is obtained by comparison to a reference cell containing only buffer. By applying centrifugal force the dissolved molecules then sediment to the bottom of the cell. Visually, sedimentation can be followed by the moving boundary of the dissolved peptide. Numerically, both the diffusional flux ($j_D(r)$; defined by Fick's

law) and the sedimentation flux ($j_s(r)$) of a molecule in a volume located at r into a neighboring volume at $r + dr$ are described by

$$j_D(r) = -D\frac{dc}{dr}$$

$$j_s(r) = -s\omega^2 rc(r)$$

with D as the diffusion coefficient, s as sedimentation coefficient, c as molecule concentration and ω as angular velocity of the rotor. Using these two equations and further assuming a sector-shaped cell, the Lamm equation

$$\frac{dc}{dt} = \frac{1}{r}\frac{d}{dr}\left[rD\frac{dc}{dr} - s\omega^2 r^2 c\right]$$

can be derived, which describes the evolution of the concentration distribution between the meniscus and the bottom of the cell in a centrifugal field over time. Computed analysis of the Lamm equation can be done on a regular PC using a dedicated software tools (e.g. Sedfit (7)).

Sedimentation velocity experiments.

We investigated the dissolved peptide in order to gain further insights into the actual mass or size distribution of the peptide assemblies observed at concentrations above 100 µM. Therefore, a sedimentation velocity experiment was performed. Importantly the time required for interference detection of the entire cell is much shorter as compared to absorbance detection (~1 s vs ~90 s, depending on settings) which is important when 7 cells are measured in series, especially in case of rapidly sedimenting particles. For this reason, we switched to interference detection because it is able to scan the cells more rapidly. A typical result is depicted in **Fig. 4.10** where the first 10 plus every 10th from 20 to 100 scans of 100 µM pen-A(pY)L in TBS are shown. The absence of a moving sedimentation boundary suggests either complete sedimentation of the peptide to the bottom of the cell faster than the instruments time resolution or that the

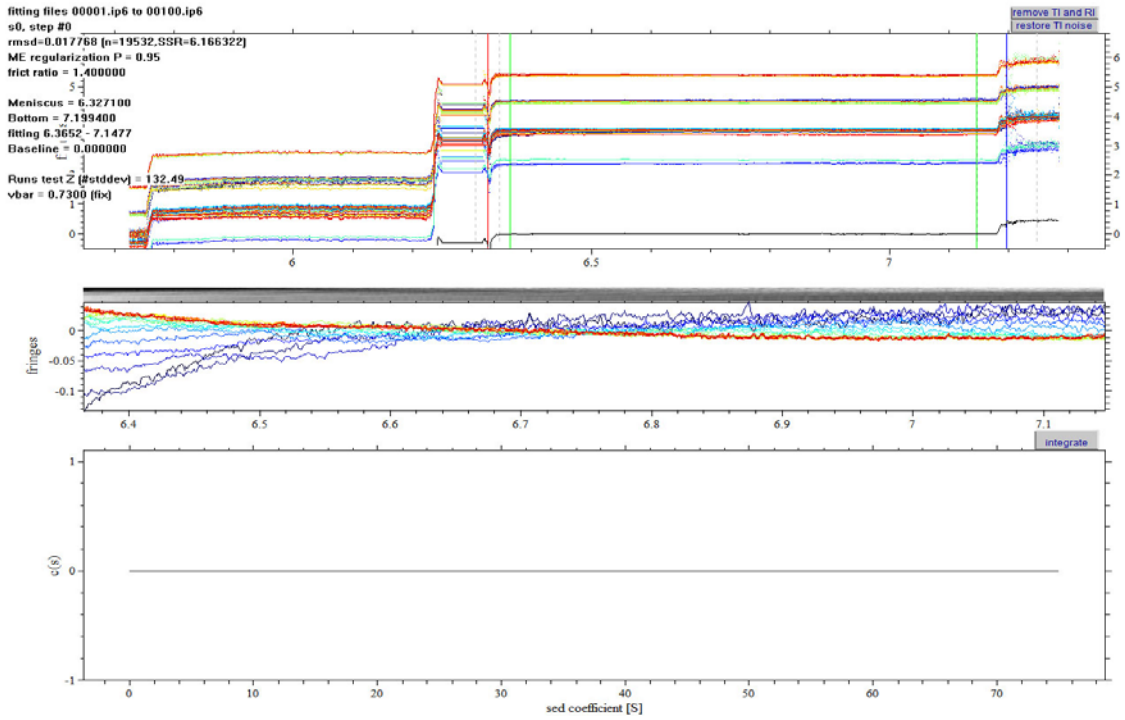

Fig. 4.10. AUC data of scans 1-10 and every 10th from 20 to 100 of 100 µM pen-A(pY)L in TBS. (Top) Raw data from interference detection which has been fitted between the indicated limits. No sedimentation is detected. **(Middle)** Residuals of the fit. **(Bottom)** Calculated size distribution of the sample which could not succeed due to the absence of the sedimentation boundary.

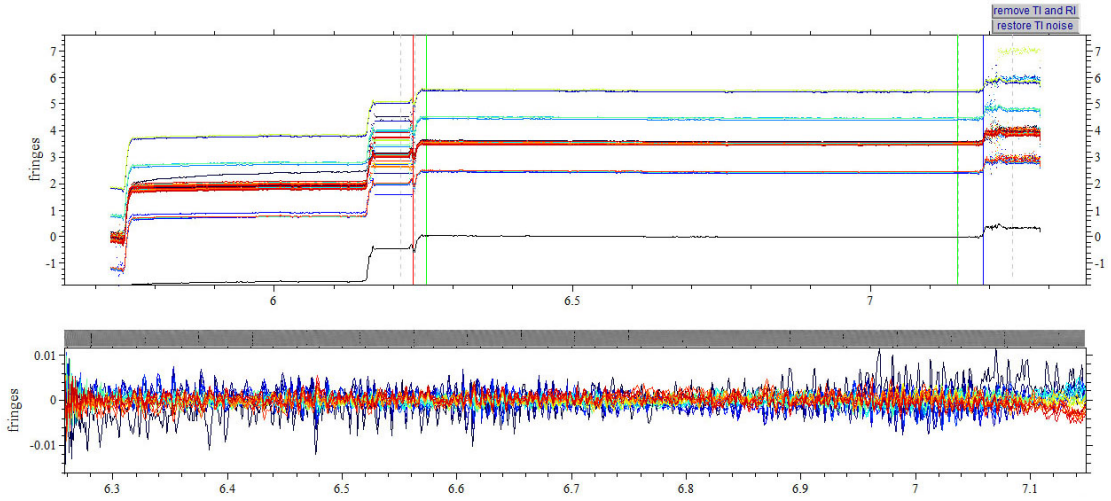

Fig. 4.11. AUC data of scans every 50th scan from 1 to 951 of 100 µM pen-A(pY)L in 20 mM Tris pH 7.4. (Top) Raw data from interference detection which has been fitted between the indicated limits. Also over the time course of 2 h no sedimentation is observed. **(Middle)** Residuals of the fit. A size distribution could not be calculated due to the absence of the sedimentation boundary.

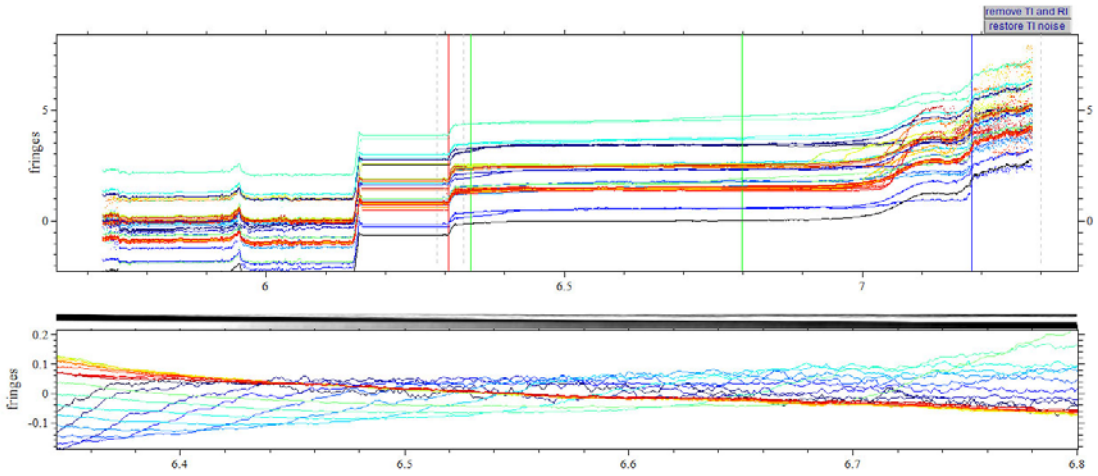

Fig. 4.12. AUC data of every 10th from the first 100 scans of 100 µM pen-AYL in 20 mM Tris 100 mM NaCl pH 7.4. (Top) Raw data from interference detection which has been fitted between the indicated limits. There is a visible boundary movement which is spun to the bottom in less than 15 min. **(Middle)** Residuals of the fit.

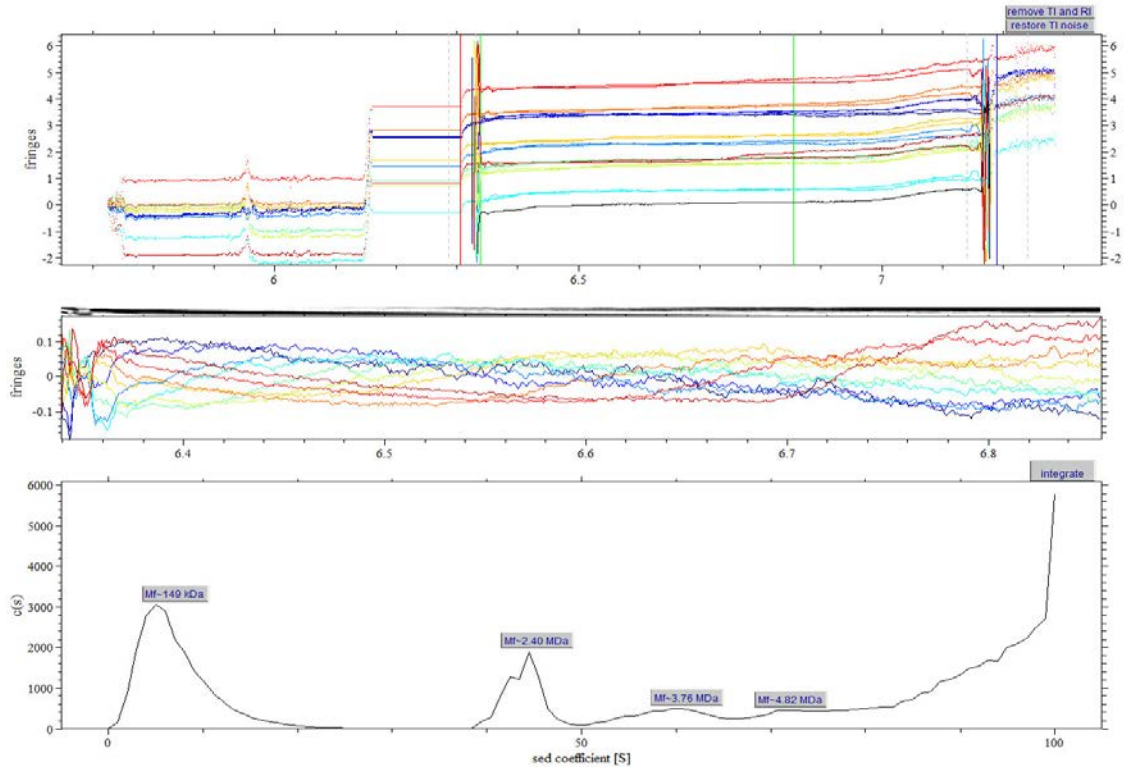

Fig. 4.13. AUC data of the first 10 scans of 100 µM pen-AYL in 20 mM Tris 100 mM NaCl pH 7.4. (Top) Raw interference data which has been fitted between the indicated limits. **(Middle)** Residuals of the fit. **(Bottom)** Size distribution of the sample showing the calculated sedimentation coefficients peaks with the corresponding indicated molecular mass.

molecules/assemblies are too small to sediment at the specific rotational speed and duration. The same observation was made if more scans were made (see **Fig. 4.11**) – we therefore chose to simply show the raw data as detected by IR.

After the AUC run of pen-AYL without salt, we further performed a concentration determination of the supernatant by means of Trp absorption to assess how much of the peptide might have sedimented to the bottom. Whereas the amount of the 1 µM peptide solution could not be detected because of insufficient signal intensity, we found peptide concentrations of 5.2 and 85 µM in the supernatant that was identical to the initial peptide concentrations in the cell of 5.0 and 84 µM (as determined prior the sedimentation velocity run; see **Tab. 4.6**), respectively. This suggests that no sedimentation of the peptide occurred.

In contrast, when adding salt, the 100 µM pen-AYL in TBS solution showed detectable sedimentation. Data of the first 100 scans shows practically no change in sedimentation any longer after 15 minutes (**Fig. 4.12**). Because of the very fast sedimentation at only 3000 rpm, the fitted size distribution and the mass of the sedimented particles have poor precision and thus high residuals in the fit. The first 10 scans are shown in **Fig. 4.13** and show a better time resolution of the sedimentation boundary movement. Numerical analysis of these data with Sedfit renders two main peaks with masses of 149 kDa and 2.4 MDa which correspond to clusters of 54 and 870 peptides, respectively ($m_{pen\text{-}AYL}$ = 2.77 kDa). In addition, the integral point to a much larger fraction at higher molecular masses which suggests that the peptide can cluster to even larger sizes as well.

4.4. Discussion

Aqueous solutions of the pen-pA(pY)L peptide showed formation of a gel-like state when prepared at low millimolar concentration (**Fig. 4.1**). This behavior was not observed for diluted solutions (< 1 mM) of the peptide. Because peptide aggregation might cause side-effects in bio-medical applications, we were interested in exploring the responsible mechanism that leads to the observed behavior.

From a physicochemical point of view (16) the peptide is not necessarily prone to aggregation. It contains a total of 5 basic amino acids (2 Arg and 3 Lys, compare **Tab. 4.1**) which overall make it highly positively charged at the used pH despite the presence of a negatively charged phosphate group on the Tyr_{10}. Because of that we would expect the peptide to rather repulse itself and not cluster in any way.

In this chapter, we used various methods, namely DLS, SLS, Trp fluorescence and AUC, to describe both size and conditions required for the observed peptide clusters.

SLS shows increased scattering only of the 1 mM pen-A(pY)L solution.

In first experiments to investigate the potential presence of peptide clusters, we used SLS. Only the 1 mM pen-A(pY)L solutions showed markedly increased scattering whereas the other solutions basically had same signal intensity. The absence of NaCl in the peptide solutions had no pronounced effect beside that the signal of the 1 mM pen-A(pY)L solution had a smaller fluctuation upon repeated measurements. This is a first indicator that ionic interactions may not be responsible for the clustering of the peptide. We also conclude that only the 1 mM pen-A(pY)L solutions contain peptide clusters that are scatter light significantly. Ultimately this is also reflected by its gel-like state on a macroscopic scale.

The DLS data shows presence of some assemblies in solutions of both pen-AYL and pen-pA(pY)L.

Investigation of 100 μM and 1 mM peptide dissolved in TBS by means of DLS showed the presence of smaller particles with a size distribution between 20 and 120 nm, but also some larger particles with sizes up to 1 μm. The fraction of large particles increased for 1 mM pen-AYL. Especially for concentrations <1 mM, the technique is not sensitive enough to measure the ratio of monomeric peptides (like pen-Antp with an estimated hydrated diameter of ~1 nm) and larger assemblies. The high content of basic amino acids rather suggests charge repulsion between the molecules than some sort of attractive force that may lead to the observed cluster formation. Drin et al. describe both

pen-Antp and pen-2AL as monomeric at concentration of ≤130 μm (3), although without providing data for this assumptions.

Comparison of the size distribution between pen-AYL and pen-A(pY)L shows no obvious differences beside the aforementioned increased number of larger particles for 1 mM pen-AYL. Pen-A(pY)L basically shows the same size distribution at both concentrations. The PDI of every measurement was high with values between 0.45 and 0.65 which indicate a high polydispersity regarding the size of the registered particles, but only low count rate and thus total number of scattering particles. Note that the potential signal of a monomeric peptide population may be overshadowed in the presence of already a few of the larger particles. We therefore cannot conclude the absence of monomeric peptide *per se* but notice the presence of larger sized particles which are assumed to be clusters of peptide. Taking further into account that we could not detect a prominent scattering signal of the pen-AYL solutions by means of SLS we assume that the observed particles are present in rather low numbers compared to the monomeric state.

The presence of large particles could be dissolved with increasing DMSO content.

The particles detected in all peptide TBS solutions could be dissolved by increasing contents of DMSO. Particle dissolution was observed at a DMSO content of ≥50% whereupon no particles could be detected anymore i.e. the measured signal approximated the value of pure solvent. The dissolution in a less polar solvent (compared to TBS) indicates a preference of these peptides for a nonpolar environment, which is an indication for hydrophobic interaction as reason for their clustering which might be the result of amphipathic self-association of the peptides.

Adsorption of pen-Antp to quartz cuvette surface is negligible.

Prior to the spectroscopic investigation of the peptide solutions we established the settings for proper conditions to determine Trp fluorescence emission shifts. Prior to that, we looked into potential adsorption of the pen-Antp to the quartz glass surface. Occurrence of peptide adsorption of polycationic peptides, such as CPPs, to glass or

fluorocarbon surfaces can introduce measurement errors as described already by several authors (9-11).

If pen-Antp adsorbed to glass surface, we would measure a decrease in the free peptide over time using spectrophotometric measurements. As this is expected to correlate with a corresponding decrease in fluorescence we assessed the absorption of pen-Antp to quartz glass by the decline in Trp fluorescence over time. According to our results, the peptide adsorbs only little to the glass surface because Trp fluorescence decreased by ~15% over 10 min when constantly stirred (**Fig. 4.5A**). Trp fluorescence decrease was much more pronounced when the solution was not stirred. The signal loss was around 60% in absence of a magnet (**Fig 4.5A**). However, this signal loss could be largely avoided by doing a single fluorescence excitation every 30 s instead of a constant excitation (**Fig. 4.5B**). This led us to the assumption that the observed fluorescence decrease is not mainly caused by adsorption of the peptide but by bleaching of the indole group. Incubation of the quartz cuvette with 1% (w/v) PEI prior these measurements accordingly managed to prevent only a minor signal decrease of ~10%.

Adsorption of pen-Antp to quartz glass surface therefore did not seem to interfere enough in our experimental setup to be further considered.

Trp fluorescence emission of pen-2AL resembles that of free L-Trp.

The maximum wavelength of fluorescence emission of the Trp indole moiety is dependent on the polarity of its environment. When brought into a nonpolar proximity, the Trp emission maximum shifts to shorter wavelengths. We harnessed this feature to gain more insight into possible clustering of the pen-Antp variants investigated during foregone studies (see chapter 2 and 3). The sequence of Pen-2AL is different from pen-AYL only by an Ala at position 10 and was described as a monomeric random coil peptide in aqueous buffer solution (3). Accordingly, we expected its Trp emission maximum to remain close to 351 nm at all conditions. Our measurements confirmed this assumption and provided us thereby with an actual reference value for a monomeric peptide.

Trp fluorescence emission of pen-AYL mostly resembles pen-2AL emission.

Pen-AYL shows the same nominal charge of +5 as pen-2AL. Just from structural considerations we expected the peptide to show the absence of a pronounced fluorescence emission shift like with pen-2AL. Overall, our results agree with this assumption and show mostly a maximal emission at wavelengths around 352 nm which suggest a polar proximity. There were, however, two noteworthy exceptions. We observed for both 100 µM and 1 mM pen-AYL in TBS and without salt, respectively, significant blue shifts of several nm which could be a sign for the 20-100 nm assemblies observed in DLS.

Only 1 mM pen-A(pY)L solutions show a significant blue shift in Trp emission.

In contrast to the other peptides, pen-A(pY)L includes a negative charge by its phosphorylated Tyr_{10}. As this is the only structural difference to the pen-AYL peptide, the observed aggregation of its 1 mM solution should be linked to the addition of the phosphate group. Interestingly, the Trp emission maximum of 1 mM pen-A(pY)L solutions is shifted down from ~351-352 nm to ~343-344 nm, which implies a change of the Trp residue into a nonpolar environment. The emission spectrum of Trp is highly sensitive to polarity changes in its proximity and already traces of polar molecules with hydrogen donors are enough to establish the hydrogen bonding interaction with the indole group that shift the emission maximum of 350 nm. For instance, the emission maximum of indole in an aqueous dioxane (80% v/v) solution or cyclohexane-ethanol (19:1 v/v) mixture are both at ~328 nm (4,17). Note that in pure dioxane the corresponding emission maximum lies at 310 nm (18) and the emission accordingly does not shift linearly with content of polar solute. The observed ~7 nm blue shift of the maximum emission wavelength therefore indicates a significant change in the proximal polarity of the Trp residue. Additionally, such a change can only stem from neighboring peptides as there are no other nonpolar components in the solution.

The blue shift takes place to almost the same extent in both presence and absence of NaCl which speaks against an ionic interaction leading to the clustering of the peptide. On the other hand, the emission maxima reside again around 351 nm at all lower peptide concentrations. We therefore conclude from the Trp fluorescence data

that cluster formation of pen-A(pY)L seems to happen above a certain concentration and between 100 μM and 1 mM. Both the blue shift of Trp in the 1 mM pen-A(pY)L solutions and the independence of the blue shift on salt further substantiates the results obtained by DLS. The pen-A(pY)L peptide thus seems to self-assembly due to hydrophobic attraction.

Almost no peptide clusters observable by means of AUC.

We further used the sedimentation velocity mode of AUC to potentially describe the observed peptide clusters in more detail regarding their size and molecular mass. Unfortunately, the sedimentation data of both peptides at concentrations of 1, 10 and 100 μM both in presence and absence of salt did not show noticeable sedimentation. In support, the ensuing concentration determination of the supernatant by means of UV-vis spectroscopy showed that the peptide was still present at the starting concentration which implies that the rotational force was too weak to move the peptide under the used conditions.

We could, however, detect a moving boundary in one of the peptide solutions. Specifically, it was monitored in 100 μM pen-AYL TBS during the very first minute. Within the first couple of scans, the signal was already spun to the bottom of the cell. Again, similar to the observation of the same solution with DLS, the finding of sedimenting particles in the pen-AYL solution, but not in the pen-A(pY)L one is surprising, but because of the sensitivity of the interference detection this might represent only a fraction of total peptide molecules.

4.4.1. Conclusion

The results of this study indicate that the pen-Antp variants pen-AYL and pen-A(pY)L may self-associate to a certain degree. The size of these clusters has a broader distribution between 20 nm to ~4 um as suggested by DLS. On the other hand, the bulk of the peptide seems to remain dissolved in either a monomeric state or very small clusters as shown by SLS and the almost unchanged peptide concentration of the supernatant after AUC. We did not investigate whether the self-association changed

after 1 day. As a precaution to reduce the (small) fraction of self-assemblies, all solutions were prepared as shortly as possible prior any measurement and prepared by a combination of vortexing and ultrasound.

Driving force of the peptide interaction seems to be hydrophobic attraction which is rather unintuitive regarding the nominal charge of these peptides, but comprehensible when referring to their amphipathic, i.e. detergent-like, structure. Accordingly, absence of salt had no influence on the peptides' behavior and the experiments exploiting Trp fluorescence suggest a change of the Trp moiety from a polar to a nonpolar proximity which can only be provided by the peptide itself. Furthermore, the peptide assemblies dissolved when brought into the less polar solvent DMSO. When comparing pen-2AL and pen-A(pY)L, it is evident that the phenol group seems to favor the peptide interaction.

4.5. References

1. Derossi, D., Joliot, A. H., Chassaing, G., and Prochiantz, A. (1994) *J Biol Chem* **269**, 10444-10450
2. Lindgren, M., Hallbrink, M., Prochiantz, A., and Langel, U. (2000) *Trends Pharmacol Sci* **21**, 99-103
3. Drin, G., Demene, H., Temsamani, J., and Brasseur, R. (2001) *Biochemistry* **40**, 1824-1834
4. Gryczynski, I., Wiczk, W., Johnson, M. L., and Lakowicz, J. R. (1988) *Biophys Chem* **32**, 173-185
5. Edelhoch, H. (1967) *Biochemistry* **6**, 1948-1954
6. Schuck, P., MacPhee, C. E., and Howlett, G. J. (1998) *Biophys J* **74**, 466-474
7. Schuck, P. (2012).
8. Lakowicz, J. R. (1999) *Principles of fluorescence spectroscopy*, 2nd ed., Kluwer Academic/Plenum, New York
9. Tosteson, M. T., Holmes, S. J., Razin, M., and Tosteson, D. C. (1985) *J Membr Biol* **87**, 35-44
10. Grant, E., Jr., Beeler, T. J., Taylor, K. M., Gable, K., and Roseman, M. A. (1992) *Biochemistry* **31**, 9912-9918
11. Persson, D., Thoren, P. E., Herner, M., Lincoln, P., and Norden, B. (2003) *Biochemistry* **42**, 421-429
12. Behrens, S. H., and Grier, D. G. (2001) *J Chem Phys* **115**, 6716-6721
13. Drin, G., Cottin, S., Blanc, E., Rees, A. R., and Temsamani, J. (2003) *J Biol Chem* **278**, 31192-31201
14. Fischer, R., Kohler, K., Fotin-Mleczek, M., and Brock, R. (2004) *J Biol Chem* **279**, 12625-12635

15. Thoren, P. E., Persson, D., Isakson, P., Goksor, M., Onfelt, A., and Norden, B. (2003) *Biochem Biophys Res Commun* **307**, 100-107
16. Caflisch, A. (2006) *Curr Opin Chem Biol* **10**, 437-444
17. Privat, J. P., Wahl, P., and Auchet, J. C. (1979) *Biophys Chem* **9**, 223-233
18. Walker, M. S., Bednar, T. W., and Lumry, R. (1967) *J Chem Phys* **47**, 1020-&

Chapter 5:

Electron-spin labels as molecular probes to monitor membrane leakage

5.1. Introduction

The basis for further understanding and exploitation of CPPs in future clinical applications requires the investigation of the involved mechanisms with appropriate techniques and models. In particular, it has been shown that limited models have produced misleading results because of the particular properties of CPPs. For instance, it could be shown that cell fixation led to peptide uptake under conditions where an active participation of the cell in this process seemed highly unlikely (1). Because the same fixation bias might have occurred in preceding studies, CPPs were expected to be able to translocate across a lipid membrane in a "passive" manner i.e. in absence of supporting proteins. Biophysical methods, in combination with various lipid membrane models and compositions, might thus help in clarifying whether the passive translocation of CPPs is likely.

In this regard, two important points have to be considered. First, the choice of a correct *membrane model* is crucial to be able to understand which physicochemical properties allow the peptide to cross the lipid bilayer. It is important to realize that the lipid bilayer portion of a biological membrane is not simply an isotropic hydrophobic film, but rather an anisotropic double layer that has a variable hydrophobicity and lateral

pressure across its normal (2) and also suffers from curvature stress in some membrane models. The most prominent membrane model to investigate the effect of any compound on a lipid bilayer of desired lipid composition are easy-to-handle and thermodynamically stable unilamellar vesicles[6] ((3, 4); their preparation of varying size is thoroughly described in **chapter 1**).

Next to translocation, also the *interaction between CPP and membrane* itself needs to be monitored in order to understand the influence of different membrane compositions on the macroscopically observed translocation. The specific changes on the molecular scale thus might help in an indirect way to understand the macroscopic level where the sum of its parts may be observed and not only individual elements. On the other hand, the techniques, which measure changes on the molecular level (usually spectroscopic methods), are often difficult to interpret in a stringent way which is explained in the following.

A widely used method for the analysis of the translocation property of CPP is the so-called leakage assay (5). The underlying principle for detection of peptide translocation across a model membrane is the following: A fluorescent molecule (hereafter referred as fluorescent dye or simply dye) is entrapped at a self-quenching concentration inside of unilamellar vesicles of desired lipid concentration (see **chapter 1** for a minute protocol). The dye-filled vesicles then get exposed from the outside to CPPs of choice that eventually bind to the lipid membrane depending on molecular properties, such as both peptide and membrane surface composition/charge (6). Whenever the peptide manages to destabilize the membrane and/or travel across the membrane it is assumed that this process concomitantly leads to an influx of the peptide, but the measurement records only the efflux of the fluorescent dye which had been trapped inside of the vesicles. The dye gets diluted to concentrations below the quenching concentration limit and this can be conveniently detected by measuring the vesicle sample by means of a spectrofluorometer.

[6] Also referred to as liposomes. Note that liposome is a general term for spherules made of lipid bilayer(s) without indication of size and lamellarity. It is thus suggested to clearly specify if the vesicles are either uni- or multilamellar, and which size they have (i.e., small, large or giant vesicles with according diameters of 30, 100 and >500 nm, respectively).

This method is very sensitive, and a spectrofluorometer is very convenient and easy to both apply and interpret. It therefore has become a popular method to demonstrate the effect of CPPs on model membranes. However, the method has some limitations when used with CPPs which can lead to eventual misinterpretation. First and especially delicate is the amount of dye leakage which is not necessarily reflecting similar proportions in peptide translocation across the membrane. Instead, it is an indication that the CPP at least temporarily destabilizes the lipid bilayer sufficiently in order to allow the dye escape from the lipid vesicle.

A second point to take into account is the ionic strength of the enclosed volume. Standard protocols usually include a concentration of >50 mM of di-, tri- and tetravalent dyes ((5, 7-9) for comparison) which correspond to considerable charge difference between both sides of the membrane. For example, we assume a charge of -4 for calcein at neutral pH, so that the ionic strength of a 50 mM solution is 400 mM (excluding other ions). The difference in ionic strength in- and outside of the vesicle then establishes a transmembrane potential which can also lead to increased membrane permeation (10).

Thirdly, negatively charged fluorescent dyes such as calcein or carboxyfluorescein are prone to electrostatic interaction with CPPs as they are highly positively charged. We thus monitored either gain or loss in fluorescent signal intensity for various dyes in presence of CPPs. Such effects may then bias the calculation of the dye leakage (e.g. mask dye leakage), leading potentially to measuring artifacts (see **Fig. 1.1 e-f** in **chapter 1** for reference).

Overall, the dye leakage method is based on a good approach by monitoring the membrane permeability in presence of the CPP. It carries however some inherent limitations e.g. by using negatively charged[7] fluorescent dye molecules that lead to peptide-dye interaction which may distort fluorescence emission of the dye. Thus, complementary methods would be helpful to include reporter molecules that do not

[7] Alternatively, a positively charged fluorescent dye such as divalent propidium iodide (which is hazardous, like all chemicals binding selectively to DNA) could be enclosed in the vesicles. In this case, however, negatively charged lipids such as POPG should be omitted in the lipid composition to prevent interaction of the dye with the membrane. In turn, this compromises the resemblance to eukaryotic cell membranes as these usually show a content of negatively charged lipid around 20% (see Pankov (2006) (11. Pankov R, Markovska T, Antonov P, Ivanova L, Momchilova A. 2006. *Chemico-Biological Interactions* 164: 167-73)).

interact with CPPs so that the signal would not be biased. Humphries proposed an interesting approach in this regard using the nitroxide spin label TEMPO-choline to detect complement-induced lysis of multilamellar vesicles by means of electron paramagnetic resonance (EPR) (12). The main advantage here is the use of a spin label which comes in the form of a nitroxide-based, persistent radical of low positive or absent charge thus not being prone to electrostatic interaction with the CPP. The following chapter therefore summarizes our attempt to establish an EPR based assay to monitor the permeabilization property of CPPs on model membranes.

5.2. Materials and methods

Materials.

The various spin labels, the fluorophores calcein and ANTS as well as the detergent Triton X-100 were all purchased from Sigma-Aldrich (Buchs, Switzerland). DPX was supplied by Molecular Probes (Eugene, OR). Lipids for preparation of large unilamellar vesicles (LUVs) were obtained from Avanti Polar Lipids (Alabaster, AL). Disposable micropipettes for EPR spectroscopy were purchased from BRAND (Wertheim, Germany).

Preparation of spin label solutions.

Each spin label stock solution was prepared by weighing appropriate amounts producing concentrations of 100 mM upon dissolution in 5 mL. For this purpose, the dry amounts were dissolved in 4.5 mL buffer (20 mM Tris 100 mM NaCl pH 7.4; TBS) and the pH was adjusted to 7.4 (or pH 5 for the solution of 4-amino-TEMPO). Thereafter, buffer was added to make the final volume of 5 mL. Solutions of lower spin label concentration (i.e., <100 mM) were prepared by dilution of the stock solution with TBS. The stock solutions were stored in glass vials and protected from light with aluminum wrap.

Preparation of LUVs.

Lipid vesicles were prepared as described in chapter 1 and 2 and were composed of POPC/POPG/DOPE-PEG (76:20:4 n/n) mixtures. Loading of LUVs with spin label was done by suspending the dried lipid film with 1 mL of the corresponding spin label stock solution (100 mM). Lipid suspensions were made by alternating gentle stirring using a vortex mixer and equilibration intervals of ~5 min until all lipid was suspended as assessed by visual inspection.

Fluorescence spectroscopy.

The fluorescence measurements were performed with the same procedure and settings as described in **chapters 1** and **2**.

EPR spectroscopy.

The spectra were recorded on a MS100 benchtop EPR spectrometer manufactured by Magnettech (Berlin, Germany) using a microwave irradiation of 9.4 GHz. Samples were measured in disposable 50 µL micropipettes, sealed with putty and subsequently placed in the measurement cavity of the instrument. For measurement of the microwave irradiation, we used a 53181A frequency counter from Agilent (Santa Clara, CA). Spectra were recorded with the following parameters: center field at 337 mT; field sweep of 6 mT over 60 s; power attenuation of 11 dB; receiver gain of 20. The denoted amplitudes and linewidths all correspond to the middle peak of the resonance signal.

5.3. Results

5.3.1. Binding of pen-AYL to Calcein reduces its fluorescence signal in a concentration dependent manner

The principle of fluorescence leakage assays resides on the concentration dependent signal of these dyes. This behavior is exemplified in **Fig. 5.1** by the common fluorescent

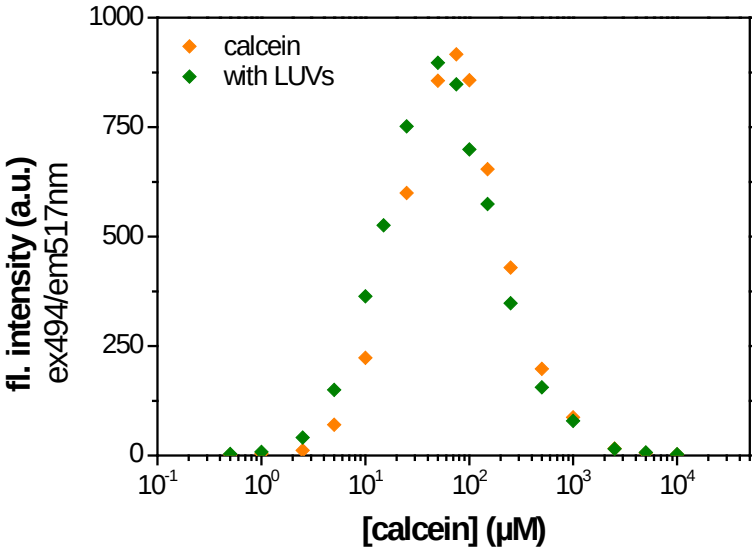

Fig. 5.1. Concentration dependence of calcein fluorescence emission intensity (orange diamonds) (PMT 200 V). The dye has its emission maximum at ~100 µM and is increasingly quenched at higher concentrations. The green diamonds show the same dependence in presence of 250 µM POPC/POPG (3:1 n/n) LUVs which do not significantly interfere with the calcein fluorescence emission.

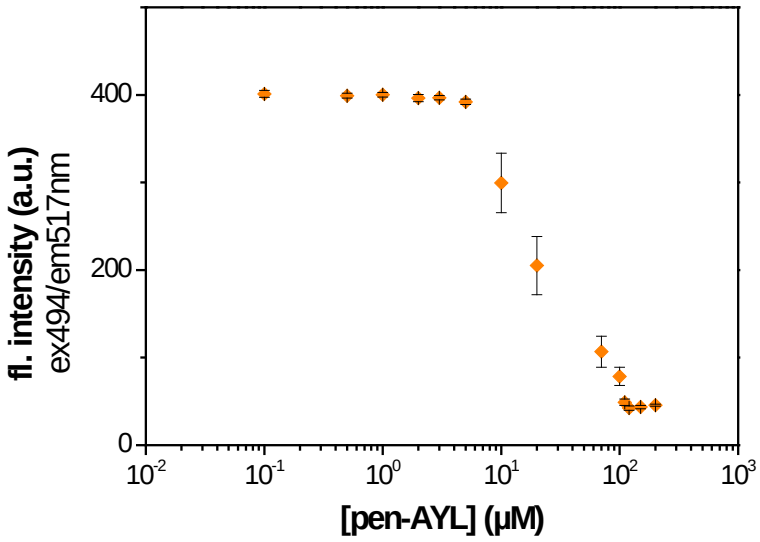

Fig. 5.2. Fluorescence emission intensity of 30 µM calcein in dependence of pen-AYL concentration (average of triplicate, PMT 220 V). 30 µM calcein corresponds to a reasonable final concentration after full vesicle lysis in a leakage assay. It is apparent that the calcein signal is strongly diminished in presence of pen-AYL concentrations above 10 µM with almost full quenching at 100 µM.

dye calcein. The signal intensity has a maximum around 100 µM and gets increasingly quenched with increasing dye concentration (self-quenching). Accordingly, the concentration at which the dye is enclosed in the vesicles of desired lipid concentration has to be carefully calculated so that release of the dye produces a concentration of maximum signal or concentrations below. At these conditions, the concentration/fluorescence intensity correlation should be linear and thus appropriate to quantify the leakage.

Instead, we have found that this relation is not linear, because fluorescence emission of negatively charged dyes was considerably disturbed in presence of CPPs. **Fig. 5.2** shows the fluorescence signal of a 30 µM calcein solution in presence of the pen-Antp mutant pen-AYL with increasing CPP concentration. The calcein signal starts to decrease at a pen-AYL concentration slightly below 10 µM and is reduced to only 11% of its original intensity at 120 µM pen-AYL. These concentrations are characteristic for the experiments done in **chapter 2** which shows that the interaction between dye and peptide may severely bias the results derived from the permeabilization assays. This observation is fundamental, because the quenching of the dye starts at low micromolar peptide concentration which is equivalent to CPP concentrations commonly observed to be taken up by living cells. Whereas pen-AYL manages to permeabilize model membranes at this concentration (as shown in **chapter 2**), it thus cannot be measured to what extend the dye had been released.

5.3.2. ANTS fluorescence is increased in presence of pen-Antp mutants

8-aminonaphthalene-1,3,6-trisulfonic acid (ANTS) is another negatively charged fluorescent dye molecule which is commonly used in fusion and leakage assays, usually in combination with its quencher *p*-xylene-bis-pyridinium bromide (DPX) (13). In analogy to calcein, we found that ANTS interacts with pen-Antp and its mutants as well, but in contrast to calcein its fluorescence intensity is increased upon interaction with the CPP. **Fig. 5.3** shows the titration of 75 µM ANTS 270 µM DPX with increasing concentration of either pen-AYL or pen-A(pY)L. The increase in

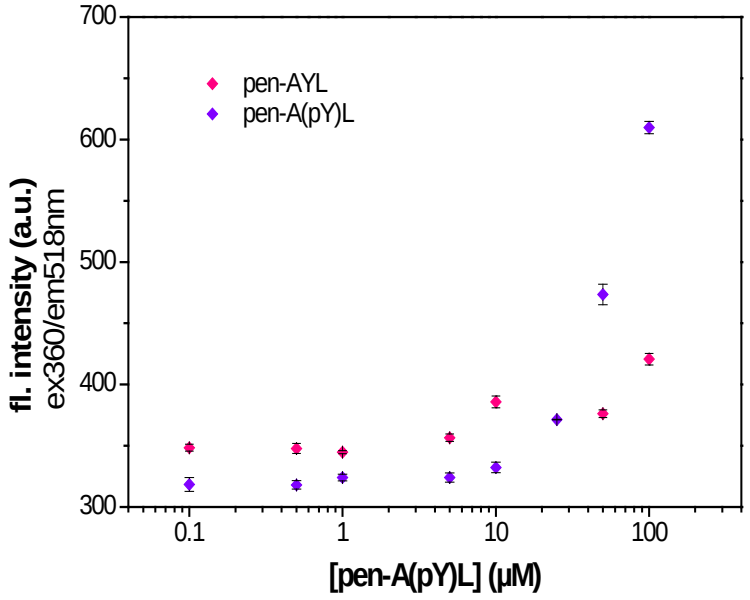

Fig. 5.3. Fluorescence emission intensity of 75 µM ANTS 270 µM DPX in presence of increasing concentration of pen-AYL and pen-A(pY)L (average of triplicate, PMT 400 V).
In contrast to calcein, interaction of the peptides with ANTS increases the fluorescence intensity. This effect is more pronounced with the phosphorylated pen-A(pY)L peptide. Note that the increase in fluorescence manifests itself again at a peptide concentration ≥10 µM.

---

fluorescence signal intensity as induced by pen-A(pY)L is considerable. For example, the fluorescence intensity in presence of 100 µM pen-A(pY)L is doubled as compared to 10 µM pen-A(pY)L, whereas the increase with 100 µM pen-AYL is only 33%. These experiments support our hypothesis that negatively charged dyes may interact electrostatically with CPPs, thereby changing their fluorescence intensity both positively or negatively. The critical concentration for this to happen starts at concentrations as low as 10 µM. In conclusion, the leakage assay might be appropriate to demonstrate membrane permeabilization, whereas fluorescence quenching by CPP binding might bias its proper quantification (or even mask the release). Alternate methods thus appear certainly complementary.

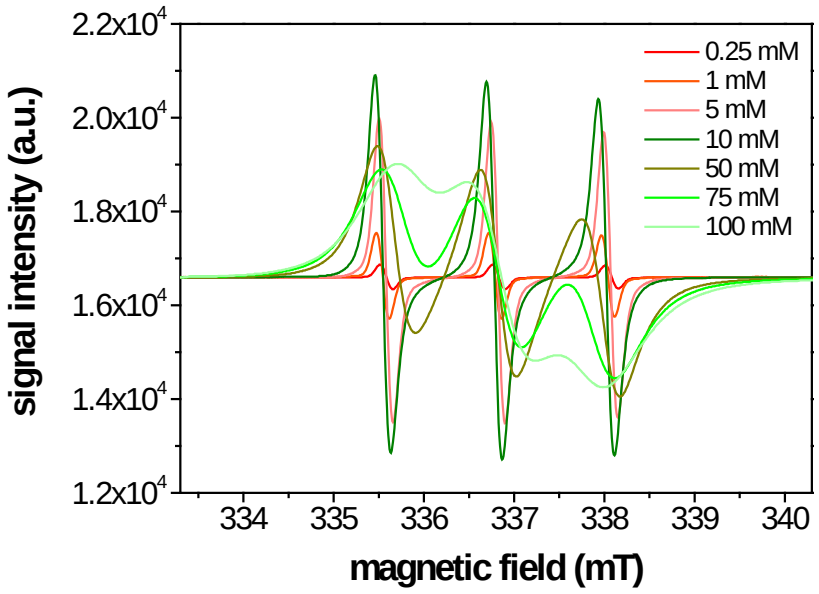

Fig. 5.4. EPR signal of 4-amino-TEMPO in dependence of concentration. Shown is the first derivative of the actual absorption lines. Below 10 mM the signal amplitude increases with spin label concentration (reddish lines). Above 10 mM, instead the line width starts to increase (green lines) due to electron-spin exchange.

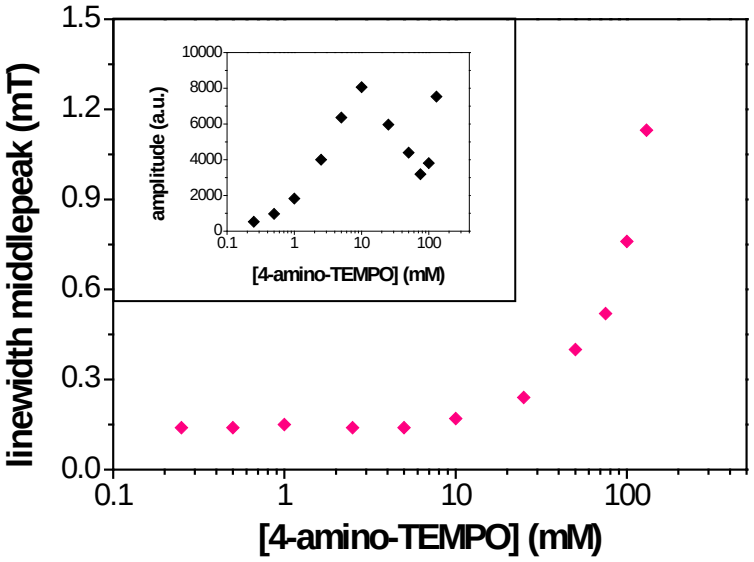

Fig. 5.5. Concentration dependence of the linewidth of the middle peak of the EPR signal of 4-amino-TEMPO. The linewidth is independent of the spin label concentration below 10 mM. **(Inset)** Concentration dependence of the amplitude of the middle peak. The amplitude increases with concentration up to 10 mM where the broadening of the linewidth starts to counteract. The signal of the two points at 100 and 130 mM is higher than that of lower concentrations because the lines coalesce due to electron-spin exchange (see **Fig. 5.4** at 100 mM).

5.3.3. Using paramagnetic spin labels as probe for membrane permeabilization

The concept of using EPR instead of fluorescence spectroscopy for the leakage assay is based on the different physical property of the molecular probe. Whereas the emission of the fluorophore was found to be changed upon electrostatic interaction with the CPP, it is likely that such a peptide-induced signal change can be avoided by using larger reporter molecules (instead of charged molecules) that do not cross the membrane because of their size (instead of charge). Inside the vesicles, the reporter molecule is chosen also at high concentration so that its mobility is hindered (with consequences on the correlation time). Upon dilution into the extravesicular space (e.g., upon membrane destabilization with CPPs), the reporter gets diluted causing a change in correlation time. In principle, these changes could be also detected with fluorescence correlation spectroscopy (FCS) of FITC-labeled dextran, for example, but the FCS was not as easily available – in contrast to the EPR instrument.

The concentration dependence of the EPR signal of 4-amino-TEMPO is shown in **Fig. 5.4.** The spectra are obviously characteristically different from the fluorescence spectra where only the signal intensity correlates with the concentration of the fluorophore. A linear increase in signal with concentration is observed in the EPR spectra as well (compare also **Fig. 5.5**). Above 10 mM, the unpaired electrons get into proximity and start to interact with each other (electron-spin exchange) leading first to broadening of the spectral line at intermediate concentrations and ultimately to coalescence at >75 mM (**Fig. 5.5**). Accordingly, the concentration of the enclosed spin label was calculated for the leakage assays, so that dilution as caused by CPP-induced leakage produces a sufficient difference between the two states of intact vesicles containing highly concentrated spin label and permeabilized and/or solubilized vesicles with diluted spin label in bulk solution, i.e. intravesicular concentration of >10 mM, and amount of lipid vesicles, such as to produce a concentration of the spin label to the linear range of <10 mM upon complete vesicle leakage

Obviously, it is possible to assess either the signal amplitude or spectral linewidth of the TEMPO resonance to detect membrane permeabilization. We decided to use the dependence of the linewidth because the half-width is not as influenced by smaller

differences in sample volume of radiofrequency excitation. Also, the linewidth is less prone to ambiguity, because the signal amplitude decreases at both above and below the concentration of maximum signal intensity. The middle peak of the resonance signal was chosen because of highest signal-to-noise ratio (all three peaks share the same linewidth at concentrations below 100 mM) and will further simply referred to as "linewidth".

5.3.4. The EPR signal of TEMPO is stable in the presence of pen-Antp mutants

As a first experiment, it was tested whether the EPR based permeabilization assay is biased by varying CPP concentrations. Also, the concentration dependence of the nitroxide label must not change in presence of both the CPP of interest and model membranes such as LUVs. It was found that the CPP did not disturb the EPR signal as shown for 10 mM TEMPO in **Fig. 5.6** where the linewidth remains constant in presence of either lipid vesicles (POPC/POPG/DOPE-PEG (76:20:4 n/n) LUVs) or peptide (pen-AYL or pen-A(pY)L). Concentrations of either component were chosen in the range where they would be used in a potential permeabilization assay.

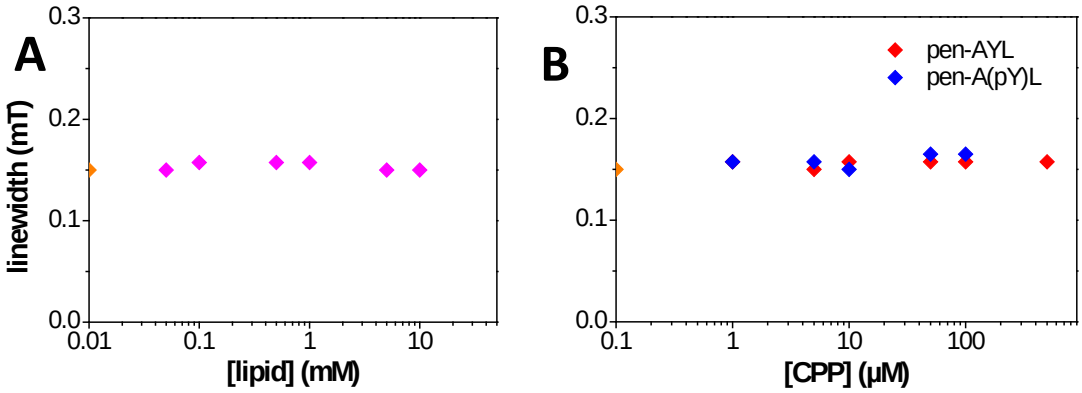

Fig. 5.6. Linewidth (of the middle peak) of 10 mM TEMPO in presence of lipid vesicles (A) or CPP (B). The signal resides at ~0.15 mT independently of the presence of either model membranes or CPP. The orange diamond on the y-axis is the linewidth of 10 mM TEMPO in buffer (TBS). **(A)** Lipid composition of LUVs is POPC/POPG/DOPE-PEG (76:20:4 n/n). **(B)** Added CPPs were pen-AYL (red diamonds) or pen-A(pY)L (blue diamonds). The independence of the spin label resonance in presence of the used CPP concentration is a clear improvement as probe for membrane permeabilization in comparison to fluorescent dyes which are susceptible for CPP-induced signal changes.

5.3.5. Preparation of nitroxide spin label-loaded vesicles

In order to investigate the CPP-induced membrane permeabilization by EPR, lipid vesicles with encapsulated spin label were prepared. In a first trial, preparation of TEMPO-loaded LUVs was done in the same way as for vesicles loaded with fluorescent dye (see chapter 1 for detailed description). We successfully managed to gather the LUVs after size size-exclusion chromatography (SEC) over a column as confirmed by both dynamic light scattering (DLS) and determination of the lipid concentration of the eluate by means of colorimetric phosphate assay. However, when the lipid-containing fractions were investigated on their EPR signal we could not detect any TEMPO. The spin label is apparently hydrophobic enough to simply diffuse across the vesicle membrane into the elution buffer. We therefore used various spin label derivatives that were either positively charged or covalently bound to polar molecules with large molecular mass to prevent passive diffusion from the LUVs.

4-amino-TEMPO.

This TEMPO derivative was chosen because of its amine group which is expected to be charged at the used pH of 7.4. We suspended the lipids in a 130 mM stock solution of 4-amino-TEMPO. Although we detected the presence of spin label in the LUV-containing fractions, it seemed to escape LUVs over time. **Fig. 5.7A** shows linewidth of the 4-amino-TEMPO signal in the lipid-containing eluate at different concentrations prior and after the addition of the detergent Triton X-100 (5% v/v in ddH_2O; TX100). All linewidths correspond to a 4-amino-TEMPO concentration $\leq$10 mM and accordingly cannot get narrower (compare **Fig. 5.5**). Upon further examination, the corresponding amplitudes of the resonance signal (**Fig. 5.7B**) decreased with concentration as we would expect upon dilution. However, the signal and linewidth remained *identical* after the addition of TX100 which indicates that the spin label could not be incorporated into the vesicles at concentrations high enough that would restrict the motility of the molecules. The diffusion of the spin label across the membrane becomes also evident by a closer look to the eluate after elution of the LUVs.

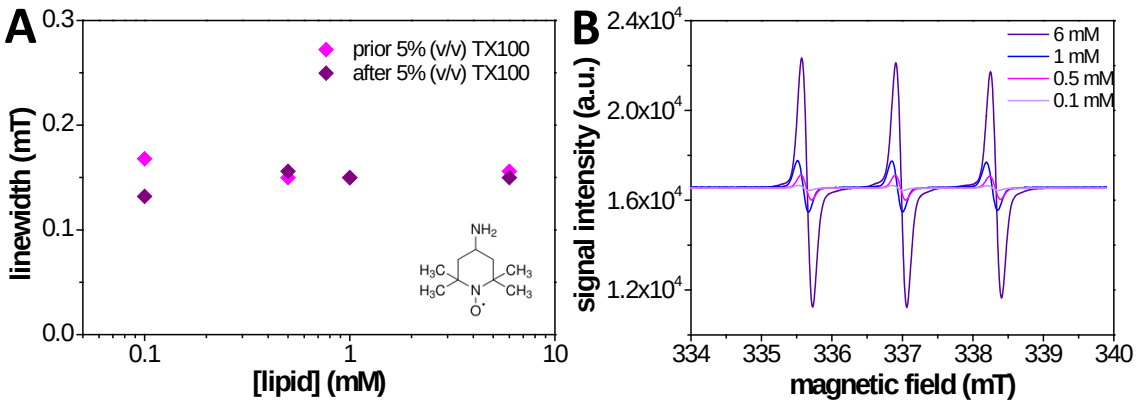

Fig. 5.7. 4-amino-TEMPO signal of the eluate after SEC at indicated lipid concentrations. (A) The linewidth of the signal does not change after addition of the strong detergent TX100 (5% v/v). Also shown in the bottom right corner is the structure of 4-amino-TEMPO[8] **(B)** Similarly, the signal amplitude remains the same after detergent addition (spectra after TX100 addition are identical and are therefore omitted; see text for details). We therefore assume that the spin label can diffuse across the membrane and the spectra depict a state where the spin label is equally distributed in- and outside of the LUVs.

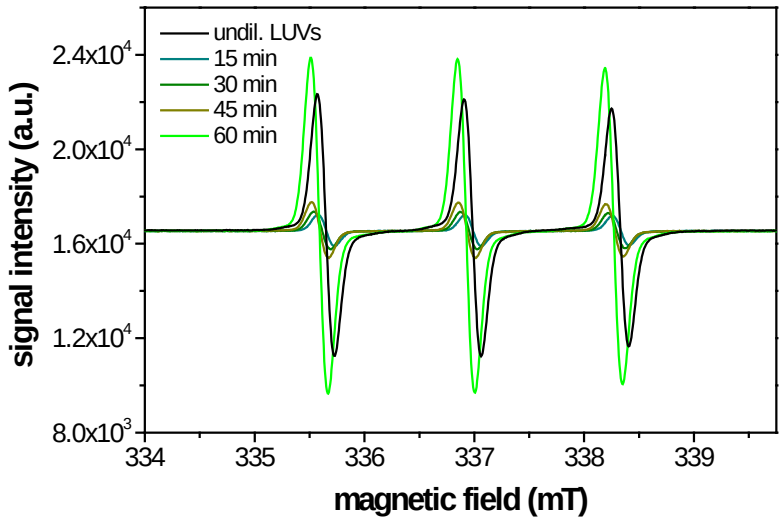

Fig. 5.8. 4-amino-TEMPO signal in fractions eluted from the gel-filtration column after passing of the LUVs. The indicated times correspond to minutes after the last gathered LUV-containing fraction. The signal increases with time but even closely to the LUVs some spin label is detected which implies constant diffusion of 4-amino-TEMPO into the elution buffer. The fraction of the originally excluded spin label (right after suspending the lipid) elutes approximately an hour after the LUVs. For comparison, the signal of the undiluted LUV-containing suspension is shown as well.

[8] TEMPO structures from http://www.sigmaaldrich.com

The signal amplitude increases steadily with time which is consistent with leakage along the column (**Fig. 5.8**).

Preparation of 4-amino-TEMPO containing LUVs was repeated with a 130 mM spin label stock solution at pH 5 to ensure a charged amine group to a similar result.

4-phosphonooxy-TEMPO.

As an alternative charged spin label we investigated the negatively charged 4-phosphonooxy-TEMPO (structure in **Fig. 5.9A**). In contrast to 4-amino-TEMPO, it does not show line broadening at a concentration up to 100 mM but the amplitude of the resonance increases with concentration (**Fig. 5.9**) as expected. However, the suspension of lipid with 100 mM 4-phosphonooxy-TEMPO yielded LUVs showing a resonance amplitude of 390 a.u. (at same radiofrequency settings) which correspond to an enclosed spin label concentration of ~5 mM (compare inset **Fig. 5.9**). Again, the signal did not change after TX100 addition. In contrast to 4-amino-TEMPO, however, the spin label did not escape into the eluate samples of the column (**Fig. 5.10**) indicating that not the escape, but the inability to incorporate sufficiently high concentrations into the LUVs was leading to the poor usability of the label for leakage experiments.

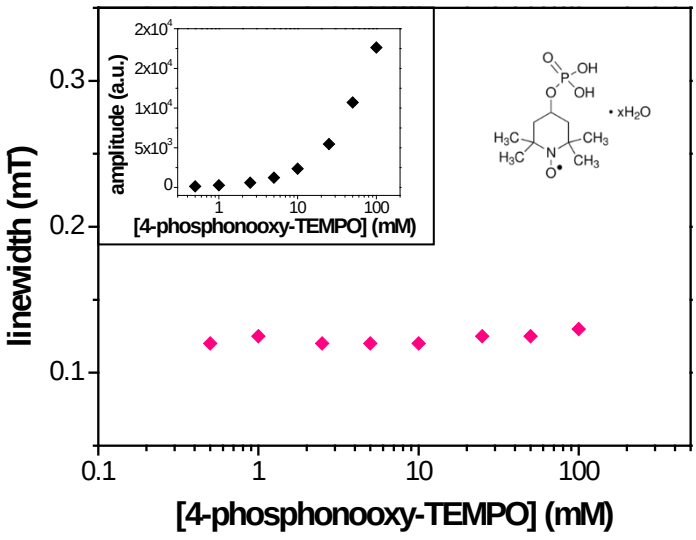

Fig. 5.9. Concentration dependence of the 4-phosphonooxy-TEMPO resonance (structure in top right corner). In contrast to 4-amino-TEMPO, the line broadening does not take place at the used concentrations. **(Inset)** The amplitude of the resonance increases with concentration.

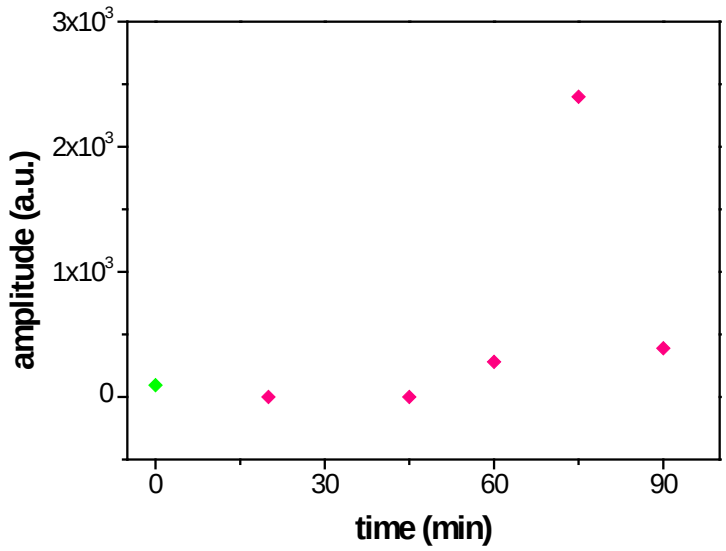

Fig. 5.10. Resonance amplitude of supposedly enclosed 4-phosphonooxy-TEMPO (green) and fractions gathered at indicated time (pink) after the LUV-containing eluate. The value of the undiluted LUV-containing sample corresponds to ~5 mM 4-phosphonooxy-TEMPO. Free spin label arrives 75 after the LUVs.

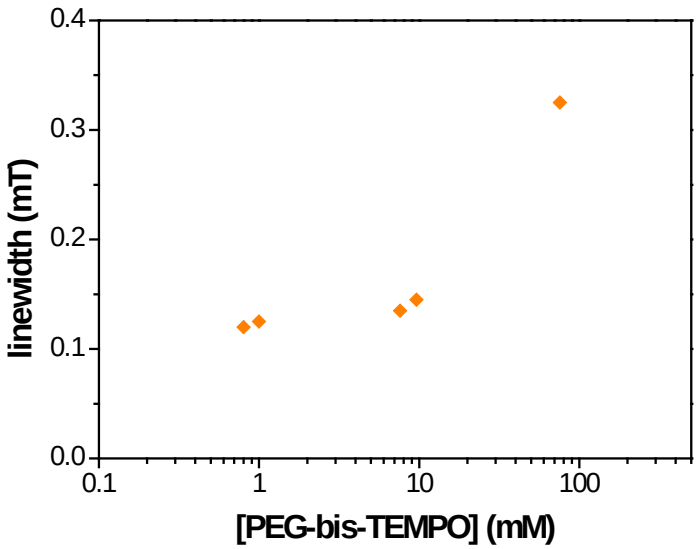

Fig. 5.11. Concentration dependence of the linewidth of the EPR signal of PEG-bis-TEMPO. Concentrations were calculated by using a labeling extent of 0.5 mmol/g weighed PEG-bis-TEMPO.

Poly(ethylene glycol)-bis-TEMPO.

After finding the rather surprisingly low concentration of charged spin labels in LUVs we tried to detain the spin label inside the vesicles by coupling it to a polymer. Poly(ethylene glycol) (PEG) is a relatively hydrophilic polymer which we use extensively as a lipid component that prevents fusion of lipid vesicles at sufficient length and content (14, 15). Unfortunately, the degree of polymerization is poorly specified by the (few) manufacturers of the spin-labeled molecules, so that we do not know the exact molecular weight and thus the exact concentration of the prepared solutions. We can, however, make a rough estimation. The extent of labeling is declared as 0.25-0.75 mmol/g which we assumed to be 0.5 mmol/g for simplicity reasons. 302 mg of PEG-bis-TEMPO were dissolved in 1 mL buffer which then would correspond to a 75.5 mM stock solution (two spin labels per PEG chain). **Fig. 5.11** shows the linewidths of a dilution series of this stock solution which are similar to the linewidths of 4-amino-TEMPO. For instance, PEG-bis-TEMPO has linewidths of 0.145 and 0.325 mT at 9.6 and 75.7 mM, respectively, compared to 0.138 and 0.414 mT for 4-amino-TEMPO at 10 and 75 mM, respectively. Assuming the above described estimation of the PEG-bis-TEMPO concentration of the stock solution we then can calculate the number of ethylene glycol polymerization: 302 mg dissolved in 1 mL give a molecular mass of 4027 Da. This corresponds to a number of about 85 ethylene glycol units that should be large enough to sterically prevent passive diffusion across the membrane.

The preparation of LUVs by pressure extrusion after solubilizing the lipid with the PEG-bis-TEMPO stock solution was difficult and only possible by starting with 400 nm pore sizes and subsequent stepwise reduction in pore size of the polycarbonate filter over 200 to 100 nm. However, the separation of vesicles and excluded spin label was again not sufficient. Similar to the previous trials the concentration of detected spin label was constant over the whole eluate, independent of the presence of LUVs (see **Tab. 5**). Additionally, there was a transition from clearly defined LUVs (indicated by constant attenuator, diameter and (low) polydispersity index) to lower concentration of similarly sized particles with higher polydispersity (fractions 16 to 45 in **Tab 5**).

Tab. 5. DLS and EPR data of the eluate of the SEC column loaded with 40 mM lipid and 302 mg PEG-bis-TEMPO (after extrusion). The linewidth of the TEMPO signal remains equal over the complete course of the column. Furthermore, the by means of DLS detected size and polydispersity of the particles in the eluate shifts slowly from clearly defined LUVs (Fractions 1-14 in light green) to smaller diameters and higher polydispersity, presumably PEG-bis-TEMPO aggregates. The chosen column material apparently is not able to separate these two species. The linewidth of the detected EPR signal corresponds to an approximate concentration of 5 mM (compare with **Fig. 5.11**).

Time (min)	Fraction	PDI	Attenuator	average diameter (nm)	linewidth (mT)
0	1	0.377	11	152.15	
1	2	0.068	5	106.1	
2	3	0.051	5	114.9	
3	4	0.058	5	107.2	
4	5	0.039	5	116.7	0.120
5	6	0.048	5	114.9	
6	7	0.065	5	108.3	
7	8	0.078	5	126.7	
8	9	0.064	5	117.6	
9	10	0.043	5	108.6	
10	11	0.026	5	119	0.125
11	12	0.059	5	116	
12	13	0.036	5	109.7	
13	14	0.026	5	121.8	
14	15	0.035	5	112	
15	16	0.033	6	113.2	0.120
16	17	0.051	6	116.2	
17	18	0.062	6	114	
18	19	0.052	6	112.6	
19	20	0.006	7	115.2	0.125
25	25	0.069	7	123.7	0.120
35	30	0.109	8	127.9	0.125
45	35	0.266	10	112.4	0.125
55	40	0.301	10	109.6	0.125
75	45	0.219	10	117	0.115

5.4. Discussion

Permeabilization assays as a valuable tool to demonstrate CPP-membrane interaction.

The mechanism of CPP translocation across biological membranes inside the cell interior is likely not unique for the various CPPs. Earlier studies pointed at an energy-independent uptake mechanism into living cells (16-18) which gave rise to several models (summarized in (19)) such as the so-called direct membrane "transduction". Recent consensus on the matter, however, shows that the cationic CPPs in general are taken up at least to some extend by surface, adhesion, followed by endocytosis-driven cellular uptake and subsequent escape from the endosome (20, 21). In analogy to the original explanations for CPP translocation across the plasma membrane, the CPPs have to escape the endosome to avoid degradation in the lysosome. In order to investigate the translocation of the CPP it is thus crucial to both i) use an appropriate model system and ii) exclude possible CPP interactions with the reported model system (and thus method bias).

The typical leakage assay suits the first of the criteria because of the close resemblance of the model membrane system such as unilamellar vesicles with the lipid part of a biological membrane.

Apparent membrane leakage may be distorted due to fluorescent dye-CPP interaction.

Regarding the second point, however, we observed unexpected limitations. We found that the fluorescence signal of the dyes calcein and ANTS is influenced by the presence of 10 μM or higher concentration of various CPPs (compare **chapter 1** for the effect of nonaarginine (WR_9) or pen-2AL on calcein fluorescence emission). The CPPs either enhanced or reduced the fluorescence intensity of the anionic fluorophore. Whereas calcein emission was strongly reduced (almost complete quenching in presence of 100 μM pen-AYL) the ANTS signal increased upon interaction with CPPs (e.g. 92% signal increase in presence of 100 μM pen-A(pY)L). It is thus not possible with the leakage assay to accurately assess the fraction of membrane leakage. These findings are substantial, because the peptides show uptake by living cells at this concentration range.

The signal change is most likely caused by the electrostatic interaction between the highly positively charged CPP and the negatively charged dye. Interestingly, the zwitterionic phosphorylated pen-A(pY)L increased the fluorescence intensity more than the more positively charged pen-AYL which might be also related to the density of the resulting complexes.

As a consequence, we suggest to exclude potential intensity changes that may be caused by interaction of the CPP of interest and the used fluorescent dye.

The EPR signal of nitroxide-based spin labels is independent of presence of CPPs.

In order to avoid the bias of the multivalent CPP on the signal of the fluorophore, we replaced the fluorescent probe with a spin label that allows detection by EPR (as similarly performed with multilamellar vesicles by Humphries (12)). Commonly used spin labels in life science research areas are derivatives of stable nitroxide radicals such as TEMPO.

The EPR signal amplitude of these spin labels is usually increasing with concentration. Its resonance amplitude shows a concentration dependence that is similar to fluorescent dyes that start to self-quench at a certain concentration threshold (e.g. ~100 µM for calcein). Accordingly, the amplitude increases with spin label concentration until its maximum and then subsequently decreases again. In addition to the amplitude, also the linewidth of the resonance showed a concentration dependence (reflecting the motional averaging). In particular, a maximum in signal amplitude is observed at concentrations where spin exchange starts to take place. Even higher concentrations then lead to a broadening of the linewidth. As a result, either the signal amplitude or the linewidth (or both together) may be used to assess membrane permeabilization upon vesicular release/dilution of the spin label.

Also the EPR signal of the spin label should not change in presence of CPP. Our measurements show that the EPR spectrum of TEMPO indeed is independent of both lipid and CPP for the concentrations between 0.1 to 10 mM and 1 to 100 µM, respectively. Thus, the principle conditions for a robust leakage assay based on detection by means of EPR are given – in contrast to the leakage assay using fluorescent dyes and detection by means of fluorescence spectroscopy.

The entrapped nitroxide-based spin labels seem to leak from LUVs.

For optimum assay performance and reproducibility of the leakage assay it is required that the probe compound remains enclosed in the vesicles for a period of some hours to days in order to differentiate dilution of the probe by passive vesicle release from destabilization of the lipid bilayer by an external component, such as the CPP.

We observed that the TEMPO molecule is hydrophobic enough to diffuse across the lipid bilayer of model membranes such as LUVs and is therefore unsuitable as probe. In analogy, we could not entrap sufficient amounts of the examined TEMPO derivatives in LUVs. In all cases, the signal of the undiluted LUVs after gel chromatography was only a fraction (corresponding to <10 mM) of the signal as compared to the spin label stock solution (>50 mM). In support of passive diffusion across the membrane, we detected increasing amounts of spin label in the column eluate right after the LUV-containing fractions which indicate leakage over the whole course of the column.

Finally, addition of detergent to the gathered LUVs did neither change the EPR signal amplitude nor linewidth illustrating the concentration inside the vesicles was not sufficiently high to cause the required motional restriction.

5.4.1 Conclusion

Usage of fluorescent dyes as molecular probe to detect leakage may be critical in the investigation of CPPs because the fluorescent signal is biased by the electrostatic interaction of the CPP with the charged dye at low micromolar concentrations that are biologically relevant. In contrast, the EPR signal of nitroxide-based spin labels is not prone to CPP-induced distortion. However, retention of the spin labels inside LUVs needs to be improved by custom synthesis in order to be a useful molecular probe for this kind of assay.

5.5. References

1. Lundberg M, Johansson M. 2001. *Nature biotechnology* 19: 713-4
2. Wiener MC, White SH. 1992. *Biophysical journal* 61: 428-33
3. Henn FA, Thompson TE. 1969. *Annual Review of Biochemistry* 38: 241-&
4. Sessa G, Weissman.G. 1968. *Journal of Lipid Research* 9: 310-&
5. Weinstein JN, Yoshikami S, Henkart P, Blumenthal R, Hagins WA. 1977. *Science* 195: 489-92
6. Ziegler A. 2008. *Advanced Drug Delivery Reviews* 60: 580-97
7. Drin G, Demene H, Temsamani J, Brasseur R. 2001. *Biochemistry* 40: 1824-34
8. Fuchs SM, Raines RT. 2004. *Biochemistry* 43: 2438-44
9. Thoren PE, Persson D, Karlsson M, Norden B. 2000. *FEBS letters* 482: 265-8
10. Terrone D, Sang SLW, Roudaia L, Silvius JR. 2003. *Biochemistry* 42: 13787-99
11. Pankov R, Markovska T, Antonov P, Ivanova L, Momchilova A. 2006. *Chemico-Biological Interactions* 164: 167-73
12. Humphrie.Gk, Mcconnel.Hm. 1974. *Proceedings of the National Academy of Sciences of the United States of America* 71: 1691-4
13. Ellens H, Bentz J, Szoka FC. 1985. *Biochemistry* 24: 3099-106
14. Holland JW, Hui C, Cullis PR, Madden TD. 1996. *Biochemistry* 35: 2618-24
15. Needham D, Mcintosh TJ, Lasic DD. 1992. *Biochimica Et Biophysica Acta* 1108: 40-8
16. Derossi D, Calvet S, Trembleau A, Brunissen A, Chassaing G, Prochiantz A. 1996. *The Journal of biological chemistry* 271: 18188-93
17. Silhol M, Tyagi M, Giacca M, Lebleu B, Vives E. 2002. *European Journal of Biochemistry* 269: 494-501
18. Vives E, Brodin P, Lebleu B. 1997. *The Journal of biological chemistry* 272: 16010-7
19. Magzoub M, Graslund A. 2004. *Quarterly Reviews of Biophysics* 37: 147-95
20. Drin G, Cottin S, Blanc E, Rees AR, Temsamani J. 2003. *The Journal of biological chemistry* 278: 31192-201
21. Duchardt F, Fotin-Mleczek M, Schwarz H, Fischer R, Brock R. 2007. *Traffic* 8: 848-66

Acknowledgements

First I would like to thank Prof. Dr. Joachim Seelig for granting me the opportunity to do this thesis and for facilitating the very pleasant and fruitful atmosphere in his research group.

I thank the other members of my thesis committee, Prof. Dr. Sebastian Hiller and Prof. Dr. Jörg Huwyler for their effort.

Very special thanks to Dr. André Ziegler for his constant guidance, advice and proof reading.

Thanks to all members of the Seelig group, the workshop of the 6th floor and all other co-workers or employees from the Biozentrum I had the pleasure to work with for providing such a nice environment and generous support.

Thanks to Andy, Marc and Fabian for being such nice fellows.

Thanks to my family and friends.

Curriculum vitae

Personal data

Reto Sauder
Born on March 3rd, 1982
in Rorschach, Switzerland

Biozentrum, University of Basel
Department Biophysical Chemistry
Klingelbergstrasse 50/70
4056 Basel, Switzerland

Education

2009 – 2012	Graduate (Ph.D.) studies in Biophysics Biozentrum of the University of Basel Thesis supervisor: Prof. Dr. Joachim Seelig Thesis title: "Peptide Phosphorylation in the Design of a Vector for Intracellular Drug Delivery based on the Cell-Penetrating Peptide Penetratin"
2007 – 2009	Master of Science (M.Sc.) in Molecular Biology Biozentrum of the University of Basel Diploma supervisor: Prof. Dr. Joachim Seelig Diploma title: "Membrane permeation as caused by amphipathic and non-amphipathic cell-penetrating peptides"
2003 – 2009	Bachelor of Science (B.Sc) in Biology Biozentrum of the University of Basel

2000 – 2002	Matura Kantonsschule Trogen, Appenzell Ausserrhoden
1998 – 2000	Teachers Seminar Mariaberg, St. Gallen